UNIVERSITÀ DEGLI STUDI DI PADOVA

DIPARTIMENTO DI INGEGNERIA CIVILE, EDILE E AMBIENTALE - ICEA

Corso di Laurea in Ingegneria Geotecnica

Tesi di Laurea Magistrale

Dissipation of pore water pressure in debris flow mixtures of different composition

Dissipazione della pressione dei pori in miscele di colate detritiche di differente composizione

Relatore: Simonetta Cola

Correlatori: Roland Kaitna

Lorenzo Brezzi

Laureando: Stefano Canto

Anno accademico

2014-2015

2015 July, Vienna

This master thesis has been achieved at the Institut für Alpine Naturgefahren (IAN), Universität für Bodenkultur, Wien.

I am grateful in particular, for the essential help, to the assistant supervisor and mentor Roland Kaitna, to the laboratory technicians Martin Falkensteiner and Friedrich Zott, to PhD Magdalena Von Der Thannen, the assistant Monika Stanzer and last but not least Franz Ottner, laboratory supervisor of Institut für Angewandte Geologie (IAG)

Questa tesi è stata realizzata all'Institut für Alpine Naturgefahren (IAN) presso l'Universität für Bodenkultur Wien BOKU di Vienna AT.

Si ringraziano in particolare per il fondamentale aiuto Roland Kaitna, correlatore e guida; i tecnici di laboratorio Martin Falkensteiner e Friedrich Zott, Magdalena Von Der Thannen, Monika Stanzer e ultimo ma non meno importante Franz Ottner, presso il laboratorio di Institut für Angewandte Geologie (IAG).

A mio padre,

che mi ha trasmesso la passione.

Table of contents

ABSTRACT

This paper focuses on natural hazards, particularly on debris flow. The goal of the research is to find, if exist, any correlation between fine particles, coarse particles and dissipation coefficient D. To reach the goal a test procedure based on the experiments of Jon Major will be used.

I tested two different debris flow samples, the first coming from a debris flow event in Switzerland (Scalärarüfe, 2001) and the latter coming from a debris flow event in Austria (St. Lorenzen im Paltental, 2012).

First of all, I proceeded with the grain size distribution (GSD) for both samples. Then I decided to carry out 32 different tests, changing both fine particles and coarse particles concentration, to investigate the possible correlations among the parameters. I led some mineralogical tests on the Scalärarüfe sample to know more about the fine particles mineralogy.

In order to carry out the tests, I used a 12.5 l of volume plexiglass cylinder, equipped with five sensors, one placed at the bottom and four on the sides paired two by two. Unfortunately, one of them was inoperative since the first tests. Other sensors, sometimes, showed some problems of reliability. I took into account that by checking manually the results.

The results showed that the more is the fine particles content, the smaller is the Dissipation coefficient. Whereas, results showed that, below a certain fine particles concentration, D coefficient is independent from the coarse particles composition. Over this fine particles concentration limit, D coefficient is related to coarse particles composition. Different results could be found testing other mixtures and fine contents.

Keywords:

Debris flow, gravity driven consolidation, fine particles, coarse particles, D coefficient.

INTRODUCTION

Before the appearance of Homo sapiens on Earth, the purely natural system ruled our planet. Many geophysical events such as earthquakes, volcanic eruptions, landslides, flooding took place threatening only the prevailing flora and fauna. Millions of years later, the human presence transformed the geophysical events into natural disasters.

The transformation of these geophysical events into natural disasters occurred simultaneously with the appearance of the human system, when human beings began to interact with nature, when fire was discovered and tools were made from the offerings of the natural habitats. The evolution of humans left behind the age in which only nature existed. It provided the starting point of the interrelation of the human system with nature.

The human system itself was subjected to significant transformations, where the concept of work and hence of social division of work, production relations and economical–political systems appeared. These transformations and their links to the natural system have served as templates of the dynamics of natural hazards and therefore, of natural disasters.

Natural hazards are indeed geophysical events, such as earthquakes, landslides, volcanic activity and flooding. They have the characteristic of posing danger to the different social entities of our planet, nevertheless, this danger is not only the result of the process per se (natural vulnerability), it is the result of the human systems and their associated vulnerabilities towards them (human vulnerability). When both types of vulnerability have the same coordinates in space and time, natural disasters can occur.

Natural disasters happen worldwide; however, their impact is greater in developing countries, where they occur very often. In most cases, the cause of natural disasters in these countries is due to two main factors. First, there is a relation with geographical location and geological–geomorphological settings. Developing or poor countries are located largely in zones largely affected by volcanic activity, seismicity, flooding, etc. The second reason is linked to the historical development of these poor countries, where the economic, social, political and cultural conditions are not good, and consequently act as factors of high vulnerability to natural disasters (economic, social political and cultural vulnerability).

Understanding and reducing vulnerability is undoubtedly the task of multi-disciplinary teams. Amongst geoscientists, geomorphologists with a geography background might be best equipped to undertake research related to the prevention of natural disasters given the understanding not only of the natural processes, but also of their interactions with the human system. In this sense, geomorphology has contributed enormously to the understanding and assessment of different natural hazards (such as flooding, landslides, volcanic activity and seismicity), and to a lesser extent, geomorphologists have started moving into the natural disaster field.

Natural hazards are threatening events, capable of producing damage to the physical and social space where they take place not only at the moment of their occurrence, but on a long-term basis due to their associated consequences. When these consequences have a major impact on society and/or infrastructure, they become natural disasters. Specifically, they are considered within a geological and hydrometeorological conception, where earthquakes, volcanoes, floods, landslides, storms, droughts and tsunamis are the main types. These hazards are strongly related to geomorphology since they are important ingredients of the Earth's surface dynamics. Natural hazards take place in a certain place and

during a specific time, but their occurrence is not instantaneous. Time is always involved in the development of such phenomena. For example, flooding triggered by hurricanes or tropical storms is developed on a time basis. Atmospheric perturbations lead to the formation of tropical storms, which may evolve into hurricanes, taking from a few hours to some days. Hence, the intensity and duration of rainfall in conjunction with the nature of the fluvial system, developed also on a time basis, would determine the characteristics of the flooding. (Alcàntara_Ayala, 2002)

1 NATURAL HAZARDS

1.1 LANDSIDES

Landslides occur in many territories and can be caused by a variety of factors including earthquakes, fire and by human modification of land. Landslides can happen quickly, often with little notice and the best way to prepare is to stay informed about changes in and around your home that could signal that a landslide is likely to befall.

Figure 1.1.a A debris flow event in the Alpine region

In a landslide, masses of rock, earth or debris move down a slope. Debris and mudflows are rivers of rock, earth, and other debris saturated with water. They develop when water rapidly accumulates in the ground, during heavy rainfall or rapid snowmelt, changing the earth into a flowing river of mud or "slurry." They can flow rapidly, striking with little or no warning at avalanche speeds. They also can travel several miles from their source, growing in size as they pick up trees, boulders, cars and other materials. Landslide problems can be caused by land mismanagement, particularly in mountain, canyon and coastal regions. In areas burned by forest and brush fires, a lower threshold of precipitation may initiate landslides. Land-use zoning, professional inspections, and proper design can minimize many landslide, mudflow, and debris flow problems.

1.2 DEBRIS FLOW

A debris flow is a moving mass of loose mud, sand, soil, rock, water and air that travels down a slope under the influence of gravity. To be considered a debris flow the moving material must be loose and capable of "flow", and at least 50% of the material must be sand-size particles or larger. Some debris flows are very fast - these require attention. In areas of very steep slopes, they can reach speeds of over 160 km/hour. However, many debris flows are very slow, creeping down slopes by slow internal movements at speeds of just 30 to 60 centimeters per year. The speed and the volume of debris flows make them very dangerous. Every year, worldwide, many people are killed by debris flows. This hazard can be reduced by identifying areas that can potentially produce debris flows, educating people who live in those areas and govern them, limiting development in debris flow hazard areas, and developing a debris flow mitigation plan.

1.2.1 Conditions Required to Produce a Debris Flow

The source area of a debris flow must have:

- very steep slope
- abundant supply of loose debris
- a source of abundant moisture
- sparse vegetation

Identifying areas where debris flows have happened in the past or where these conditions are present is the first step towards developing a debris flow mitigation plan.

1.2.2 What Causes Debris Flows?

Debris flows can be triggered by many different situations. Here are a few examples:

Addition of Moisture: A sudden flow of water from heavy rain, or rapid snowmelt can be channeled over a steep valley filled with debris that is loose enough to be mobilized. The water soaks down into the debris, lubricates the material, adds weight, and triggers a flow.

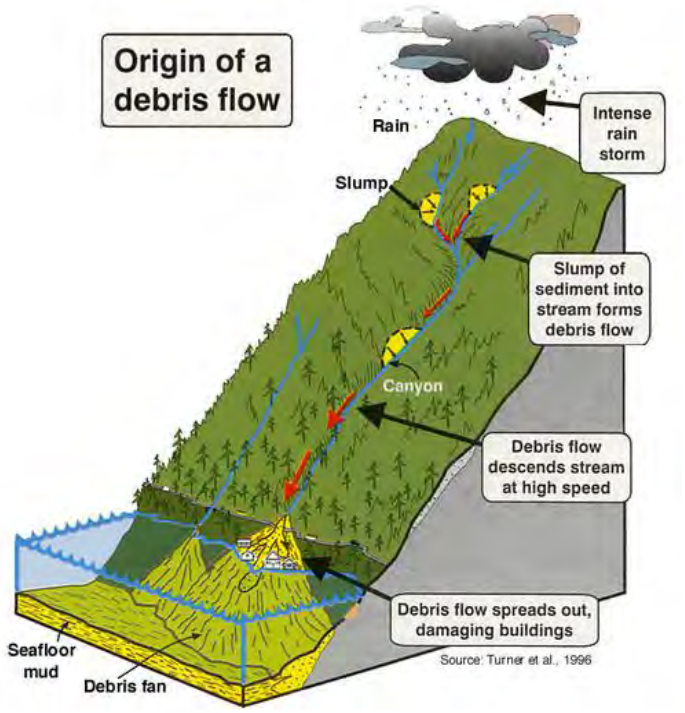

Figure 1.2.a Sketch of debris flow origin

Removal of Support: Streams often erode materials along their banks. This erosion can cut into thick deposits of saturated materials stacked high up the valley walls. This erosion removes support from the base of the slope and can trigger a sudden flow of debris.

Failure of Ancient Landslide Deposits: Some debris flows originate from older landslides. These older landslides can be unstable masses perched up on a steep slope. A flow of water over the top of the old landslide can lubricate the slide material or erosion at the base can remove support. Either of these can trigger a debris flow.

Wildfires or Timbering: Some debris flows occur after wildfires have burned the vegetation from a steep slope or after logging operations have removed vegetation. Before the fire or logging the vegetation's roots anchored the soil on the slope and removed water from the soil. The loss of support and accumulation of moisture can result in a catastrophic failure. Rainfall that was previously absorbed by vegetation now runs off immediately. A moderate amount of rain on a burn scar can trigger a large debris flow.

Volcanic Eruptions: A volcanic eruption can flash melt large amounts of snow and ice on the flanks of a volcano. This sudden rush of water can pick up ash and pyroclastic debris as it flows down the steep volcano and carry them rapidly downstream for great distances. In the 1877 eruption of Cotopaxi Volcano in Ecuador, debris flows traveled over 300 kilometers down a valley at an average speed of about 27 kilometers per hour. Debris flows are one of the deadly "surprise attacks" of volcanoes. (King, 2006)

2 THESIS' PURPOSE

This paper focuses on landslides and flood: the so-called debris flow. They are very dangerous in built-up areas and the more they run-off, the more damages could be considerable. Run-off distance mainly depends on the characteristics of the mixture and the topography. In this work, I focus on the mixture characteristics, especially in mixture composition and grain-size distribution, because I would to investigate how the composition of the mixture may influence pore water pressure dissipation. In fact, debris flows are subjected to the soil laws: we have to consider the interactions between the fluid stage and the solid one. As the one-dimensional consolidation, a debris flow running down a slope shows a hyper-hydrostatic pore fluid pressure that will be dissipated whit time depending on the mixture composition.

In case of natural debris flows, we usually refer to the gravity driven consolidation that arises from the one-dimensional consolidation, studied by Terzaghi. Despite the one dimensional consolidation, where the soil compacts under an external loading, in the gravity driven one we have no external loading applied, but the material's consolidation is due to the gravity force acting on it. Therefore, it is quite interesting to know how they bulk mixture dissipates the excess pore water pressure. It is remarkable to remember that, according to the Terzaghi stress principle, the higher pore pressure the lower the effective stress. The effective stress drives the frictional stress, according the simplest Coulomb's principle.

As result, the lower is the frictional stress, longer the debris flows might run off. Therefore, by understanding the behavior of the pore pressure, we can express some hypothesis on the run off and consequently on debris flows hazard assessment.

In this thesis, my aim is to find, if exists, any correlation between the dissipation coefficient and the basic parameters involved in debris flows: water content, fine-grained particles and coarse-grained particles. Alternately, I want to investigate about which parameter is more important to the dissipation coefficient and what kind of relation it is possible to use. In order to get the aim of this research, I will test a real debris flow sample collected in Switzerland in Scalärarüfe near Trimmis/Chur in Eastern Switzerland after the event of 3rd May 2001 and the Lorenzerbach event of 21st July 2012 in St. Lorenzen im Paltental.

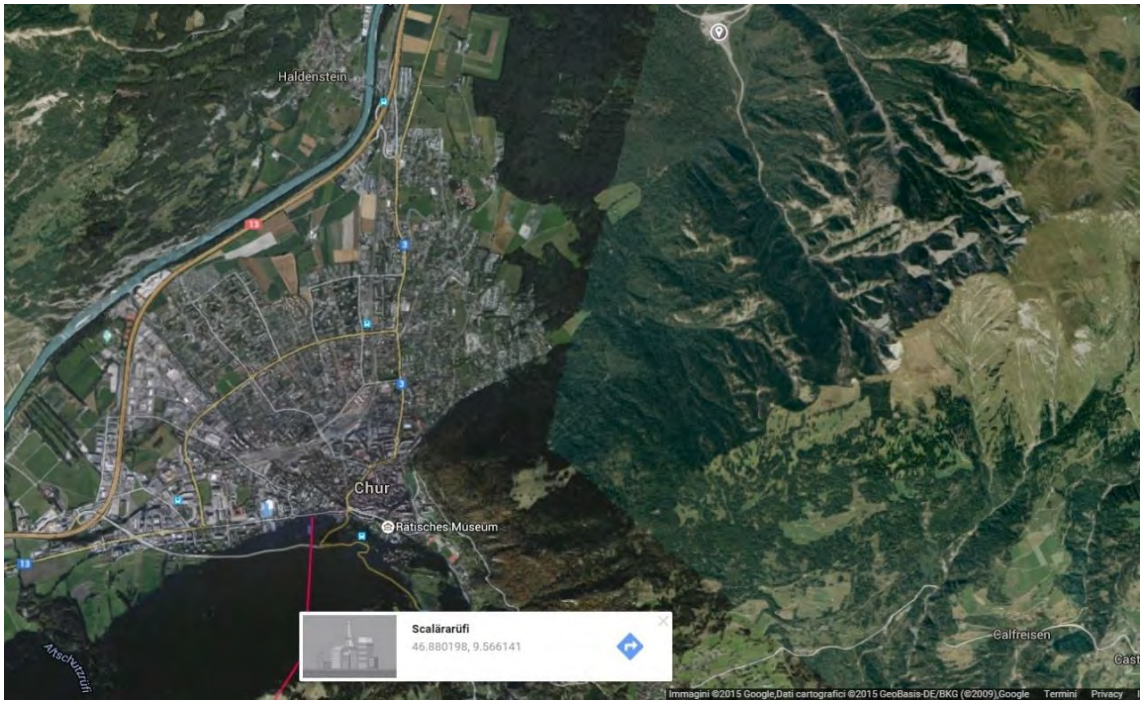

Figure 2.a Satellite view of the area of Scalärarüfe debris flow event of 3rd May 2001 in Switzerland

Figure 2.b Satellite view of St. Lorenzen im Paltental, area of Lorenzerbach debris flow event of 21st July 2012

2.1 DOCUMENTATION OF THE LORENZERBACH EVENT

2.1.1 General Description

Figure 2.1.a Lorenzerbach event damages

The village of St. Lorenzen, in the Styrian Palten valley, is situated on the banks of the Lorenz torrent, in which a debris flow event occurred in the early morning hours of the 21st of July 2012, causing catastrophic damage to residential buildings and other infrastructural facilities. The catchment area encompasses a 5.84 km^2 area that is situated geologically in the Rottenmanner Tauern. The upper catchment lies within the High Tauern's basement complex (gneissic rock of the Bösenstein massif), whereas the middle section of the catchment lies within the greywacke zone (Muerz shale deposits, phyllite and sericite schist) and the lower catchment is located in greywacke-, green- and graphitic schist; the sedimentary cover is made up of alluvium. The flood water discharge and bedload volume associated with a 150 year return time was estimated at 34 m^3/s and 25.000 m^3 respectively for the 5,84 km2 catchment area. The bedload transport capacity of the torrent was classified as ranging from "heavy" to "capable to produce debris flows". Large parts of the village were designated as red zones in the hazard zone map, while the remaining part of the alluvial fan upon which the village is situated was designated as belonging to the yellow zone. The Lorenzer torrent has always been known to present a danger and the construction of the first technical protection measures started in 1924. The extensive constructions undertaken by the Austrian Service for Torrent and Avalanche Control over the past few decades have however surely prevented and an even worse catastrophe from occurring. A bed deepening was in particular prevented along the tiered series of check dams.

Figure 2.1.b Lorenzerbach event damages

Figure 2.1.c Lorenzerbach event damages

2.1.2 Meteorology and Precipitations

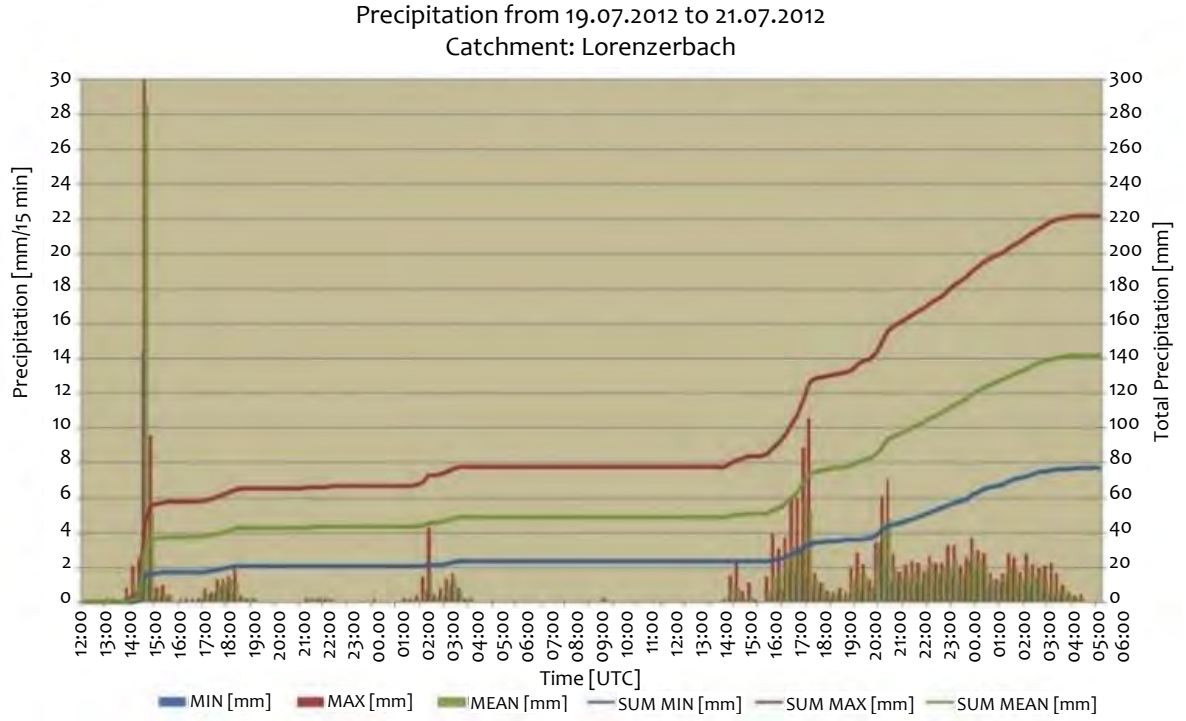

Figure 2.1.d Precipitation table of previous days

The precipitation event that ultimately triggered this debris flow began at 13 .00 UTC on the 19th July and ended 5.30 UTC on 21st July. The largest single-point 15 min precipitation rate registered within the catchment basin comprises nearly 40.4 mm. The average of for the entire catchment area amounts to slightly more than 141 mm. The catastrophic impact of the event is however not only due to the rainfall intensity of this precipitation event itself, but also in combination with the precipitation of the previous weeks.

2.1.3 Event Description

The dominant process type of the mass movement event may described as a fine-grained debris flow. The damage in the residential area of St.Lorenzen was caused by a debris flow pulse in lower reach of the Lorenz torrent. This debris flow pulse was in turn caused by numerous landslide along the middle reaches of the torrent, some of which caused blockages, ultimately leading to an outburst event in the main torrent. Following the event, comprehensive documentation work was undertaken on the debris cone, along the channel length and on the later slopes of the channel. Back-calculation of velocities, based on a 2-parameter model by Perla and Rickenmann, yielded an average debris flow velocity along the middle reaches of torrent between 11 and 16 m/s. An average velocity of 9 m/s was calculated for the debris flow at the neck of the alluvial fan directly the center of the village. The back-calculated debris flow peak discharge was around 500 m^3/s. A total of 67 buildings were damaged along the torrent, 7 of them were totally destroyed. In the town center, flooding heights of up to 3 m were measured. (S. Janu, 2015).

3 THEORETICAL SYSTEM

3.1 CONTINUUM

When applying concepts of mechanics to problems in Earth sciences, we are interested in forces applied to, and deformation and flow of idealized continuous bodies (a continuum). But what constitutes a continuum? Is it such an idealization appropriate or adequate? A continuum is an idealized region of space filled with matter having properties that, when averaged over appropriate spatial scales, vary continuously across that space. Under this simplifying concept, we disregard molecular structure of material. At the macroscopic scale, we ignore discontinuities and assume that material can be adequately characterized by averaged properties. Clearly, such idealized matter does not exist, as discontinuities are present at virtually all scales. In some instances, discontinuities may place bounds on the region that can be considered a continuum. However, if a scale appropriate for the problem is selected, discontinuities at a smaller scale can be tolerated and average properties of the matter can be assumed to vary smoothly across the scale of interest.

3.1.1 Force

Newton's second law states that the time rate of change of momentum of a body is proportional to the sum of the forces acting upon that body (e.g., Johnson, 1970; Middleton and Wilcock, 1994). Because momentum is defined as the product of mass and velocity, Newton's second law can be written as $F = d(mv)/dt$ where *F* represents the forces acting on the body, d/dt the total derivative that represents rate of change with time, *m* the mass of the body, and *v* its velocity. For constant mass, this expression becomes $F = m\, dv/dt$ and because d/dt is the definition of acceleration, we get the familiar expression $F = ma$.

From the above expression, we see that force has a unit of $Kg\ m/s^2$, which is called a newton (N). In mechanics, two classes of forces can be defined: body forces and surface forces. Body forces act equally on every element of mass within a body and are proportional to its mass or volume. An example of a body force is the force of gravity; the weight of an element is the product of its mass and the acceleration of gravity, *g*. Surface, or contact, forces, on the other hand, act on the bounding surface of a body. Unlike a body force, the influence of a surface force is proportional to the size of the area over which it acts; furthermore, it acts in a specific direction and in a specific position. An example of surface forces acting on a body can be illustrated by envisioning a person pushing a box across a table. As the box is pushed, there is not only a force acting perpendicular to the face being pushed, but also a component of that force acting tangentially along the surface of the box in contact with the table. As long as the magnitude of the tangential force exceeds the force of friction resisting sliding the box will slide. We can also envision that a box having a small footprint might be easier to push than one having a large footprint, because the magnitude of the tangential force transmitted to the base of the small box is focused across a smaller area and can more easily overcome the frictional force resisting sliding. Because the influence of a surface force is proportional to the size of the area over which it acts, an inherent geometric effect influences the changes in a body caused by that force. Therefore, having a common way of quantifying the effect of a surface force regardless of the size of the area over which it acts is useful. The best way to remove the geometric effect of a surface force acting on a body is to normalize the force by the area over which it acts, which leads to the concept of stress.

3.1.2 Stress

Stress, by definition, is the surface force per unit area exerted on a body of material and is given in units of newtons per square meter N/m^2 or pascals (Pa). Stress is a very useful concept for understanding the impact a surface force has on a body. Intuitively, the more broadly a surface force is distributed, the lower the stress. The broader concept of stress with respect to continuum mechanics is related to the stress acting at a point or the force acting on an area in the limit as the size of the area diminishes to zero (e.g., Malvern, 1969; Middleton and Wilcock, 1994).

3.1.3 Total Stress

Stress is conveniently resolved into two components: a normal stress, which acts perpendicular to a surface, and a shear stress, which acts tangential to a surface. Figure 3.1.a shows the normal and shear stresses acting on an elemental control volume defined in accordance with the Cartesian *x,y,z* coordinate system. Each stress is identified using a pair of subscripts: the first subscript refers to the direction perpendicular to the surface on which the stress is acting and the second subscript refers to the direction of the stress. Thus, normal stresses have identically paired subscripts, whereas shear stresses have unequal subscripts. Three stresses are defined on each surface perpendicular to a coordinate direction: a normal stress acting perpendicular to the surface and two orthogonal shear stresses acting along the surface. Hence, nine different stresses act on the three-dimensional volume, and assuming there is no acceleration, stresses equal in magnitude but acting in opposing directions are imposed on the other three faces. The forces associated with the normal stresses act to stretch or compress the elemental volume, whereas the forces associated with the shear stresses attempt to distort and rotate the elemental volume about each axis. For an element in equilibrium, the moments about each axis must balance. Therefore, the shear stresses are symmetric, i.e. $\sigma_{xy} = \sigma_{yx}$. Whereas nine stresses are defined in three dimensions, only six of those stresses are independent. To properly account for the direction in which the stresses act, a sign convention for positive and negative stresses must be defined. In soil mechanics, it is common to consider compressive stresses positive, because compression is the most common state of soils dealt with by geotechnical engineers. Despite the seeming convenience of aligning the positive sign convention with the most common state of stress in Earth, there are both mathematical and physical reasons that trump this convenience. Mathematically, the outward-normal direction on the Cartesian elemental volume has a positive sense of direction on a positive face and a negative sense of direction on a negative face (see Figure 3.1.a). The normal stresses acting in those positive senses, thus, tend to pull the element in opposite directions leading to a state of tensile stress. The adopted sign convention also is consistent with physical changes that occur during normal strain, in which elongation associated with tension (a positive value because the ending state is longer than the starting state) is defined as positive strain. Shear stresses are defined as positive if they act in a positive direction on a positive face, and in a negative direction on a negative face. Stresses acting at a point can be represented in mathematical form as σ_{ij}. This mathematical notation, in which *i* and *j* represent the coordinate axes as numbers (*1, 2, 3*) or letters (*x, y, z*), defines a stress matrix, also known as a stress tensor:

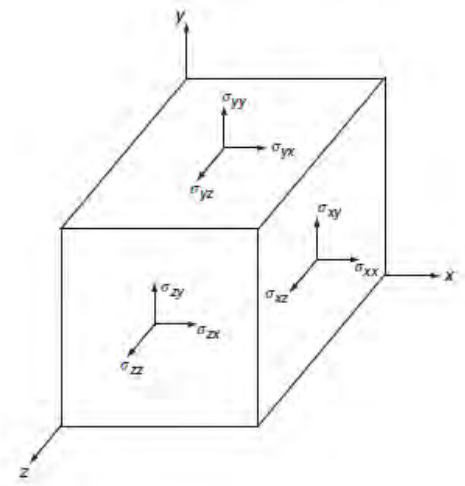

Figure 3.1.a

$$\sigma_{ij} = \begin{pmatrix} \sigma_{11} & \sigma_{12} & \sigma_{13} \\ \sigma_{21} & \sigma_{22} & \sigma_{23} \\ \sigma_{31} & \sigma_{32} & \sigma_{33} \end{pmatrix} = \begin{pmatrix} \sigma_{xx} & \sigma_{xy} & \sigma_{xz} \\ \sigma_{yx} & \sigma_{yy} & \sigma_{yz} \\ \sigma_{zx} & \sigma_{zy} & \sigma_{zz} \end{pmatrix}$$

In this matrix, the terms along the diagonal represent the normal stresses and the off-diagonal terms represent the shear stresses. Because pairs of shear stresses must be equal for an element in equilibrium, $\sigma_{ij} = \sigma_{ji}$. We can use the stress matrix to define the mean normal stress acting on the element as

$$\bar{\sigma} = \frac{1}{3}\left(\sigma_{xx} + \sigma_{yy} + \sigma_{zz}\right)$$

The mean normal stress can, furthermore, be equated with a mechanical mean pressure acting on the element. Because pressure is typically defined as positive in compression, we can define the mechanical mean pressure as

$$-\bar{p} = \frac{1}{3}\left(\sigma_{xx} + \sigma_{yy} + \sigma_{zz}\right) \quad (1)$$

This expression tells us that a positive mean normal stress (tension) is equivalent to a negative mechanical mean pressure, whereas a negative mean normal stress (compression) is equivalent to a positive mechanical mean pressure. In some analyses, it is useful to separate the mean normal stress (pressure) acting on a medium from the overall stress by subtracting the mean normal stress from the total stress. Separating stresses in this manner allows us to isolate explicitly those stresses that deviate from the mean stress. For an incompressible material, the stresses that deviate from the mean normal stress are those that cause deformation. Hence, the "*deviatoric stress*" is defined as the difference between the total stress and the mean normal stress (e.g., Engelder, 1994). The deviatoric stress matrix can be written as

$$\sigma_{ij}^{D} = \begin{pmatrix} \sigma_{xx} - (-\bar{p}) & \sigma_{xy} & \sigma_{xz} \\ \sigma_{yx} & \sigma_{yy} - (-\bar{p}) & \sigma_{yz} \\ \sigma_{zx} & \sigma_{zy} & \sigma_{zz} - (-\bar{p}) \end{pmatrix} = \begin{pmatrix} \sigma_{xx} + \bar{p} & \sigma_{xy} & \sigma_{xz} \\ \sigma_{yx} & \sigma_{yy} + \bar{p} & \sigma_{yz} \\ \sigma_{zx} & \sigma_{zy} & \sigma_{zz} + \bar{p} \end{pmatrix} \quad (2)$$

From this matrix, we see that only the normal stresses are affected; shear stresses are unaffected by variations in mean normal stress. Clearly, another way to write the total stress tensor is

$$\sigma_{ij} = -\bar{p}\,\delta_{ij} + \sigma_{ij}^{D} \quad (3)$$

where δ_{ij} is the identity matrix, known as the Kronecker delta, which is equal to 1 when *i* is equal to *j*, and zero otherwise. Thus far, discussion of stresses has been implicitly restricted to homogenous, nonporous media. In porous media, the pressure of the fluid that fills the pores can influence stresses causing deformation. That influence necessitates discussion of pore fluid, pore-fluid pressure, and the concept of effective stress. Because the most common fluid in porous material at Earth's surface is water, the discussion below is restricted to pore water and pore-water pressure.

3.1.4 Pore Water, Hydraulic Head, and Pore-Water Pressure

Regolith (the mantle of fragmented material that overlies bedrock) and highly fractured rock at Earth's surface – here termed soil – contain voids (pores) that are variously wetted or filled with water (pore water). Forces acting on pore water establish gradients of fluid potential, the work required to move a

unit quantity of fluid from a datum to a specified position, and pore water flows in response to these gradients.

The concept of hydraulic head, a measure of the energy in a fluid-filled porous medium, usefully describes pore-water potential. Total hydraulic head, or potential per unit weight of fluid, can be defined in terms of two fundamental forms of energy: potential energy, defined in terms of gravitational and pressure potential energy, and kinetic energy, the energy associated with fluid motion. In a typical soil subject to Darcian (seepage) flow, the flow velocity is usually very low and the kinetic energy is negligibly small compared to the total potential energy. Thus, for an incompressible fluid (fluid having a constant density; ρ_w for water) the total hydraulic head (h) in a water filled soil is given

$$h = \psi + \frac{p}{\varrho_w g} \quad (4)$$

where ψ is the gravitational, or elevation, potential, and $p/\rho_w g$ the pressure potential, in which p is the gauge pressure of the pore water relative to atmospheric pressure and g gravitational acceleration in the coordinate direction. Pore-water pressure, therefore, constitutes one of the two dominant components of the fluid potential in soils. Pore-water pressure is isotropic, meaning that it is has the same magnitude in all directions, but it varies with position relative to the water table within a soil (the depth horizon where pore-water pressure is atmospheric, which defines the zero-pressure datum) and with the proportion of soil weight carried by contacts among the soil grains (intergranular contacts). Below the water table, pore water pressure is greater than atmospheric and positive; above the water table, pore-water pressure is less than atmospheric and negative owing to tensional capillary forces exerted on pore water. If soil is saturated and water statically fills pore space, then the pore-water pressure is hydrostatic and varies with depth below the surface as a function of the overlying weight of water. Pore-water pressure can exceed or fall short of hydrostatic under hydrodynamic conditions or if a soil compacts or dilates under load. Below the water table, soil compaction will cause a transient increase in pore-water pressure, the duration and magnitude of which are governed mainly by the rate of compaction and the permeability of the soil. An increase in pore-water pressure can lead to a loss of soil strength. If compaction thoroughly disrupts intergranular contacts, then the pore fluid may bear the entire weight of the solid grains, and the soil will liquefy.

3.1.5 Effective Stress

The behavior of porous media having fluid-filled pores depends not only on the total state of stress to which the material is subjected, but also on the pressure of the pore fluid. The state of stress that causes solid-body deformation is the stress that acts on the skeleton of solid material that makes up the porous medium; however, that stress is modulated by the pressure of the pore fluid. Therefore, when dealing with porous media the total state of stress is commonly partitioned into components that describe the fluid pressure and the stress acting on the solid skeleton. Such partitioning of stress leads to the concept of effective stress, a concept partly recognized by Charles Lyell as early as the late 1800s (Skempton, 1960), but not explicitly articulated until Terzaghi (1923, 1943) proposed a simple theoretical framework for soil consolidation. The concept of effective stress is elegantly simple and is defined as the difference between total stress and pore-fluid pressure. The mathematical formulation most useful for describing effective stresses in soils and other compressible porous media is given

$$\sigma'_{ij} = \sigma_{ij} + p\delta_{ij} \quad (5)$$

where σ'_{ij} are the effective stresses acting on the solid skeleton, σ_{ij} the total stresses acting on the porous medium, and *p* the pore-fluid pressure. Note that the effective stress in this formulation appears to be an additive function of total stress and pore-fluid pressure, but recall that normal stresses are defined negative in compression whereas pore-fluid pressure is defined positive in compression. Partitioning the total stress in terms of effective stress and fluid pressure illuminates crucial physical insights. Consider a saturated porous medium in which water statically fills the pores. If that saturated medium is now submerged beneath a water surface, both the total stress exerted on the medium and the pore-water pressure increase by an equal amount. As a result, the effective stress remains unchanged. Hence, simply increasing the fluid pressure does not cause a volume change of the medium. Now consider a container of laterally confined saturated porous material, let's say saturated sediment. If a vertical load is added instantaneously to the sediment surface across an impermeable barrier that prevents pore-water drainage, the total stress within the sedimentary body increases. In response to that stress change, the sediment grains attempt to pack closer together. However, because the pore water cannot escape and because we shall assume that both the water and the sediment grains are incompressible, particle rearrangement cannot occur. As a result, the intergranular stresses acting on the sediment grains cannot change, the sedimentary body cannot compact, and the water pressure increases by an amount equal to the change in total stress. Again, we find that simply increasing pore-water pressure does not cause volume change. Now consider the case in which the vertical load is applied across a drainage panel atop the sediment body, which allows pore water to drain. Because the water pressure within the sedimentary body has increased above hydrostatic in this example, pore water flows toward the drainage panel at the deposit surface (where the water pressure is zero) in response to the change in gradient of the hydraulic head caused by the change in pore-water pressure. As pore water seepage progresses, the pressure in excess of hydrostatic is gradually diminished and transferred to the stress acting on the sediment grains and the deposit compacts. Compaction, or volume change, therefore, occurred in response to changes in the intergranular, or effective, stress. Thus, in porous media, the measureable effects from changes in stress, such as volume change, distortion, or changes in shearing resistance, are due exclusively to changes in effective stress (Terzaghi, as quoted in Skempton, 1960). We can solidify the thought experiment in more concrete terms by examining fluid pressure and total stress within a shallow, one-dimensional, water-saturated sediment deposit in which the vertical coordinate direction, y, is defined positive upward (Figure 3.1.b). If water statically fills the pores within the sediment body, then the hydrostatic fluid pressure, P_h, of a column of water extending from the surface to a depth *H-y* is

$$P_h = \varrho_w g(H - y) \quad (6)$$

where ρ_w is the density of water, *g* the gravitational acceleration in the coordinate direction, and H the coordinate value identifying the body surface (e.g., Major, 2000). The total stress acting on the sediment body, extending from the surface to the same depth, is

$$\sigma_{yy} = -\varrho_t g(H - y) \quad (7)$$

where ρ_t is the total mass density of the water-saturated sediment. (The negative sign follows the convention that total stress is defined as negative in compression, whereas pore fluid pressure is defined as positive in compression.) The total mass density for the body can be written in terms of water density, ρ_w, grain density, ρ_s, and porosity, *n* (assumed here to be uniform throughout the depth of the shallow body), as

$$p_t = \varrho_w n + \varrho_s(1 - n) \quad (8)$$

Substitution of eqn (8) into eqn (7), and some algebraic manipulation, leads to

$$\sigma_{yy} = -[\varrho_{tw} + (\varrho_w - \varrho_s)(1-n)]g(H-y) \quad (9)$$

This expression shows that the total stress at depth in a column of uniformly porous, water-saturated sediment depends on the weight of the overlying water plus the buoyant weight of the column of overlying solids. Suppose now the saturated sediment is loaded rapidly but with no change of stress at the deposit surface caused (i.e. by rapid deposition of a uniform thickness of similar saturated sediment). As a result, the pore-water pressure changes because the water that fills the pores is incompressible and it resists particle rearrangement. That resistance leads to a temporary increase in fluid pressure. The total pore-water pressure can then be written as $P_t = P_h + P_*$, where P_h represents the hydrostatic portion of the pressure and P_* represents the water pressure that is in excess of hydrostatic. Under rapid loading, water does not drain instantaneously from the pores; instead, it temporarily bears the weight of the new load. If the water bears the entire total stress imposed on the system, the sediment is said to be liquefied. Setting the total water pressure equal to the total stress in eqn (9) and recasting the expression leads to

$$P_t = \varrho_w g(H-y) + [(\varrho_w - \varrho_s)(1-n)]g(H-y) \quad (10)$$

The first term on the right-hand side of this expression is the hydrostatic pressure and the second term is the non-equilibrium or excess water pressure. This expression shows that the excess water pressure is equal to the buoyant unit weight of the sediment (Figure 3.1.b). Thus, when a sedimentary deposit is liquefied, gravity induces a downward flux of the sediment toward the bed, and the excess fluid pressure is equal to the buoyant unit weight of the sediment:

$$P_* = (\varrho_w - \varrho_s)(1-n)g(H-y) \quad (11)$$

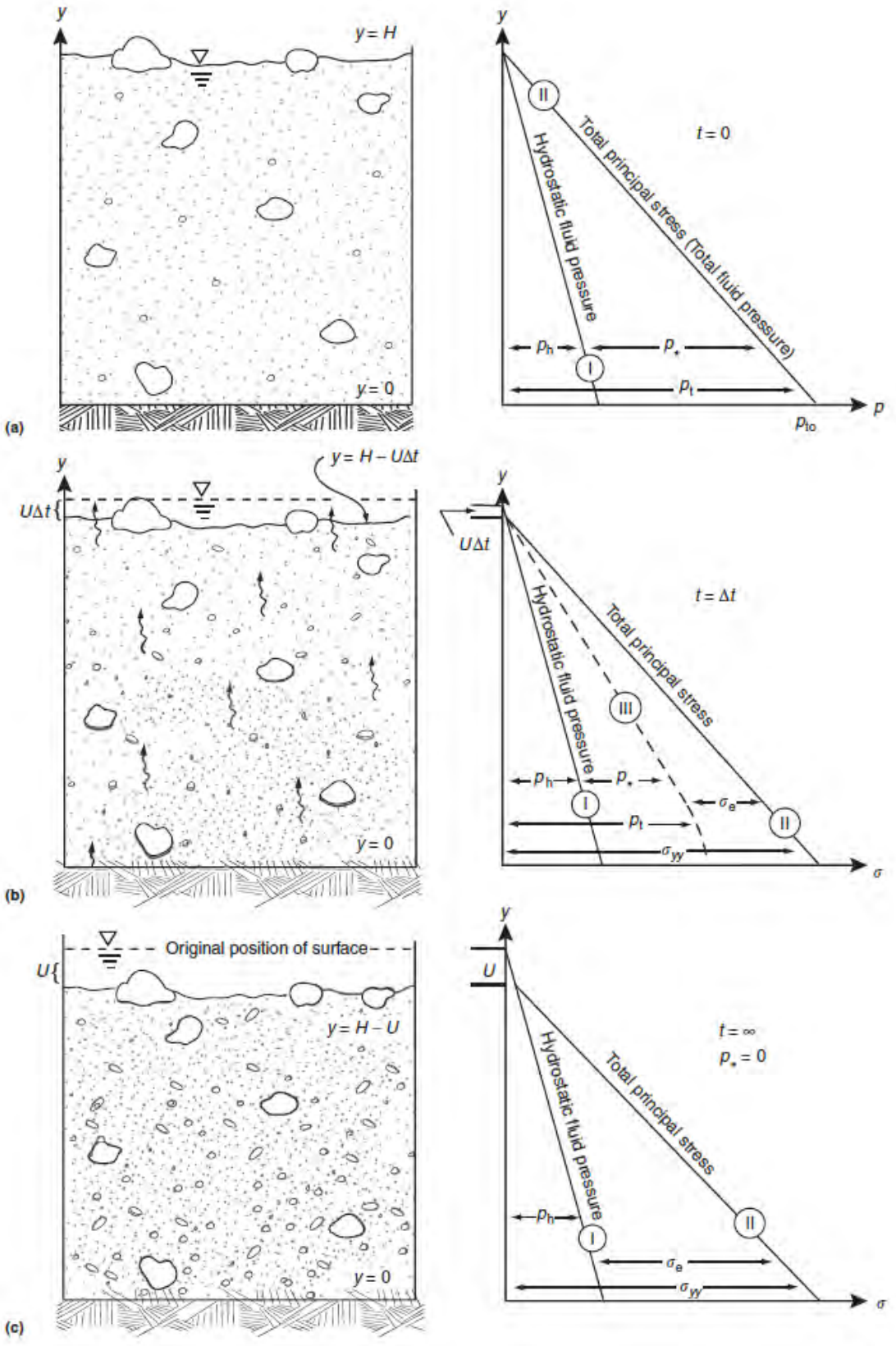
y
y = H
y = 0
(a)
II
Total principal stress (Total fluid pressure)
Hydrostatic fluid pressure
t = 0
p_h
p_e
I
p_t
p
p_to
y = H – UΔt
UΔt
t = Δt
III
σ_e
σ_yy
σ
(b)
Original position of surface
U
y = H – U
t = ∞
p_e = 0
(c)

Figure 3.1.b

Owing to the head gradient that is established because of the nonequilibrium water pressure, the pore water will flow down gradient, from high head to low head. As it does, the excess water pressure will diffuse and the effective stress acting on the solid skeleton will increase (Figure 3.1.b). At infinite time, all of the excess water pressure will have dissipated, the sediment deposit will have consolidated, and the effective stress will equal the difference between the total stress acting on the system and the hydrostatic water pressure – an equilibrium state in which no further volume change can occur. Terzaghi originally coupled deposit deformation to effective stress through a linearly elastic rheology, and restricted the theory to a state of infinitesimal strain. Subsequent sophisticated refinements of consolidation theory include coupling of strain to both sediment stress and fluid pressure, consideration of nonlinear and non-elastic sediment rheology, and accommodation of large. Self-weight consolidation of these types of slurries under low effective stresses can occur following sudden deposition by a debris flow, as demonstrated by the temporal response of fluid pressure at the base of several flume deposits.

3.2 ONE-DIMENSIONAL CONSOLIDATION THEORY

3.2.1 Theoretical Expression

Expressions for the diffusion of excess fluid pressure provide the basis for analysis of quasistatic consolidation (i.e. Terzaghi 1943; Gambolati 1973; Sills 1975; Lambe and Whitman 1969; Craig 1992). An expression for one-dimensional linear consolidation in terms of diffusion of excess fluid pressure p^*, is given by

$$\frac{\partial P_*}{\partial t} - D\frac{\partial^2 P_*}{\partial z^2} = 0 \quad (12)$$

Where the diffusion coefficient D is given by

$$D = kE_c/\mu \quad (13)$$

in which

- E_c is the constrained modulus, a measure of the bulk stiffness of a porous medium under confined uniaxial strain (reciprocal of compressibility);
- k is the hydraulic permeability of the porous medium;
- μ is the dynamic viscosity of the pore fluid.

Derivation of this expression can be found in many standard texts. Development of this linear diffusion equation is predicated on several key assumptions:

I. bulk compressibility of a sedimentary deposit is more important than the compressibility of water or sediment grains;
II. strain is uniaxial $\varepsilon_{zz} \neq \varepsilon_{yy} = \varepsilon_{xx} = 0$
III. strain is linearly related to vertical effective stress, $\varepsilon_{zz} = (\frac{1}{Ec})\sigma_{zz}$
IV. specific fluid discharge, q, is described by Darcy's law, which can be written in terms of excess fluid pressure as
V. $q = -\left(k/\mu\right)\left(\frac{\partial P_*}{\partial Z}\right)$
VI. solids are uniformly distributed throughout the deposit;
VII. total vertical stress is time invariant.

Assumptions *i–v* provide reasonable first-order approximations describing conditions in wide, thin deposits of saturated, poorly sorted sandy debris subject to low-magnitude stresses. Assumption *vi* reasonably describes the state of total vertical stress, as measured at the base of several debris-flow deposits. The diffusion equation (12) is applicable to both externally driven and gravity-driven consolidation. The primary difference between those two styles of consolidation rests in the state of stress and initial fluid pressure that develop following instantaneous loading.

3.2.2 Initial and Boundary Conditions

Appropriate initial and boundary conditions are needed to solve the equation (12). An initial fluid pressure can be approximated if we assume that loading is rapid relative to transient fluid flow. This assumption is appropriate for rapidly deposited slurries; fluid pressures in flume deposits remained elevated for a few seconds to several tens of minutes following. During instantaneously undrained loading, volume change is negligible. Thus, no vertical strain occurs and $\varepsilon_{zz} = 0$ at $t = 0$. As a result, the effective stress is initially negligible $\varepsilon_{zz} \propto \sigma'_{zz}$, the pore fluid bears the unit weight of the saturated debris, and $\sigma_{zz} = P_t$. Therefore, a rapidly deposited saturated slurry that is instantaneously undrained should be liquefied temporarily, and the total fluid pressure should approach the liquefaction pressure described by eqn (11). Fluid pressures of this magnitude have been measured following deposition of experimental debris flows. The non- hydrostatic component of that liquefaction pressure, described by eqn (12), establishes the initial condition fluid pressure. The boundary conditions considered are simple: fluid is allowed to drain freely across the upper boundary, thus $P^* = 0$ at $z = H$; no fluid flow is permitted across the basal boundary (Figure 4.1.a) so, $\partial P^*/\partial z = 0$ at $z = 0$.

3.2.3 Analytic Solution

Subject to the appropriate boundary and initial conditions described, the transient excess-fluid-pressure field for a no-flux basal boundary condition is given by Carslaw and Jaeger:

$$P_* = 8P_{*0} \sum_{n=0}^{\infty} \frac{1}{(2n+1)^2\pi^2} \cos(\lambda_n z)\, e^{-\lambda_n^2 Dt} \quad (14)$$

where

- P_{*0} represents the initial excess pore-fluid pressure at $z = 0$ (cf. eqn 11),
- λ_n are eigenvalues, $\lambda_n = \frac{(2n+1)\pi}{2H}$.

3.2.4 Plasticity – the Coulomb Failure Rule

One of the principal empiricisms in soil mechanics that is used widely in geomorphology relates the mean shearing stress acting on a potential failure surface in a soil mass to soil cohesion, normal stress, and the angle of internal friction. This empiricism, commonly referred to as Coulomb's law or Coulomb's failure rule, is generally written as

$$\tau = C + \sigma' \tan\varphi \quad (15)$$

where τ is the mean shearing stress, C the apparent material cohesion (non-frictional component of the soil strength), σ' the effective normal stress (negative in compression) acting on the potential failure surface, and φ characterizes the friction among soil particles and is called the angle of internal friction of the soil. Apparent soil cohesion depends on electrostatic forces that act between clay particles, on cementation of soil particles owing to secondary mineralization, on surface tension in water films

between particles, and on the strength of roots that infiltrate soil. The dominant control on soil (and rock) strength, however, is frictional resistance between particles and the interlocking among particles and the product σ' tanφ determines the frictional component of shear strength. In general, apparent cohesion of soils is small and not an important contributor to soil strength except in very clay-rich soils, in near-surface soil pervasively penetrated by roots or in soils where effective stresses are low. The effect of pore-water pressure on the shearing strength of soil becomes explicit by substituting the expression for effective stress eqn (5) into eqn (15), which gives

$$\tau = C + (\sigma + p)\tan\varphi \quad (16)$$

This deceptively simple expression is commonly used to assess the factors that govern slope failure. However, this expression is incomplete in that it does not account for the stress and pore-pressure fields that determine the mean shear stress, the effective stress and the pore-fluid pressure acting on a potential failure surface. The magnitude and spatial distribution of pore-fluid pressure (which is related to the distribution of hydraulic head) and the spatial distribution of solid-grain stress determines the Coulomb failure potential of a soil. (Major, Stress, Deformation, Conservation, and Rheology: A Survey of Key Concepts in Continuum Mechanics, 2013) (Swan)

3.3 GRAIN SIZE DISTRIBUTION

Grain size is the most fundamental property of sediment particles, affecting their entrainment, transport and deposition. Grain size analysis therefore provides important clues to the sediment provenance, transport history and depositional conditions (e.g. Folk and Ward, 1957; Friedman, 1979; Bui et al., 1990). The various techniques employed in grain size determination include direct measurement, dry and wet sieving, sedimentation and measurement by laser granulometer, X-ray sedigraph and Coulter counter. These methods describe widely different aspects of 'size', including sieve diameter and equivalent spherical diameter, and are to a greater or lesser extent influenced by variations in grain shape, density and optical properties. All techniques involve the division of the sediment sample into a number of size fractions, enabling a grain size distribution to be constructed from the weight or volume percentage of sediment in each size fraction.

Since a given soil is often made up of grains of many different dimension, sizes are measured in terms of grain-size distribution (GSD), that can be of value in providing initial rough estimates of a soil's engineering properties such as permeability, strength, expansivity, etc. A subject of active research interest today is the accurate prediction of soil properties based largely on GSDs, void ratios, and soil particle characteristics. Now, though, such research has not yet produced results that are usable in standard engineering practice. When measuring GSDs for soils, two methods are generally used:

- For grains larger than 0.063mm sieving is used;
- For grains in the range of .063mm > D > 0.5μm, the hydrometer test is used.

Procedure for Sieve Testing of Soils:

- Pour oven–dried soil of mass M_o into the top sieve of the stack;
- Shake and agitate the stack of sieves until all soil grains are retained on the finest sized sieve through which they can possibly pass;
- Weigh the mass of soil M_i retained on each sieve.

- For each sieve size used, compute N_i, the percentage by mass of the soil sample that is finer than *i*-th sieve size. For example:

$$N_i = \left({}^{1}/_{M_0}\right)\sum_{j=1+1}^{n} M_j * 100\% = \left(1 - \sum_{j=1}^{i} {}^{M_j}\Big/_{M_0}\right) * 100\% \quad (17)$$

- Plotting N_i versus D_i for $i = 1, 2, \ldots, n$ on special five–cycle semi–logarithmic GSD paper gives the following types of curves:

When GSDs are plotted on standard semi–log paper, they look different since the grain size will increase from left to right.

The Hydrometer Test is generally adopted for fine–grained soils (0.5mm < D < 75 mm). It is assumed, as a first approximation, that fine–grained soil particles can be idealized as small spheres. According to Stokes Law, the viscous drag force F_D on a spherical body moving through a laminar fluid at a steady velocity *v* is given by:

$$F_D = 3\pi\mu v D \quad (18)$$

where:

- *m* is the viscosity of the fluid (Pa·s)

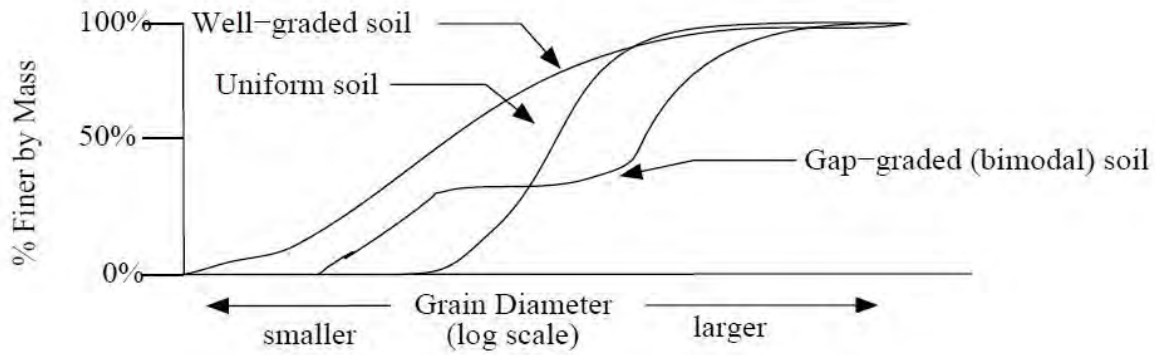

Figure 3.3.a Different kind of GSD for soils

- *v* is the steady velocity of the body (m/s)
- *D* is the diameter of the sphere (m)

If we drop a grain of soil into a viscous fluid, it eventually achieves a terminal velocity v where there is a balance of forces between viscous drag forces, gravity weight forces, and buoyant forces, as shown below:

$$F_g - F_b = (1/6) * (G_s - 1) * \gamma_w \pi D^3 \quad (19)$$

where:

- G_s is the specific gravity of the soil grain
- γ_w is the unit weight of water (kN/m^3)

For equilibrium of the soil grain: $F_D = F_g - F_b$. From this equation, we solve for the equilibrium or terminal velocity v of the soil grain as :

$$v = \frac{(G_s - 1)\gamma_w D^2}{18\mu} \quad (20)$$

Observe: $v \propto D^2$

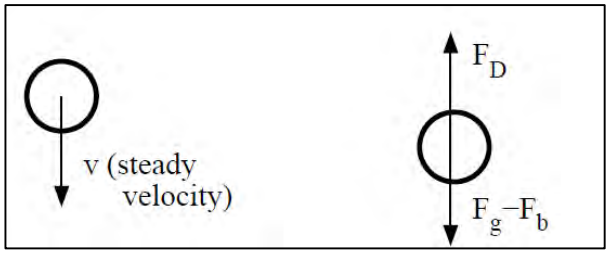

Figure 3.3.b

Thus, the larger a soil grain is, the faster it settles in water. This critical fact is used in the hydrometer testing to obtain GSDs for fine-grained soil. Engineers frequently like to use a variety of coefficients to describe the uniformity versus the well-graduation of soils. Although particle shape and angularity definitely affect the macroscopic behavior of soils, they are very difficult to quantify. Hence, these measures are not used in practice nearly as often as grain-size distributions and related grading coefficients. GSD measurements, which can be performed quickly and inexpensively, tell us whether a given soil is predominantly sandy, silty, or clayey. This simple information is often of great help in trying to anticipate a soil's possible mechanical properties. Some commonly used measures are: the Uniformity Coefficient: $C_u = D_{60}/D_{10}$ (soils with $Cu \leq 4$ are considered to be "poorly graded" or uniform); the Coefficient of Gradation: $C_c = (D_{30})^2/(D_{60} * D_{10})$ (For well-graded soils, $Cc \sim 1$); the Sorting Coefficient: $S_o = (D_{75}/D_{25})^{1/2}$ (this measure tends to be used more by geologists than engineers. The larger S_o, the more well-graded the soil); the "effective size" of the soil: D_{10} (empirically, D_{10} has been strongly correlated with the permeability of fine-grained sandy soils) (Swan).

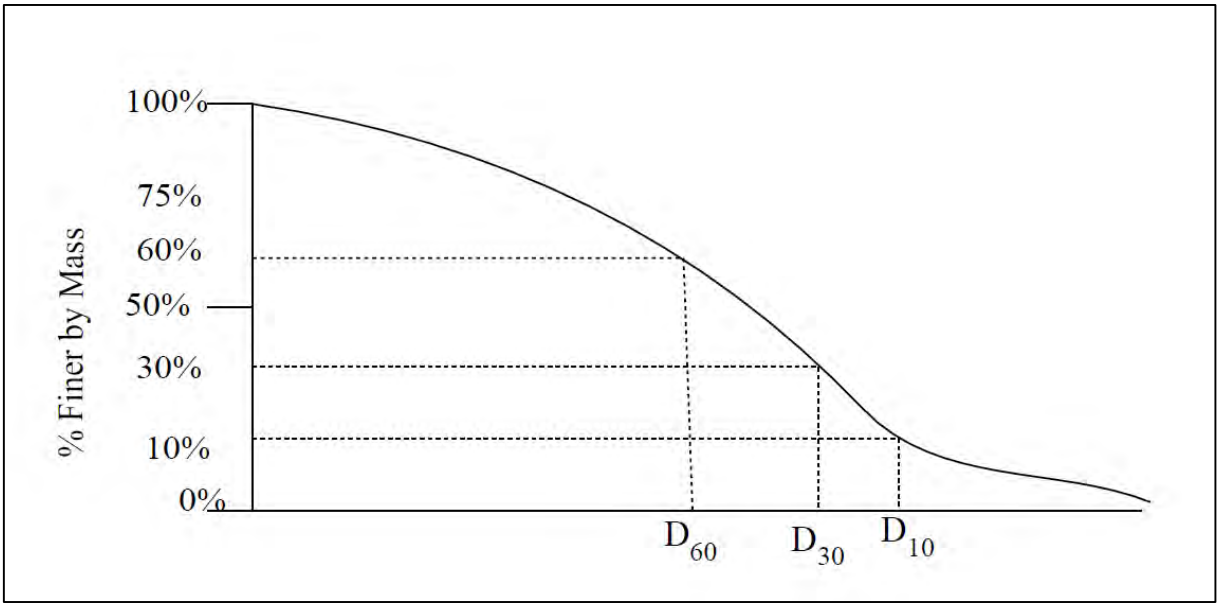

Figure 3.3.c GSD quick measures for soil classification

4 METHODS

4.1 EQUIPMENTS

The tests have been carried out using a plexiglass cylinder equipped with pressure sensors. The cylinder is 60 cm deep, with an internal diameter of 18 cm. For 12,5 l of volume it takes 45 cm filling height. Five pressure sensors are placed in it to measure the pore water pressure decay: one at the bottom, and four on the sides, paired two by two at the height of 20 cm and 35 cm from the bottom. Two side sensors have an oil-filled cell adapter. Pressure measurements with a frequency of 50 Hz will be recorded by using the CatmanEasy © software (in German). The following data analysis have been performed by using Matlab ©.

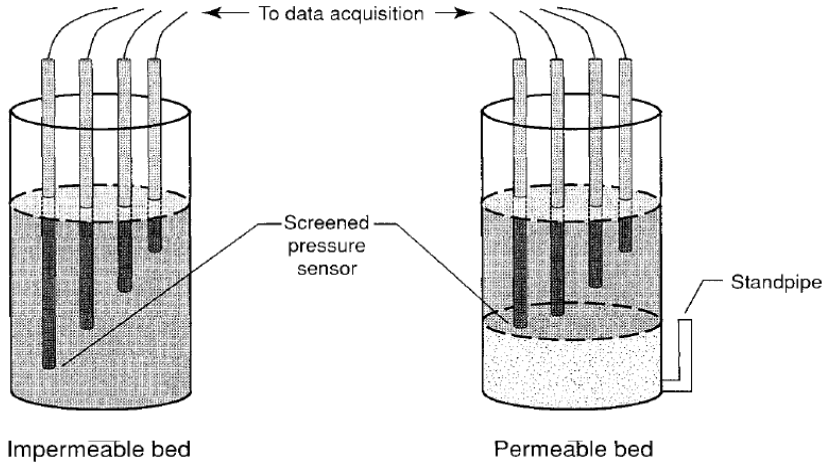

Figure 4.1.a Sketch of the cylinder test used by Major

4.2 TESTS PLAN

In order to have a wide range of different cases to test, I chose to focus both on fines and coarse grained particles. I took a big amount from the initial sample, mix it accurately to obtain a homogeneous sample and then I sifted it to split the coarse-grained particles (size > 1 mm) and the fine-grained particles (size 1 < mm). I decided this sieve dimension to assign the fine and coarse particles because sensors have a protection grid of 1 mm link, so particles smaller than 1 mm are not stopped by the grid and it is possible to think them as part of fluid. Afterwards, I sifted the coarse-grained particles in order to build up the coarse-grained size distribution curve. Keeping the D50 as much as possible constant, I changed the C_U (this means I will change the curve steepness) without modifying the total volume of the testing mixture. The need of keeping the total volume constant produces a series of issues as described below:

- For a fixed fine particles weight, changes in the coarse C_U produce a different coarse particles volume (simple packing problem). I decided to solve it by measuring, at the onset of the experiments, the bulk specific weight of the natural coarse particles γ_s. Assuming an initial ratio between $\gamma_s / \gamma_w = 5$, I could roughly estimate the amount of material I need for each test. This amount needed to be correct to take into account the porosity *n* of the coarse particles and the fine particles.
- Varying the weight of the fine particles, I used more water than the "natural" case to fill the cylinder to reach the designed volume. So, it was not possible to define in advance the fluid C_v

and C_{Vtot} values: I back-calculated them since I will know the water the fines particles and coarse particles weights.

I will test four different fine-grained particles amounts (0.5 F, 0.75 F, 1F, 1.25 F) and for each of them I will test four different coarse composition (C1, C2, C3, C4). In the end, I tested 16 mixtures of Scalärarüfe and 16 of Lorenzerbach debris flow. About the fine particles, since I have clay and silt, I provided some test at the *Institut für Angewandte Geologie* to know more about the mineralogy and composition of the sample. The following table represents the complete chart of what I tested: T1 to T16 are the codes for the tests, while C1 to C4 are the codes for the coarse composition. The fine-graded particles composition are shown as F0,5 to F1,25, that means I started with the "natural" fine content (F1,00) and gradually changed the composition with a 25% gap of weight. C1 is the original composition of the coarse particles in the samples, as found in the grain size distribution. C2 is a modified coarse composition tending to reduce the biggest size part and adding it to a smaller fraction. In C3 I removed completely the smallest coarse fraction (#1) and added the same amount in weight to the mean (D50) fraction. C4 for Scalärarüfe remove the #1 and #2 fractions and adds the amount in weight to mean fraction, whereas for Lorenzerbach C4 removes #16 fraction and split the amount in weight among fraction#1 and #2. So, the expected indications after this choice are similar for the Scalärarüfe and Lorenzerbach sample up to C3: D coefficient smaller than C1 for C2, bigger for C3, while it should be bigger for C4 of Scalärarüfe and smaller for C4 of Lorenzerbach.

TABLE OF EXPERIMENTS						
FINE / COARSE		0,5	0,75	1	1,25	codes key
Scalärarüfe	C1	T1	T2	T3	T4	Original granulometry distribution, no changes
	C2	T5	T6	T7	T8	-50% in weight of fraction #16, added in weight to fraction #1
	C3	T9	T10	T11	T12	no fraction #1, added in weight to fraction #8
	C4	T13	T14	T15	T16	no fraction #1 and #2, added in weight to fraction #8
Lorenzerbach	C1	T17	T18	T19	T20	Original granulometry distribution, no changes
	C2	T21	T22	T23	T24	no fraction #16, added in weight to fraction #4
	C3	T25	T26	T27	T28	no fraction #1, added in weight to fraction #4
	C4	T29	T30	T31	T32	no fraction #16, added 50% in weight to fraction #1 and 50% in weight to #2

Table 4.2.1 Tests table

4.3 SCALÄRARÜFE SAMPLE PARAMETERS

4.3.1 Grain size distribution

The solid material was taken from a fresh deposit of a small debris flow, which occurred on May 3, 2001 in the Scalärarüfe near Chur in Eastern Switzerland. The geology of the area is dominated by formations of schist, a sediment susceptible to weathering. As a result, large volumes of loose sediment with a considerable amount of fine material are produced every year, which encourage the formation of

debris flows. 4 m^3 of an undisturbed frontal deposition tongue of the debris flow were excavated three days after deposition.

The excavated material was brought by lorry to a gravel-sorting factory where the material dried naturally during one month. Then a full grain size analysis of the 4 m^3 material was conducted requiring a total of six days: The grain size distribution of the fraction 0.063 ≤ d ≤ 100 mm was obtained through sieve analysis and the distribution of d ≤ 0.063 mm by the aerometer test (time of sedimentation within clear water for specific fine material fractions). Finally, the grain size distribution of the complete debris flow material was obtained by the superposition of the distributions of the two different analysis. The grain size distribution of the complete material is shown in Table 4.3.1. The material is characterized by a considerable content of fine material: particles smaller than 0.04 mm represent 9 % of the total material. The particles of the block, stone and gravel fraction are dominantly flat and angular. With focus on the sand, silt and clay fraction these general features remained similar, even though for the very small particles (d ≤ 0.25 mm) particle shape could not be assessed as precisely as for the very large particles. With reference to the solid density ρs, Steiger (1999) obtained ρs = 2.74 g/cm3 for the solid material of the catchment area by analyzing the particles smaller than 0.5 mm in the glass pyknometer. By contrast, measuring the weight and the volume of 30 stones (120 mm < d ≤ 150 mm) by immerging them in a water bath, a solid density ρs = 2.60 ± 0.62 g/cm3 was obtained. According to Steiger (2001) this discrepancy in the solid density ρs is due to the fact that, within the large and very large particles (mainly in the gravel, stone and block fraction), cavities of crevices and fissures exist which are not filled with water during the latter experiment (Schatzmann, 2005).

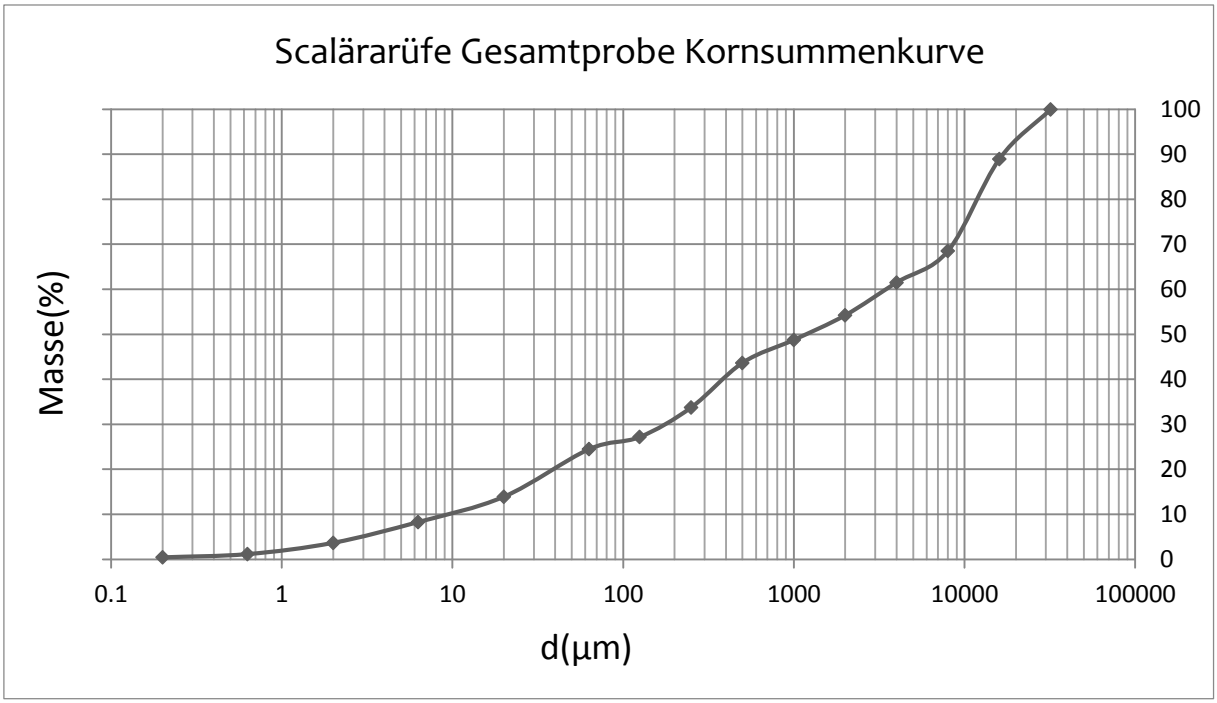

Table 4.3.1 Complete GSD for Scalärarüfe sample

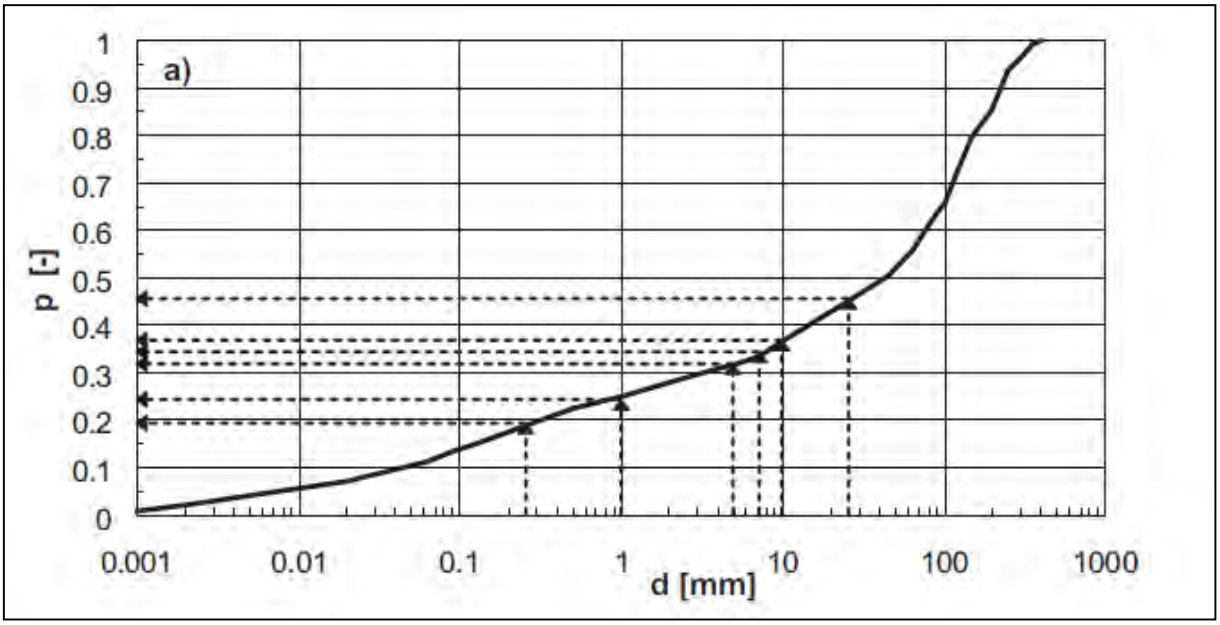

Figure 4.3.a Complete GSD for Scalärarüfe sample as found by Prof. Dr.-Ing. H.-E. Minor in Zurich analysis

Figure 4.3.b Scalalarufe sample after sieving

4.3.2 Mineralogy

In order to know the mineralogical composition of the different size parts of the starting sample, I carried out some test at *Institut für Angewandte Geologie* lab. From a 500 g amount of material, I did the following tests:

- Wet sifting (6300, 2000, 63, 20 µm) in order to split the gravel, the sand and the fine fraction;
- Sedigraphic analysis in order to recognize the percentage composition of the fine fraction;
- X-Rays analysis of gravel, sand and fine fraction in order to get the mineralogical composition of each size part;
- Scheibler test to confirm the X-Rays analysis by the measurement of the carbonate volume in a 50 g material's sample.

I obtained that, compared to the finer fraction, the coarser fraction has less chlorite content. The reduced amount of chlorite in the fine fraction is due to the weathering effects. Sand and gravel fraction show a very similar percentage composition, and small differences are probably due to statistics errors, so I consider them as a unique sample for the diagrams. The following composition of clay minerals was found: calcite (44 %), mica (11 %), Quarz (35 %), Chlorite (10 %). Based on the composition it can be concluded that the clays of the present debris flow material are hardly or not swelling at all. Due to the strong presence of mica the material exhibits lubricating effects when mixed with water (Kahr 2001). Consequently, thixotropic effects are not expected with the present debris flow material. There is a larger *Paragonite* (a sodium mica) peak in the fine fraction. Furthermore, it is possible to state that responsible for mass movement are mica and chlorite. It is not convenient to carry out a clay mineral analysis due to the very small content (just 4%) in total weight. The material is characterized by a considerable content of fine material: particles smaller than 0.04 mm represent 9 % of the total material. With focus on the sand, silt and clay fraction these general features remained similar. The obtained results are in good agreement with the results showed in (Schatzmann, 2005)

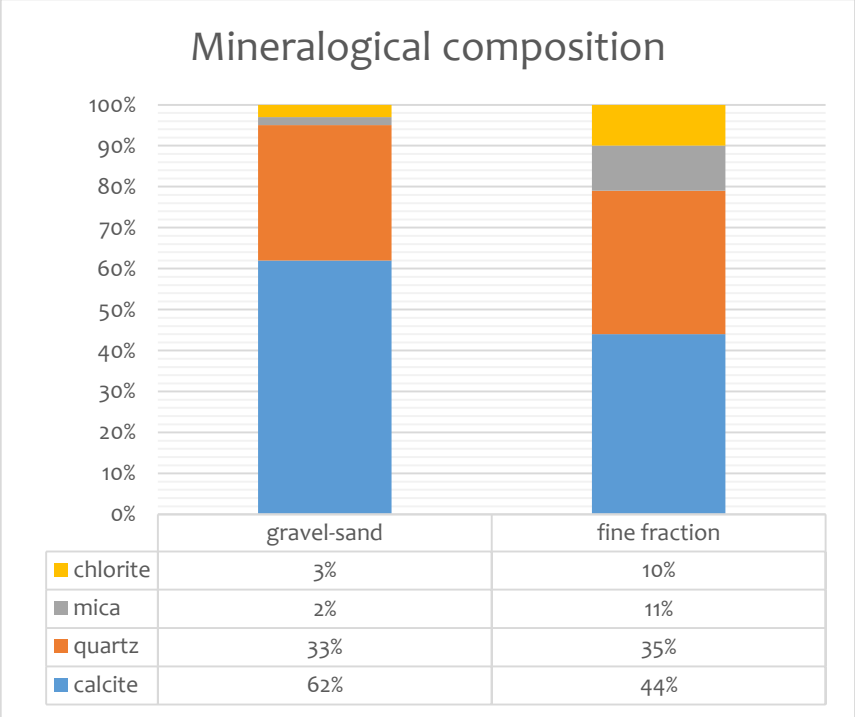

Figure 4.3.c

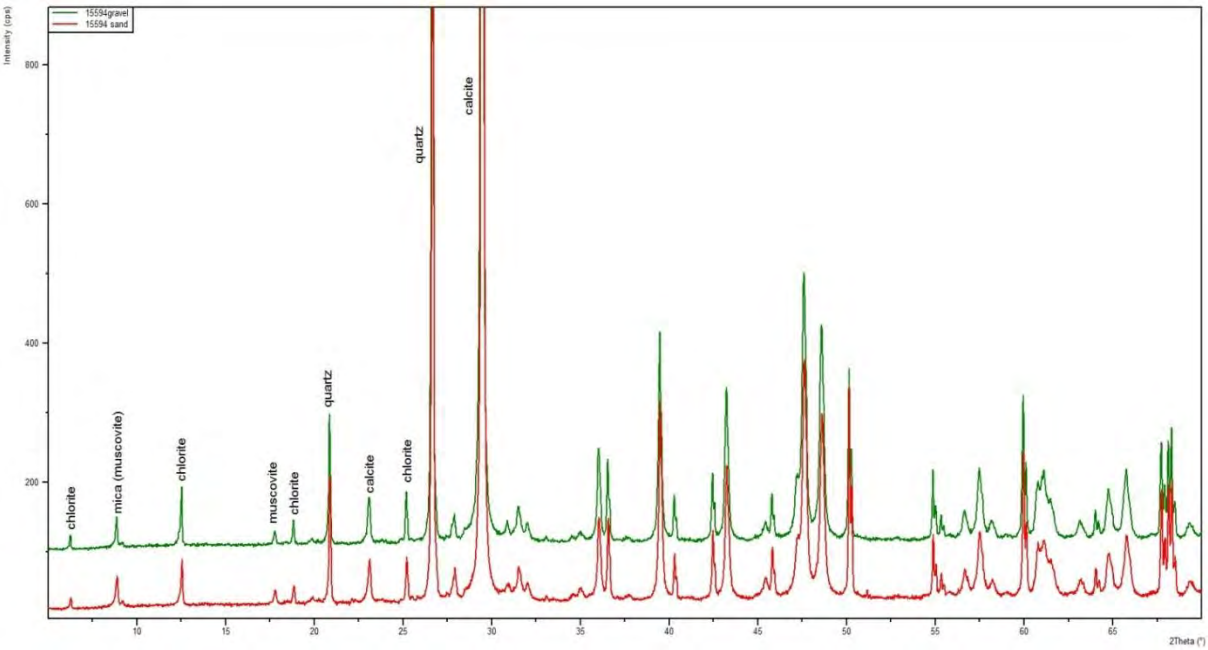

Figure 4.3.d X-ray analysis for the Scalalarufe sample.

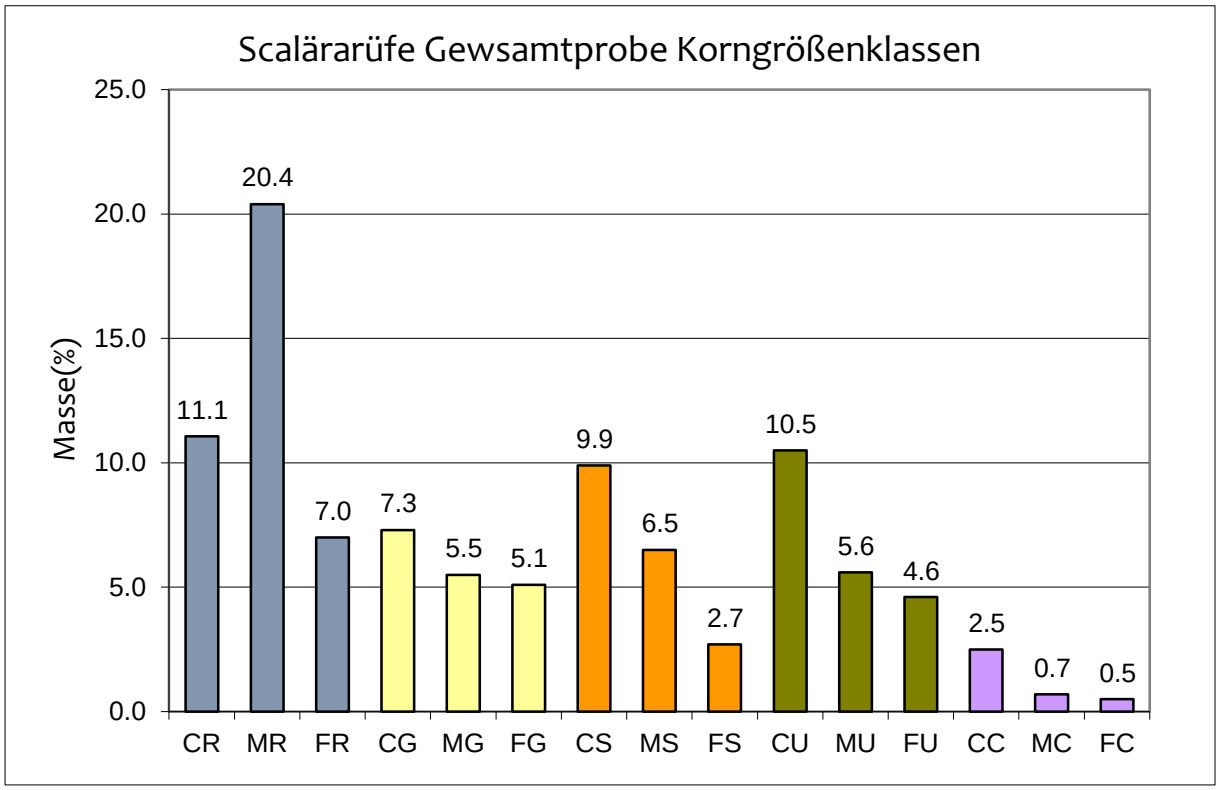

Figure 4.3.e Mineralogic composition in % for the different classes of size.

4.4 LORENZERBACH PARAMETERS

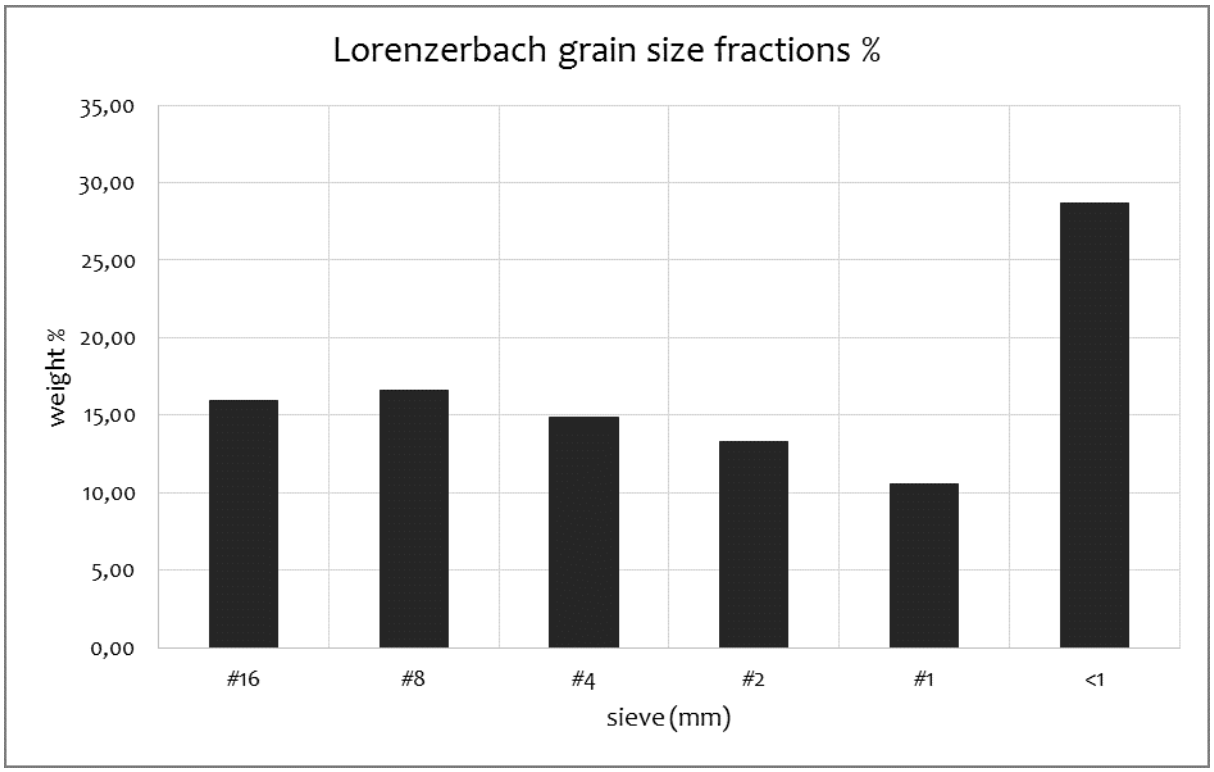

Figure 4.4.a

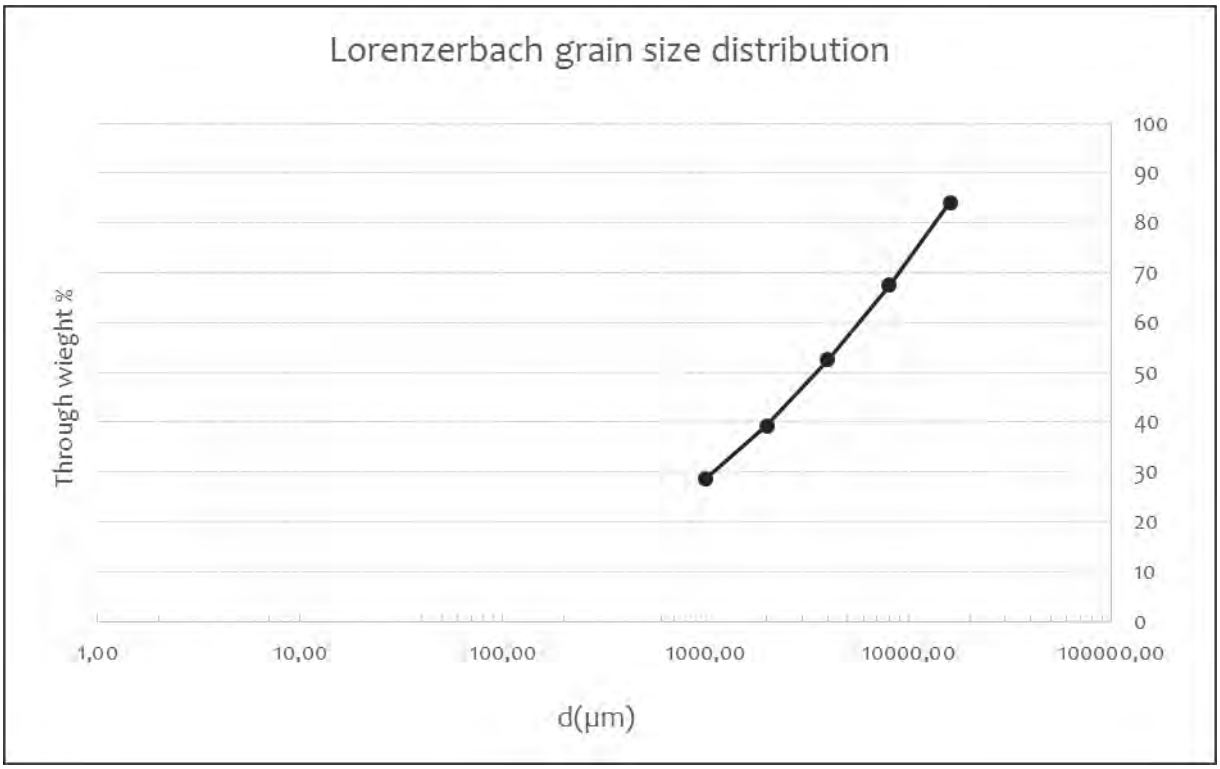

Figure 4.4.b Lorenzerbach coarse-grained particles distribution

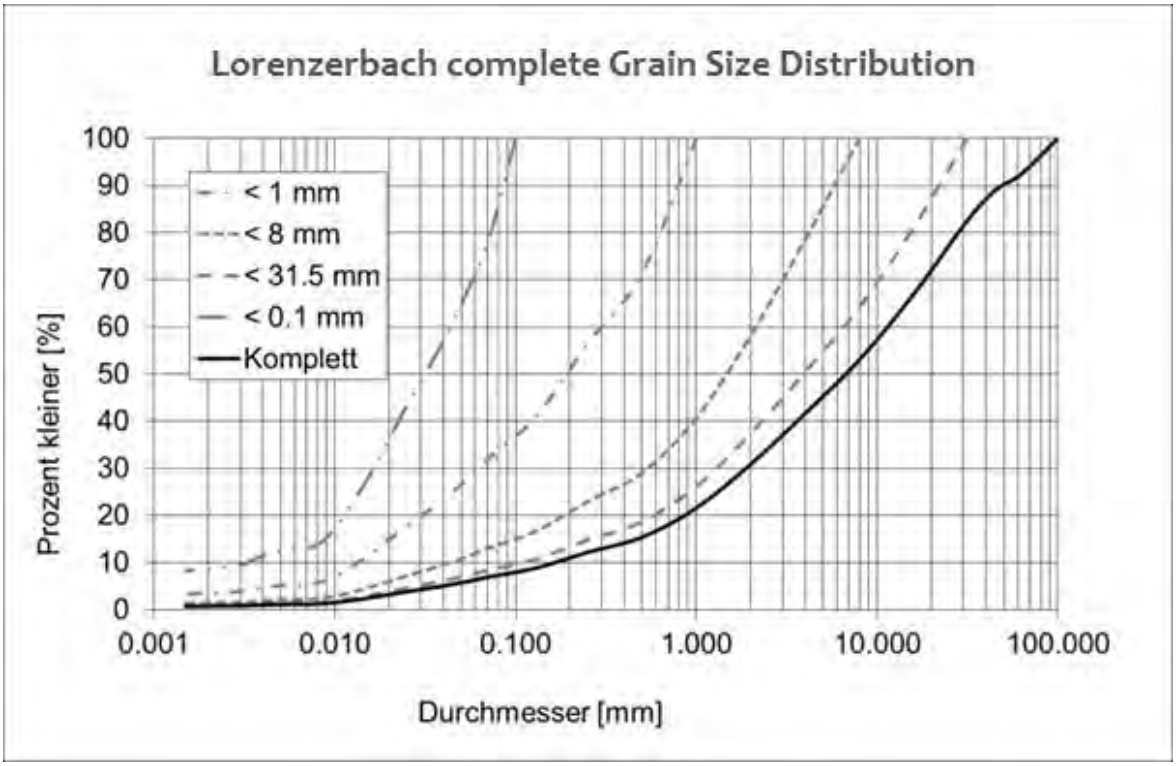

Figure 4.4.c

Figure 4.4.d Lorenzerbach sample after sieving.

4.5 SAMPLES AND TESTS PICTURES

The following pictures have been taken during the working time in the lab. First two images show the lab of Franz Schwackhöfer Haus, while Figure 4.3.2.c is about a Scalarufe sample test and Figure 4.3.2.d show a test on Lorenzerbach sample.

Figure 4.5.a

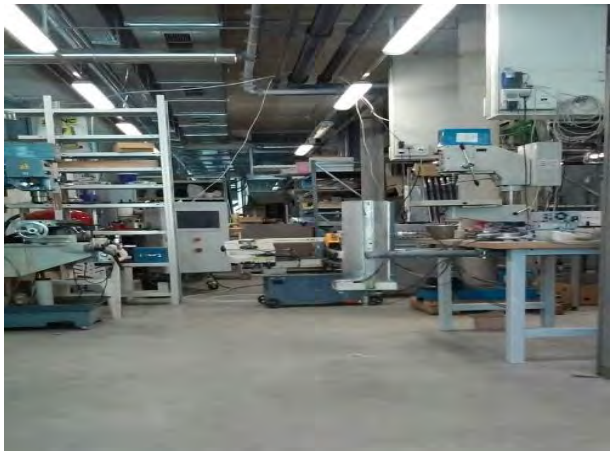

Figure 4.5.b

Figure 4.5.c

Figure 4.5.d

4.6 RELATIONS BETWEEN TOTAL MIXTURE AND MODIFIED MIXTURES

The following tables show the coarse compositions, including weights and volumes in liters for each test. Volume concentration of coarse-grained particles, fine-grained particles, total volume concentration, porosity and total and solid density (ρ_t, ρ_s) are indicated on the right part of each table. First 16 tables refer to Scalärarüfe samples, latter 16 to the Lorenzerbach one.

4.6.1 Scalärarüfe

	fraction	Vol [%]	Vol [l]	m [%]	m [kg]	Cv [-]	
SC_F0,50_C1	#16	0,12	1,53	16,4%	4,12	coarse	0,50
	#8	0,22	2,78	29,7%	7,48	fine	0,20
	#4	0,11	1,43	15,3%	3,85	total	0,60
	#2	0,02	0,26	2,7%	0,69	porosity	0,40
	#1	0,02	0,25	2,7%	0,68		
	<1	0,10	1,25	13,4%	3,37	density	[Kg/l]
	water	0,40	5,00	19,8%	5,00	ρ_t	2,02
	∑	100,0%	12,50	100,00%	25,19	ρ_s	2,69

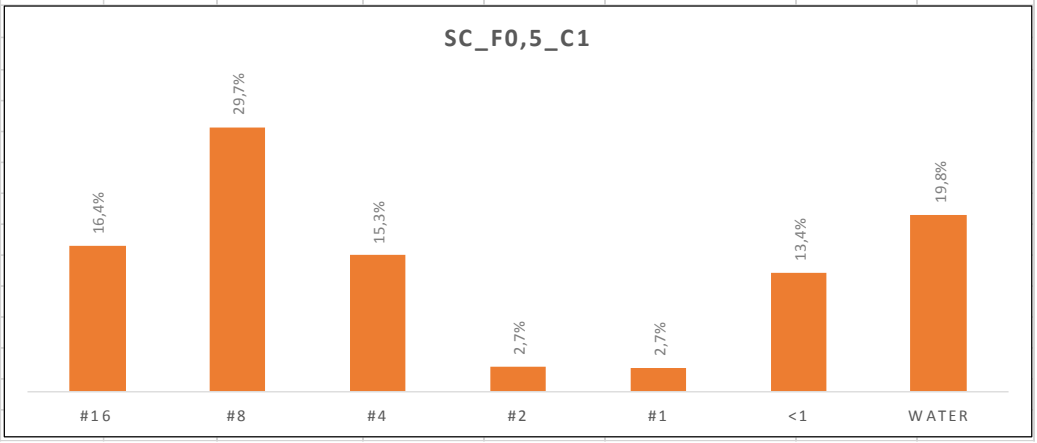

Table 4.6.1

	fraction	Vol [%]	Vol [l]	m [%]	m [kg]	Cv [-]	
SC_F0,75_C1	#16	0,13	1,56	15,8%	4,12	coarse	0,50
	#8	0,23	2,84	28,7%	7,48	fine	0,20
	#4	0,12	1,46	14,8%	3,85	total	0,66
	#2	0,02	0,26	2,6%	0,69	porosity	0,34
	#1	0,02	0,26	2,6%	0,68		
	<1	0,15	1,92	19,4%	5,06	density	[Kg/l]
	water	0,34	4,20	16,1%	4,20	ρ_t	2,09
	∑	100,0%	12,50	100,00%	26,08	ρ_s	2,64

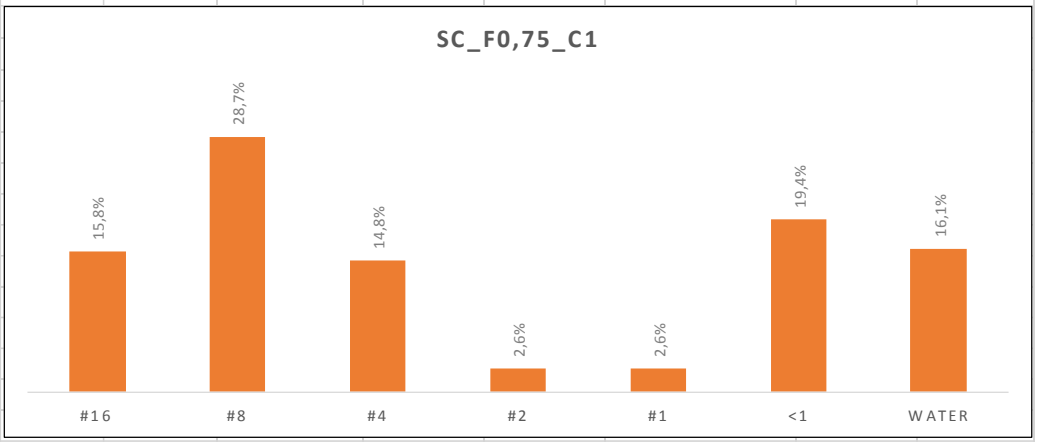

Table 4.6.2

	fraction	Vol [%]	Vol [l]	m [%]	m [kg]	Cv [-]	
SC_F1,00_C1	#16	0,12	1,49	14,9%	4,12	coarse	0,50
	#8	0,22	2,70	27,1%	7,48	fine	0,20
	#4	0,11	1,39	14,0%	3,85	total	0,68
	#2	0,02	0,25	2,5%	0,69	porosity	0,32
	#1	0,02	0,25	2,5%	0,68		
	<1	0,19	2,43	24,5%	6,74	density	[Kg/l]
	water	0,32	4,00	14,5%	4,00	ρ_t	2,20
	∑	100,0%	12,50	100,00%	27,56	ρ_s	2,77

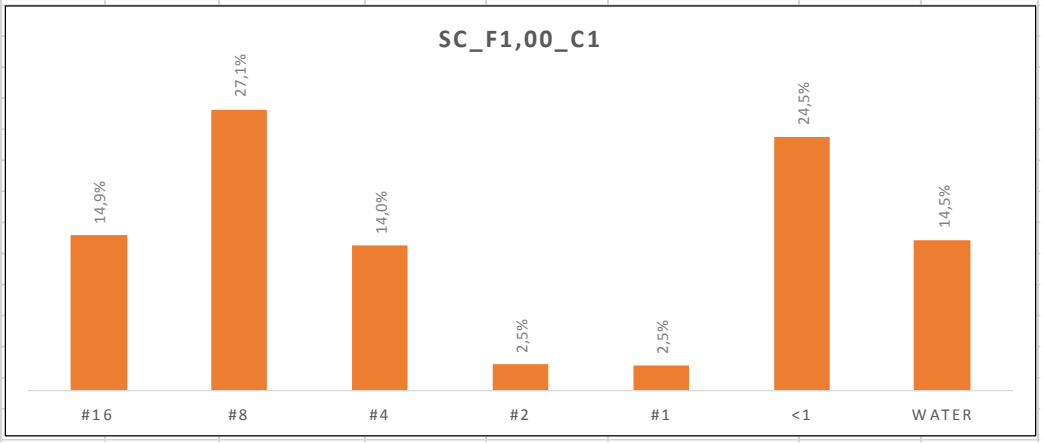

Table 4.6.3

	fraction	Vol [%]	Vol [l]	m [%]	m [kg]	Cv [-]	
SC_F1,25_C1	#16	0,12	1,47	14,3%	4,12	coarse	0,50
	#8	0,21	2,67	26,0%	7,48	fine	0,20
	#4	0,11	1,37	13,4%	3,85	total	0,72
	#2	0,02	0,25	2,4%	0,69	porosity	0,28
	#1	0,02	0,24	2,4%	0,68		
	<1	0,24	3,00	29,3%	8,43	density	[Kg/l]
	water	0,28	3,50	12,2%	3,50	ρ_t	2,30
	∑	100,0%	12,50	100,00%	28,75	ρ_s	2,81

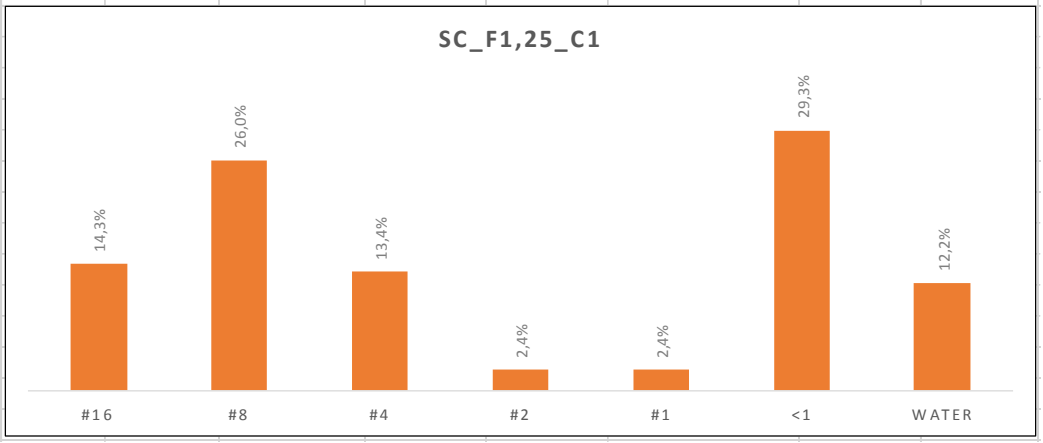

Table 4.6.4

	fraction	Vol [%]	Vol [l]	m [%]	m [kg]	Cv [-]	
SC_F0,50_C2	#16	0,06	0,77	8,2%	2,06	coarse	0,50
	#8	0,22	2,79	29,8%	7,48	fine	0,20
	#4	0,11	1,43	15,3%	3,85	total	0,60
	#2	0,02	0,26	2,7%	0,69	porosity	0,40
	#1	0,08	1,00	10,7%	2,68		
	<1	0,10	1,26	13,4%	3,37	density	[Kg/l]
	water	0,40	5,00	19,9%	5,00	ρ_t	2,01
	∑	100,0%	12,50	100,00%	25,13	ρ_s	2,68

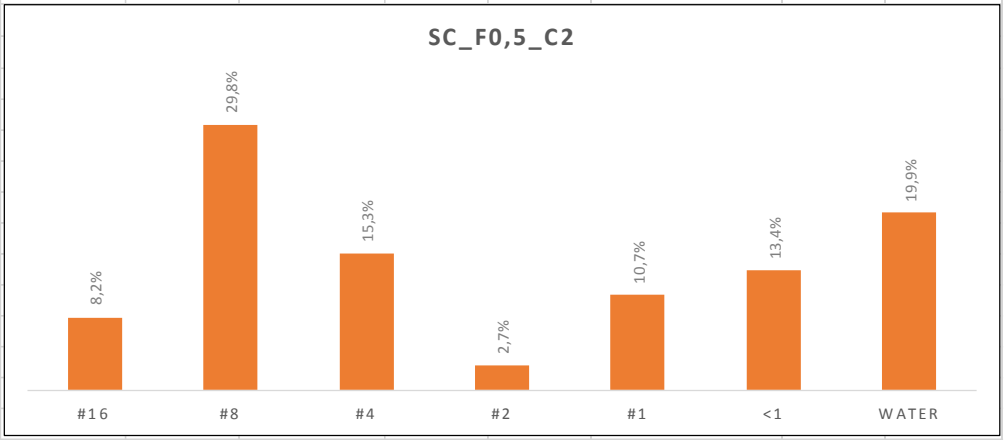

Table 4.6.5

	fraction	Vol [%]	Vol [l]	m [%]	m [kg]	Cv [-]	
SC_F0,75_C2	#16	0,06	0,78	7,9%	2,06	coarse	0,50
	#8	0,23	2,85	28,7%	7,48	fine	0,20
	#4	0,12	1,46	14,8%	3,85	total	0,66
	#2	0,02	0,26	2,7%	0,69	porosity	0,34
	#1	0,08	1,02	10,3%	2,68		
	<1	0,15	1,92	19,4%	5,06	density	[Kg/l]
	water	0,34	4,20	16,1%	4,20	ρ_t	2,08
	∑	100,0%	12,50	100,00%	26,02	ρ_s	2,63

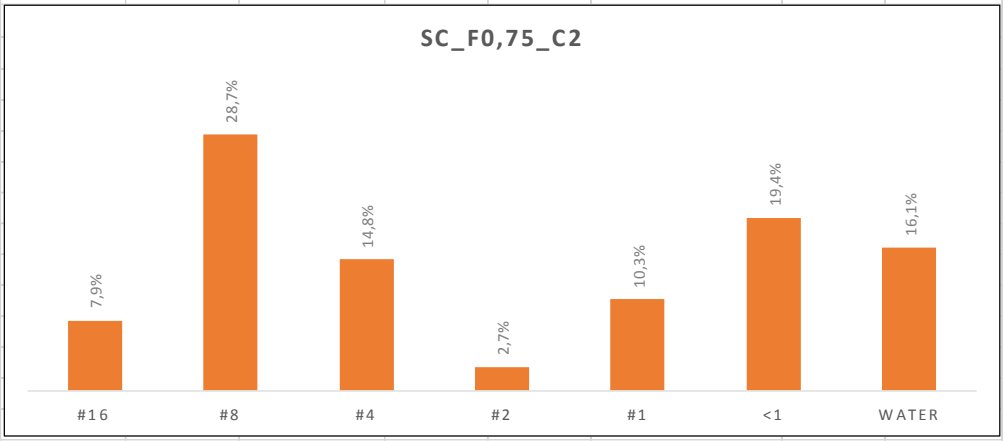

Table 4.6.6

	fraction	Vol [%]	Vol [l]	m [%]	m [kg]	Cv [-]	
SC_F1,00_C2	#16	0,06	0,75	7,5%	2,06	coarse	0,50
	#8	0,22	2,71	27,2%	7,48	fine	0,20
	#4	0,11	1,39	14,0%	3,85	total	0,68
	#2	0,02	0,25	2,5%	0,69	porosity	0,32
	#1	0,08	0,97	9,7%	2,68		
	<1	0,20	2,44	24,5%	6,74	density	[Kg/l]
	water	0,32	4,00	14,5%	4,00	ρ_t	2,20
	∑	100,0%	12,50	100,00%	27,50	ρ_s	2,76

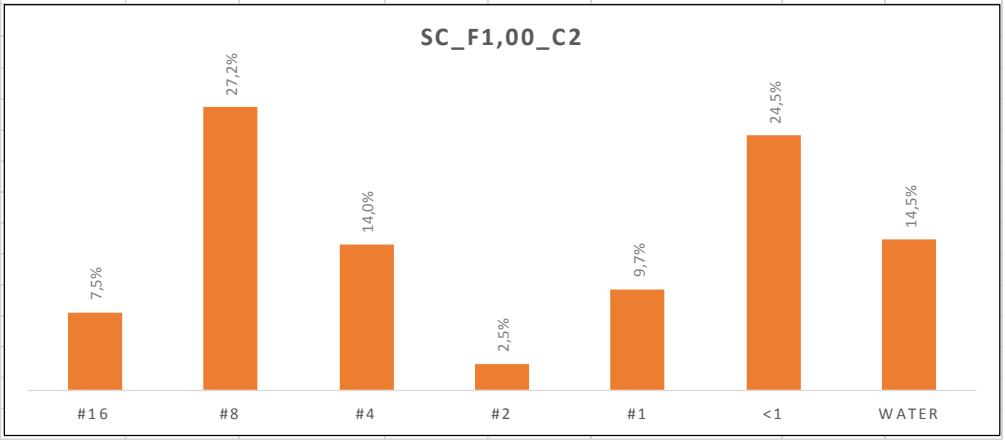

Table 4.6.7

	fraction	Vol [%]	Vol [l]	m [%]	m [kg]	Cv [-]	
SC_F1,25_C2	#16	0,06	0,74	7,2%	2,06	coarse	0,50
	#8	0,21	2,67	26,1%	7,48	fine	0,20
	#4	0,11	1,38	13,4%	3,85	total	0,72
	#2	0,02	0,25	2,4%	0,69	porosity	0,28
	#1	0,08	0,96	9,3%	2,68		
	<1	0,24	3,01	29,4%	8,43	density	[Kg/l]
	water	0,28	3,50	12,2%	3,50	ρ_t	2,30
	∑	100,0%	12,50	100,00%	28,69	ρ_s	2,80

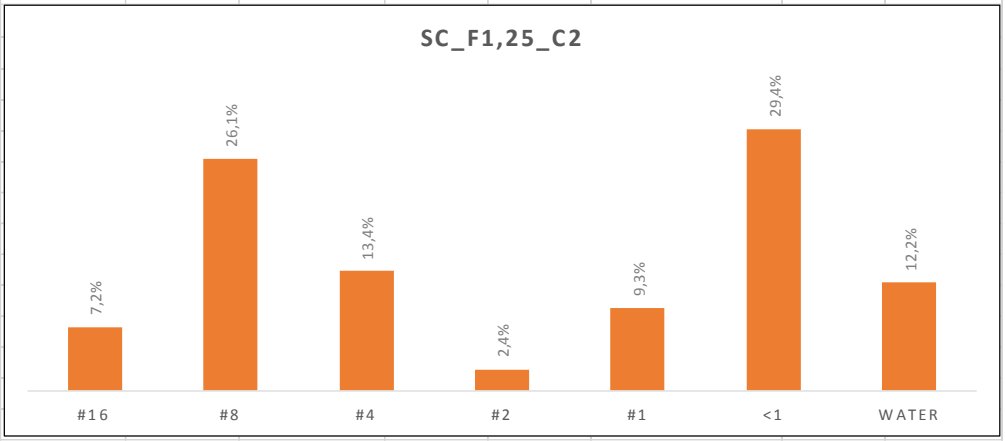

Table 4.6.8

	fraction	Vol [%]	Vol [l]	m [%]	m [kg]	Cv [-]	
SC_F0,50_C3	#16	0,12	1,51	16,2%	4,12	coarse	0,50
	#8	0,23	2,85	30,6%	7,80	fine	0,20
	#4	0,13	1,66	17,8%	4,53	total	0,60
	#2	0,02	0,25	2,7%	0,69	porosity	0,40
	#1	0,00	0,00	0,0%	0,00		
	<1	0,10	1,23	13,2%	3,37	density	[Kg/l]
	water	0,40	5,00	19,6%	5,00	ρ_t	2,04
	∑	100,0%	12,50	100,00%	25,51	ρ_s	2,73

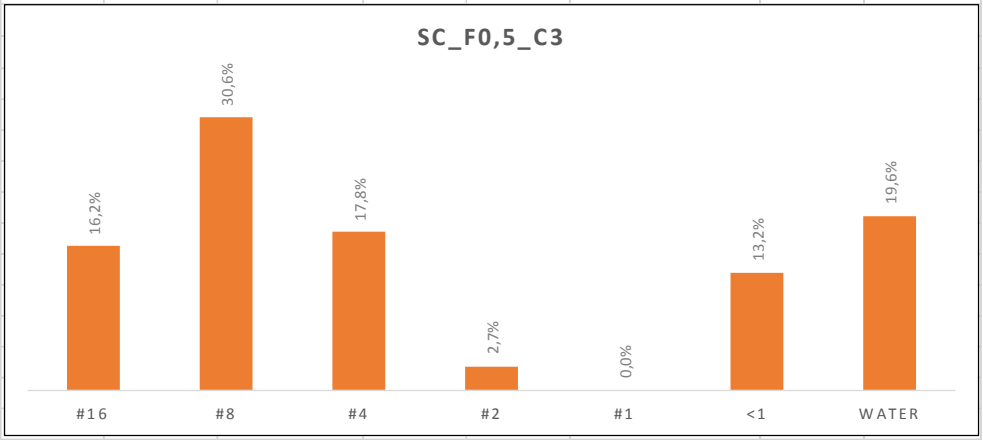

Table 4.6.9

	fraction	Vol [%]	Vol [l]	m [%]	m [kg]	Cv [-]	
SC_F0,75_C3	#16	0,12	1,54	15,6%	4,12	coarse	0,50
	#8	0,23	2,92	29,5%	7,80	fine	0,20
	#4	0,14	1,69	17,2%	4,53	total	0,66
	#2	0,02	0,26	2,6%	0,69	porosity	0,34
	#1	0,00	0,00	0,0%	0,00		
	<1	0,15	1,89	19,2%	5,06	density	[Kg/l]
	water	0,34	4,20	15,9%	4,20	ρ_t	2,11
	∑	100,0%	12,50	100,00%	26,40	ρ_s	2,67

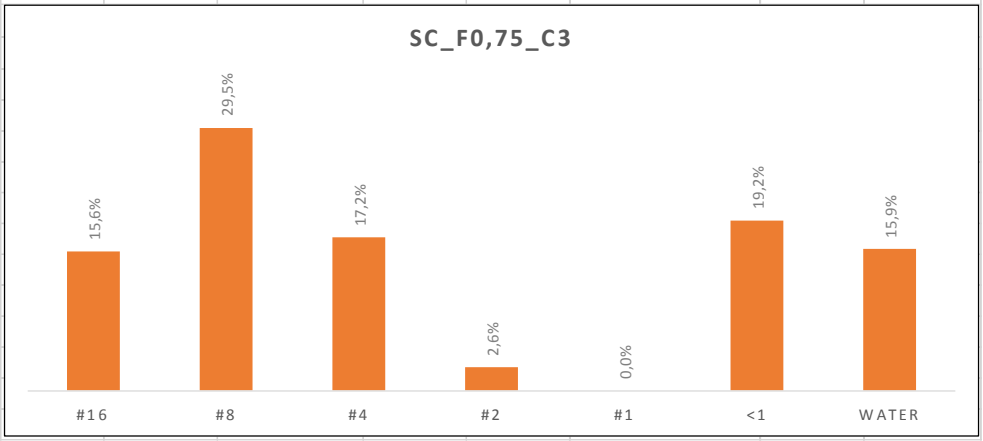

Table 4.6.10

	fraction	Vol [%]	Vol [l]	m [%]	m [kg]	Cv [-]	
SC_F1,00_C3	#16	0,12	1,47	14,8%	4,12	coarse	0,50
	#8	0,22	2,78	28,0%	7,80	fine	0,20
	#4	0,13	1,61	16,2%	4,53	total	0,68
	#2	0,02	0,25	2,5%	0,69	porosity	0,32
	#1	0,00	0,00	0,0%	0,00		
	<1	0,19	2,40	24,2%	6,74	density	[Kg/l]
	water	0,32	4,00	14,3%	4,00	ρ_t	2,23
	∑	100,0%	12,50	100,00%	27,88	ρ_s	2,81

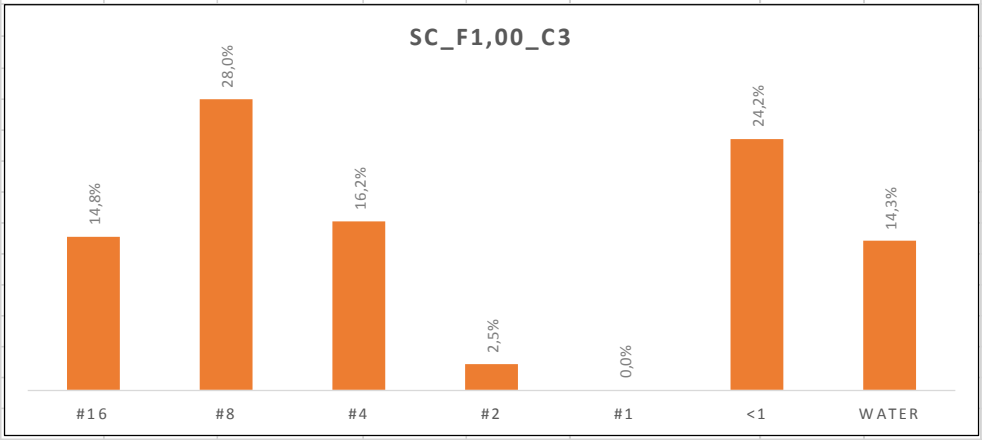

Table 4.6.11

	fraction	Vol [%]	Vol [l]	m [%]	m [kg]	Cv [-]	
SC_F1,25_C3	#16	0,12	1,45	14,2%	4,12	coarse	0,50
	#8	0,22	2,75	26,8%	7,80	fine	0,20
	#4	0,13	1,59	15,6%	4,53	total	0,72
	#2	0,02	0,24	2,4%	0,69	porosity	0,28
	#1	0,00	0,00	0,0%	0,00		
	<1	0,24	2,97	29,0%	8,43	density	[Kg/l]
	water	0,28	3,50	12,0%	3,50	ρ_t	2,33
	∑	100,0%	12,50	100,00%	29,07	ρ_s	2,84

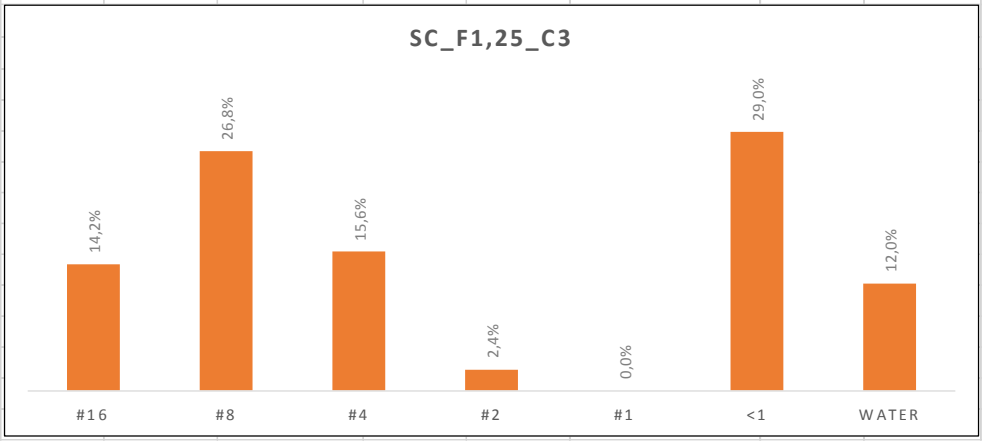

Table 4.6.12

	fraction	Vol [%]	Vol [l]	m [%]	m [kg]	Cv [-]	
SC_F0,50_C4	#16	0,12	1,53	16,4%	4,12	coarse	0,50
	#8	0,22	2,78	29,7%	7,48	fine	0,20
	#4	0,15	1,93	20,6%	5,19	total	0,60
	#2	0,00	0,00	0,0%	0,00	porosity	0,40
	#1	0,00	0,00	0,0%	0,00		
	<1	0,10	1,25	13,4%	3,37	density	[Kg/l]
	water	0,40	5,00	19,9%	5,00	ρ_t	2,01
	∑	100,0%	12,50	100,00%	25,16	ρ_s	2,69

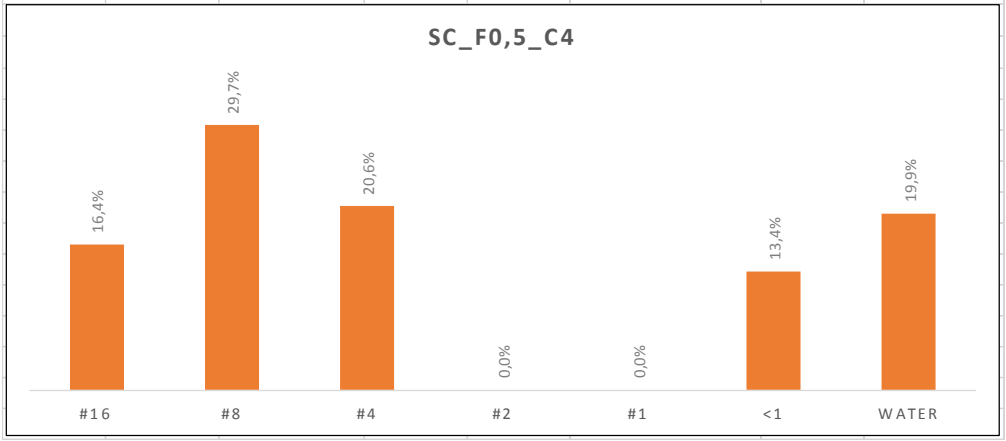

Table 4.6.13

	fraction	Vol [%]	Vol [l]	m [%]	m [kg]	Cv [-]	
SC_F0,75_C4	#16	0,13	1,57	15,8%	4,12	coarse	0,51
	#8	0,23	2,84	28,7%	7,48	fine	0,31
	#4	0,16	1,97	19,9%	5,19	total	0,66
	#2	0,00	0,00	0,0%	0,00	porosity	0,34
	#1	0,00	0,00	0,0%	0,00		
	<1	0,15	1,92	19,4%	5,06	density	[Kg/l]
	water	0,34	4,20	16,1%	4,20	ρ_t	2,08
	∑	100,0%	12,50	100,00%	26,05	ρ_s	2,63

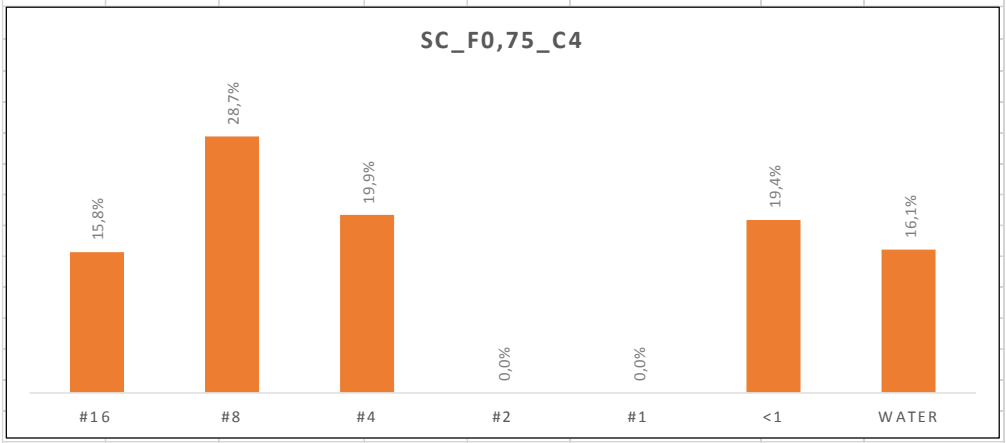

Table 4.6.14

	fraction	Vol [%]	Vol [l]	m [%]	m [kg]	Cv [-]	
SC_F1,00_C4	#16	0,12	1,49	15,0%	4,12	coarse	0,51
	#8	0,22	2,70	27,2%	7,48	fine	0,30
	#4	0,15	1,87	18,9%	5,19	total	0,68
	#2	0,00	0,00	0,0%	0,00	porosity	0,32
	#1	0,00	0,00	0,0%	0,00		
	<1	0,19	2,43	24,5%	6,74	density	[Kg/l]
	water	0,32	4,00	14,5%	4,00	ρ_t	2,20
	∑	100,0%	12,50	100,00%	27,53	ρ_s	2,77

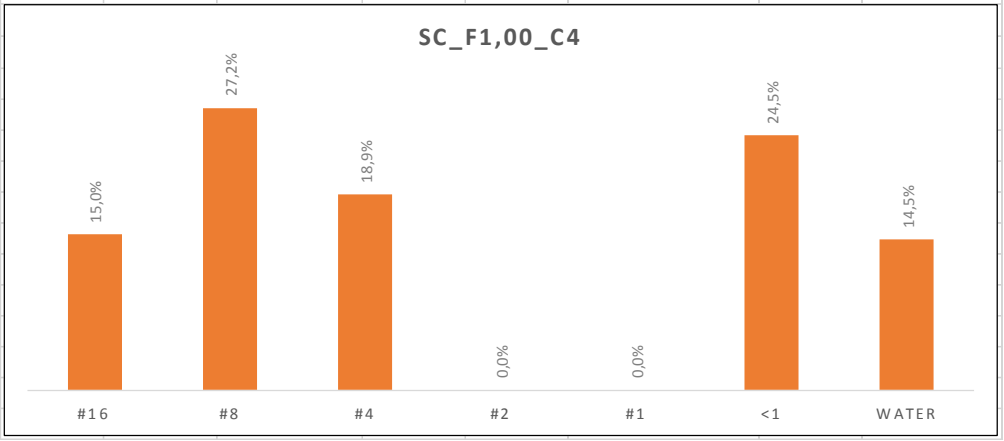

Table 4.6.15

	fraction	Vol [%]	Vol [l]	m [%]	m [kg]	Cv [-]	
SC_F1,25_C4	#16	0,12	1,47	14,3%	4,12	coarse	0,51
	#8	0,21	2,67	26,0%	7,48	fine	0,30
	#4	0,15	1,85	18,1%	5,19	total	0,72
	#2	0,00	0,00	0,0%	0,00	porosity	0,28
	#1	0,00	0,00	0,0%	0,00		
	<1	0,24	3,01	29,4%	8,43	density	[Kg/l]
	water	0,28	3,50	12,2%	3,50	ρ_t	2,30
	∑	100,0%	12,50	100,00%	28,72	ρ_s	2,80

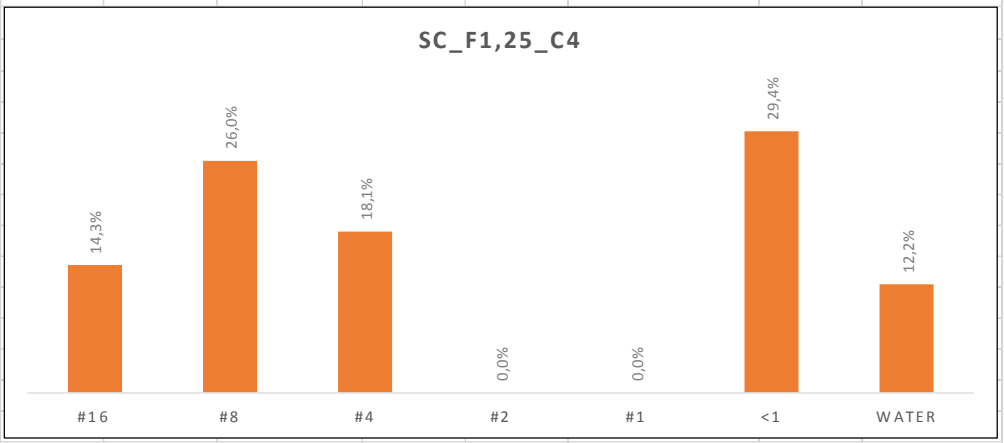

Table 4.6.16

4.6.2 Lorenzerbach

	fraction	Vol [%]	Vol [l]	m [%]	m [kg]	Cv [-]	
LB_F0,50_C1	#16	9,1%	1,14	13,3%	3,25	coarse	0,43
	#8	10,2%	1,27	14,8%	3,62	fine	0,16
	#4	9,1%	1,14	13,3%	3,25	total	0,52
	#2	8,2%	1,02	11,9%	2,91	porosity	0,48
	#1	6,5%	0,81	9,4%	2,30		
	<1	8,8%	1,11	12,8%	3,14	density	[Kg/l]
	water	48,0%	6,00	24,5%	6,00	ρ_t	1,96
	∑	100,0%	12,50	100,00%	24,47	ρ_s	2,84

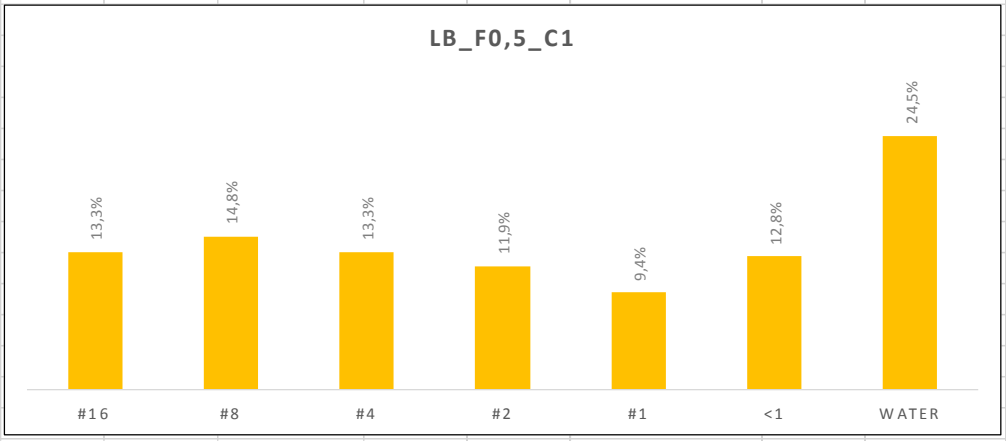

Table 4.6.17

	fraction	Vol [%]	Vol [l]	m [%]	m [kg]	Cv [-]	
LB_F0,75_C1	#16	9,3%	1,17	12,8%	3,25	coarse	0,43
	#8	10,4%	1,30	14,3%	3,62	fine	0,16
	#4	9,3%	1,17	12,8%	3,25	total	0,58
	#2	8,4%	1,05	11,5%	2,91	porosity	0,42
	#1	6,6%	0,83	9,1%	2,30		
	<1	13,5%	1,69	18,6%	4,71	density	[Kg/l]
	water	42,4%	5,30	20,9%	5,30	ρ_t	2,03
	∑	100,0%	12,50	100,00%	25,34	ρ_s	2,78

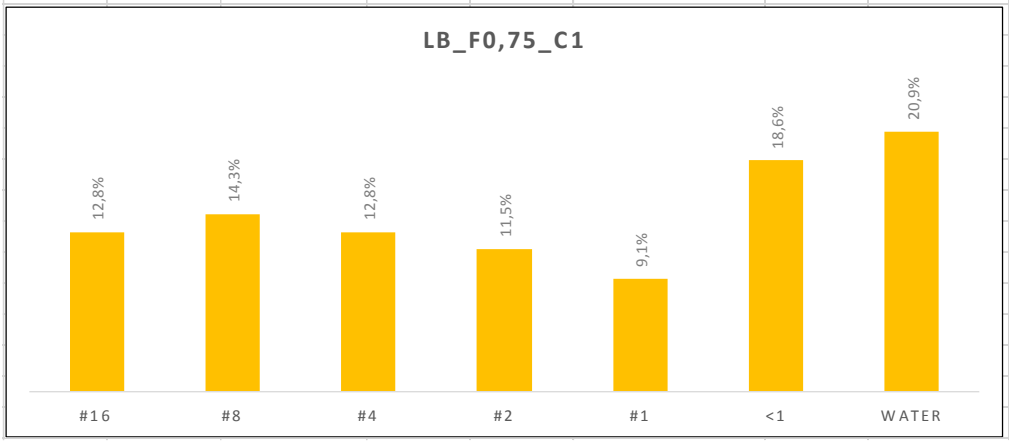

Table 4.6.18

	fraction	Vol [%]	Vol [l]	m [%]	m [kg]	Cv [-]	
LB_F1,00_C1	#16	9,5%	1,19	12,4%	3,25	coarse	0,43
	#8	10,6%	1,32	13,8%	3,62	fine	0,16
	#4	9,5%	1,19	12,4%	3,25	total	0,63
	#2	8,5%	1,06	11,1%	2,91	porosity	0,37
	#1	6,7%	0,84	8,8%	2,30		
	<1	18,4%	2,30	24,0%	6,28	density	[Kg/l]
	water	36,8%	4,60	17,5%	4,60	ρ_t	2,10
	∑	100,0%	12,50	100,00%	26,21	ρ_s	2,74

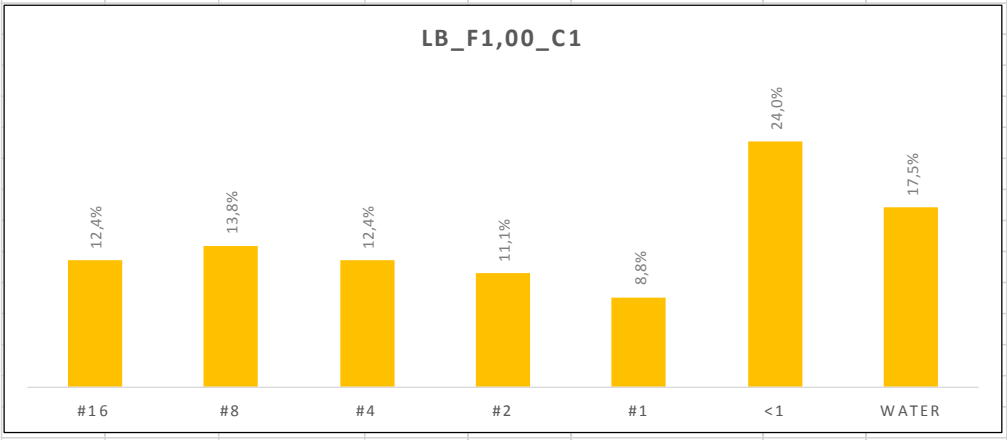

Table 4.6.19

	fraction	Vol [%]	Vol [l]	m [%]	m [kg]	Cv [-]	
LB_F1,25_C1	#16	10,1%	1,26	12,2%	3,25	coarse	0,43
	#8	11,2%	1,41	13,6%	3,62	fine	0,16
	#4	10,1%	1,26	12,2%	3,25	total	0,72
	#2	9,0%	1,13	10,9%	2,91	porosity	0,28
	#1	7,1%	0,89	8,6%	2,30		
	<1	24,4%	3,05	29,4%	7,85	density	[Kg/l]
	water	28,0%	3,50	13,1%	3,50	ρ_t	2,13
	∑	100,0%	12,50	100,00%	26,68	ρ_s	2,58

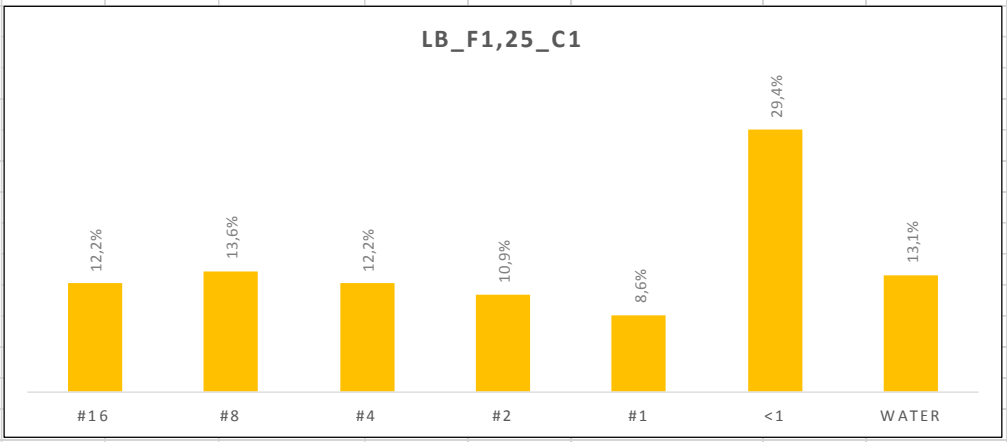

Table 4.6.20

	fraction	Vol [%]	Vol [l]	m [%]	m [kg]	Cv [-]	
LB_F0,5_C2	#16	0,0%	0,00	0,0%	0,00	coarse	0,66
	#8	10,2%	1,27	14,8%	3,62	fine	0,22
	#4	18,4%	2,30	26,8%	6,57	total	0,52
	#2	8,2%	1,02	11,9%	2,91	porosity	0,48
	#1	6,5%	0,81	9,4%	2,30		
	<1	8,8%	1,10	12,8%	3,14	density	[Kg/l]
	water	48,0%	6,00	24,4%	6,00	ρ_t	1,96
	∑	100,0%	12,50	100,00%	24,54	ρ_s	2,85

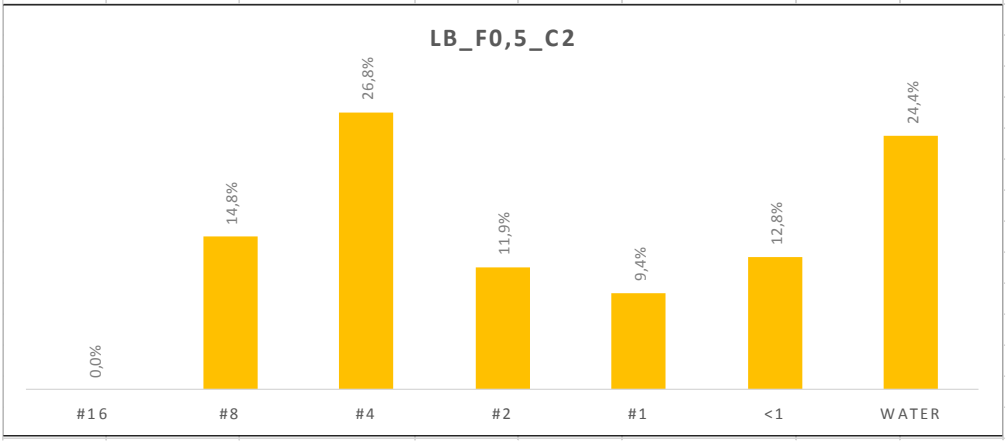

Table 4.6.21

	fraction	Vol [%]	Vol [l]	m [%]	m [kg]	Cv [-]	
LB_F0,75_C2	#16	0,0%	0,00	0,0%	0,00	coarse	0,66
	#8	10,4%	1,30	14,2%	3,62	fine	0,22
	#4	18,8%	2,35	25,9%	6,57	total	0,52
	#2	8,3%	1,04	11,5%	2,91	porosity	0,48
	#1	6,6%	0,82	9,1%	2,30		
	<1	13,5%	1,69	18,5%	4,71	density	[Kg/l]
	water	42,4%	5,30	20,9%	5,30	ρ_t	2,03
	∑	100,0%	12,50	100,00%	25,41	ρ_s	2,79

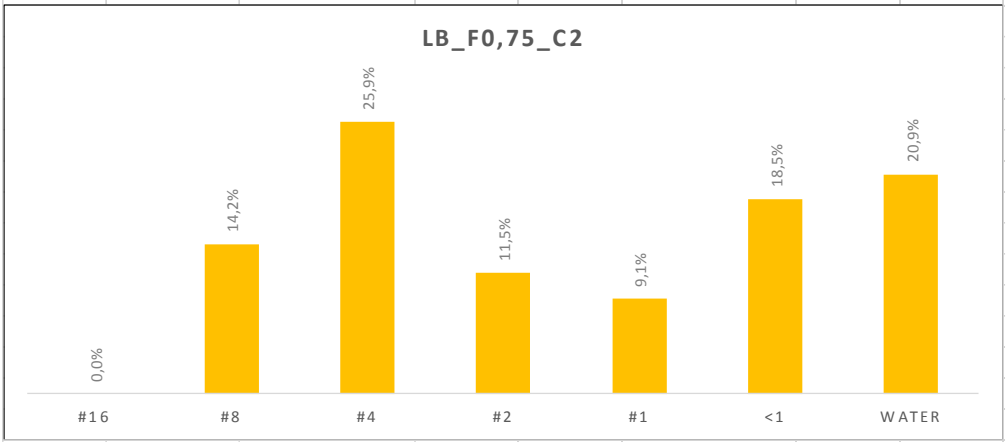

Table 4.6.22

	fraction	Vol [%]	Vol [l]	m [%]	m [kg]	Cv [-]	
LB_F1,00_C2	#16	0,0%	0,00	0,0%	0,00	coarse	0,66
	#8	10,6%	1,32	13,8%	3,62	fine	0,22
	#4	19,2%	2,39	25,0%	6,57	total	0,52
	#2	8,5%	1,06	11,1%	2,91	porosity	0,48
	#1	6,7%	0,84	8,8%	2,30		
	<1	18,3%	2,29	23,9%	6,28	density	[Kg/l]
	water	36,8%	4,60	17,5%	4,60	ρ_t	2,10
	∑	100,0%	12,50	100,00%	26,28	ρ_s	2,74

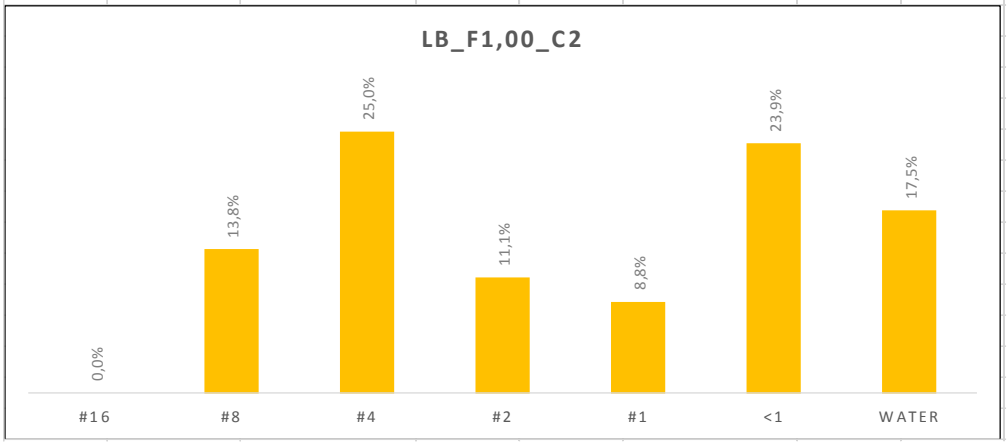

Table 4.6.23

	fraction	Vol [%]	Vol [l]	m [%]	m [kg]	Cv [-]	
LB_F1,25_C2	#16	0,0%	0,00	0,0%	0,00	coarse	0,66
	#8	11,2%	1,40	13,5%	3,62	fine	0,22
	#4	20,3%	2,54	24,6%	6,57	total	0,52
	#2	9,0%	1,13	10,9%	2,91	porosity	0,48
	#1	7,1%	0,89	8,6%	2,30		
	<1	24,3%	3,04	29,3%	7,85	density	[Kg/l]
	water	28,0%	3,50	13,1%	3,50	ρ_t	2,14
	∑	100,0%	12,50	100,00%	26,75	ρ_s	2,58

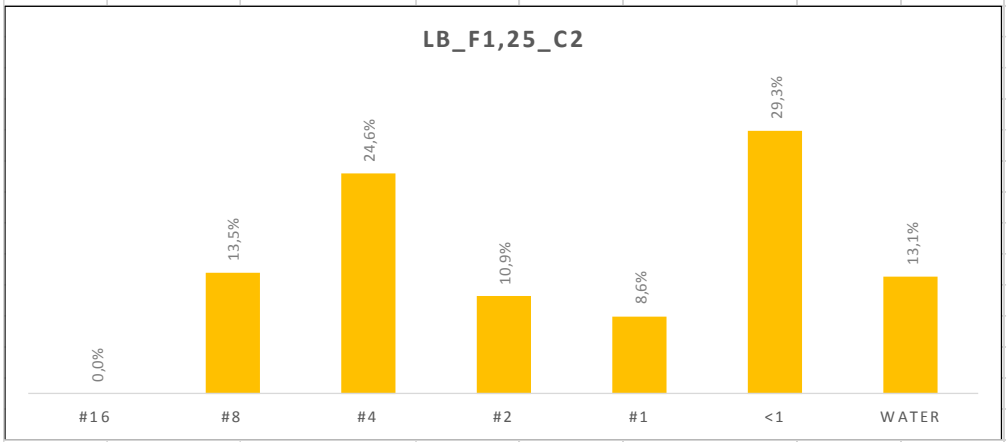

Table 4.6.24

	fraction	Vol [%]	Vol [l]	m [%]	m [kg]	Cv [-]	
LB_F0,5_C3	#16	9,1%	1,14	13,3%	3,25	coarse	0,66
	#8	10,2%	1,27	14,8%	3,62	fine	0,22
	#4	15,7%	1,96	22,8%	5,57	total	0,52
	#2	8,2%	1,02	11,9%	2,91	porosity	0,48
	#1	0,0%	0,00	0,0%	0,00		
	<1	8,8%	1,10	12,8%	3,14	density	[Kg/l]
	water	48,0%	6,00	24,5%	6,00	ρ_t	1,96
	∑	100,0%	12,50	100,00%	24,50	ρ_s	2,85

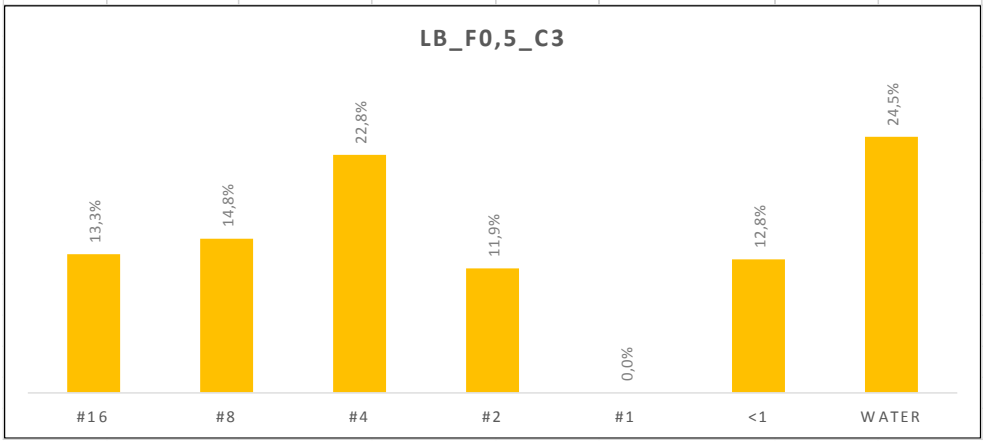

Table 4.6.25

	fraction	Vol [%]	Vol [l]	m [%]	m [kg]	Cv [-]	
LB_F0,75_C3	#16	9,3%	1,17	12,8%	3,25	coarse	0,66
	#8	10,4%	1,30	14,3%	3,62	fine	0,22
	#4	16,0%	2,00	22,0%	5,57	total	0,52
	#2	8,4%	1,04	11,5%	2,91	porosity	0,48
	#1	0,0%	0,00	0,0%	0,00		
	<1	13,5%	1,69	18,6%	4,71	density	[Kg/l]
	water	42,4%	5,30	20,9%	5,30	ρ_t	2,03
	∑	100,0%	12,50	100,00%	25,36	ρ_s	2,79

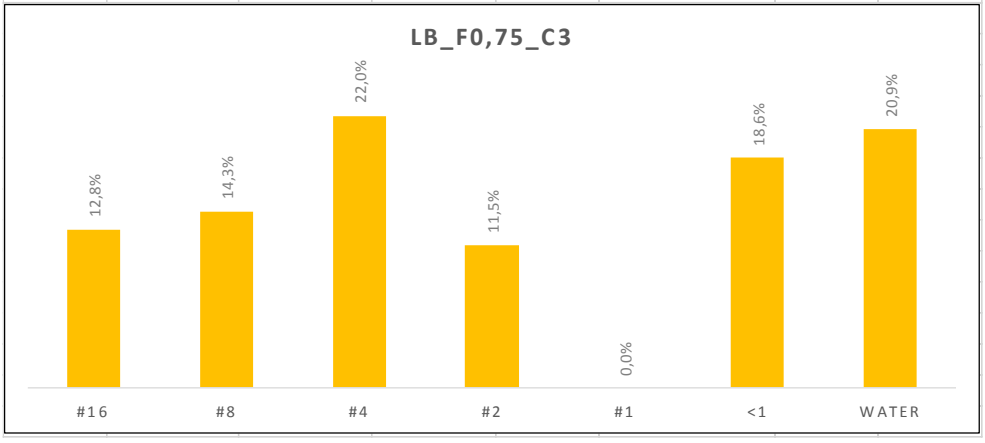

Table 4.6.26

	fraction	Vol [%]	Vol [l]	m [%]	m [kg]	Cv [-]	
LB_F1,00_C3	#16	9,5%	1,19	12,4%	3,25	coarse	0,66
	#8	10,6%	1,32	13,8%	3,62	fine	0,22
	#4	16,3%	2,04	21,2%	5,57	total	0,52
	#2	8,5%	1,06	11,1%	2,91	porosity	0,48
	#1	0,0%	0,00	0,0%	0,00		
	<1	18,3%	2,29	23,9%	6,28	density	[Kg/l]
	water	36,8%	4,60	17,5%	4,60	ρ_t	2,10
	∑	100,0%	16,26	100,00%	26,23	ρ_s	2,74

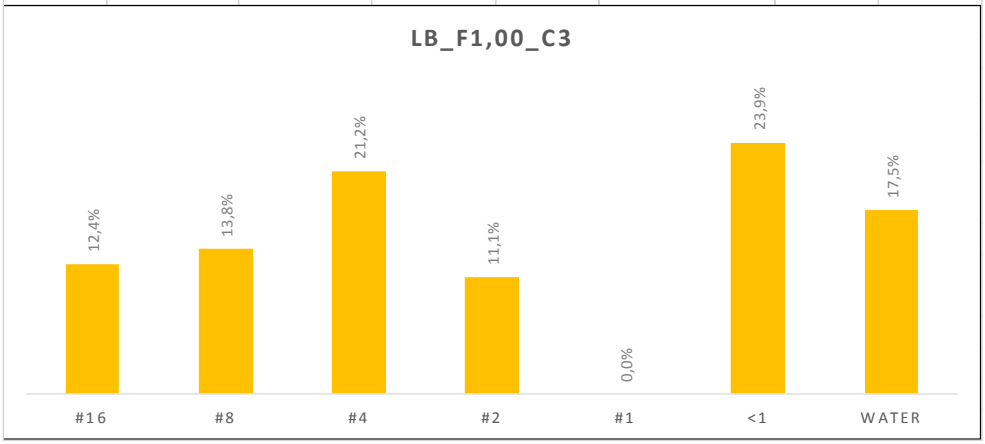

Table 4.6.27

	fraction	Vol [%]	Vol [l]	m [%]	m [kg]	Cv [-]	
LB_F1,25_C3	#16	10,1%	1,26	12,2%	3,25	coarse	0,66
	#8	11,2%	1,40	13,6%	3,62	fine	0,22
	#4	17,3%	2,16	20,9%	5,57	total	0,52
	#2	9,0%	1,13	10,9%	2,91	porosity	0,48
	#1	0,0%	0,00	0,0%	0,00		
	<1	24,4%	3,04	29,4%	7,85	density	[Kg/l]
	water	28,0%	3,50	13,1%	3,50	ρ_t	2,14
	∑	100,0%	12,50	100,00%	26,70	ρ_s	2,58

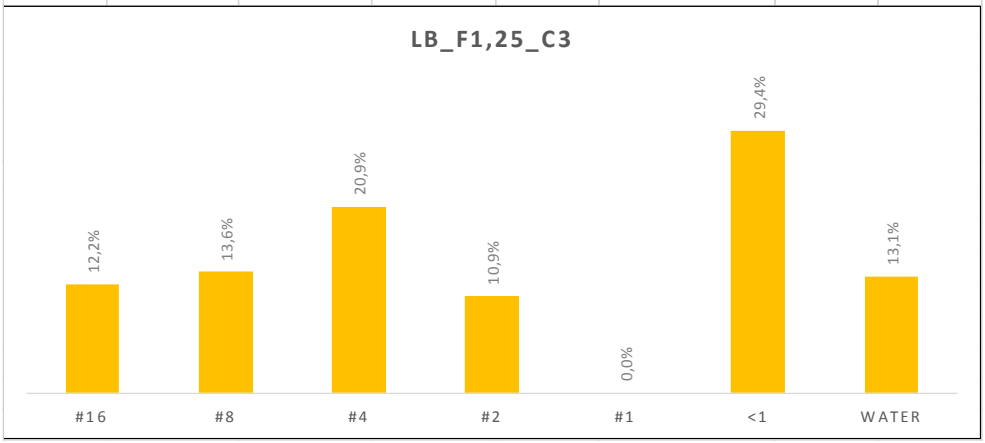

Table 4.6.28

	fraction	Vol [%]	Vol [l]	m [%]	m [kg]	Cv [-]	
LB_F0,5_C4	#16	0,0%	0,00	0,0%	0,00	coarse	0,66
	#8	10,2%	1,27	14,8%	3,62	fine	0,22
	#4	9,1%	1,14	13,3%	3,25	total	0,52
	#2	12,9%	1,61	18,7%	4,59	porosity	0,48
	#1	11,0%	1,38	16,0%	3,93		
	<1	8,8%	1,10	12,8%	3,14	density	[Kg/l]
	water	48,0%	6,00	24,5%	6,00	ρ_t	1,96
	∑	100,0%	12,50	100,00%	24,53	ρ_s	2,85

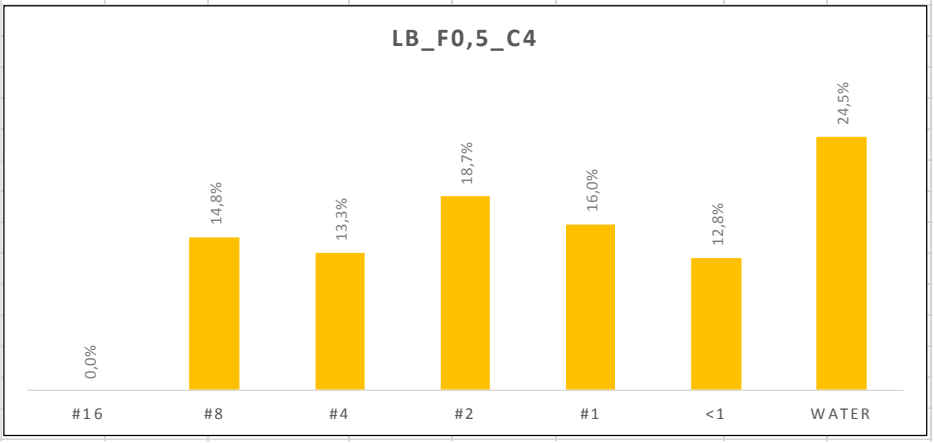

Table 4.6.29

	fraction	Vol [%]	Vol [l]	m [%]	m [kg]	Cv [-]	
LB_F0,75_C4	#16	0,0%	0,00	0,0%	0,00	coarse	0,66
	#8	10,4%	1,30	14,3%	3,62	fine	0,22
	#4	9,3%	1,16	12,8%	3,25	total	0,52
	#2	13,1%	1,64	18,1%	4,59	porosity	0,48
	#1	11,3%	1,41	15,5%	3,93		
	<1	13,5%	1,69	18,5%	4,71	density	[Kg/l]
	water	42,4%	5,30	20,9%	5,30	ρ_t	2,03
	∑	100,0%	16,10	100,00%	25,40	ρ_s	2,79

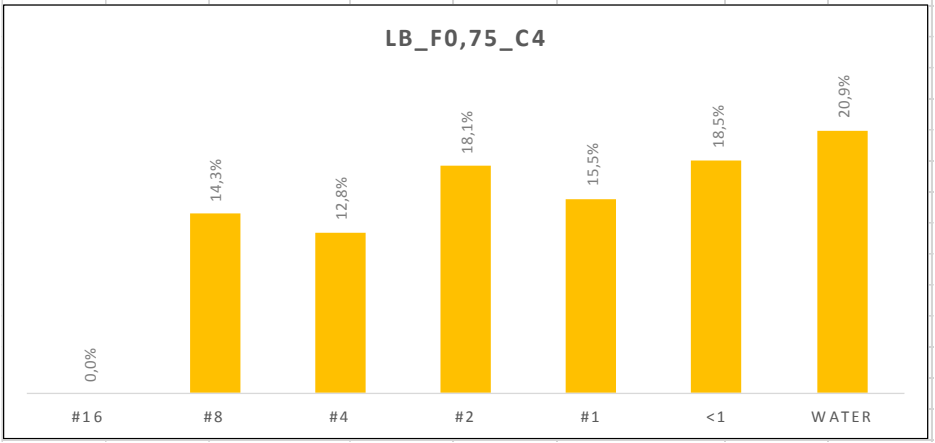

Table 4.6.30

	fraction	Vol [%]	Vol [l]	m [%]	m [kg]	Cv [-]	
LB_F1,00_C4	#16	0,0%	0,00	0,0%	0,00	coarse	0,66
	#8	10,6%	1,32	13,8%	3,62	fine	0,22
	#4	9,5%	1,18	12,4%	3,25	total	0,52
	#2	13,4%	1,67	17,5%	4,59	porosity	0,48
	#1	11,5%	1,43	15,0%	3,93		
	<1	18,3%	2,29	23,9%	6,28	density	[Kg/l]
	water	36,8%	4,60	17,5%	4,60	ρ_t	2,10
	∑	100,0%	12,50	100,00%	26,27	ρ_s	2,74

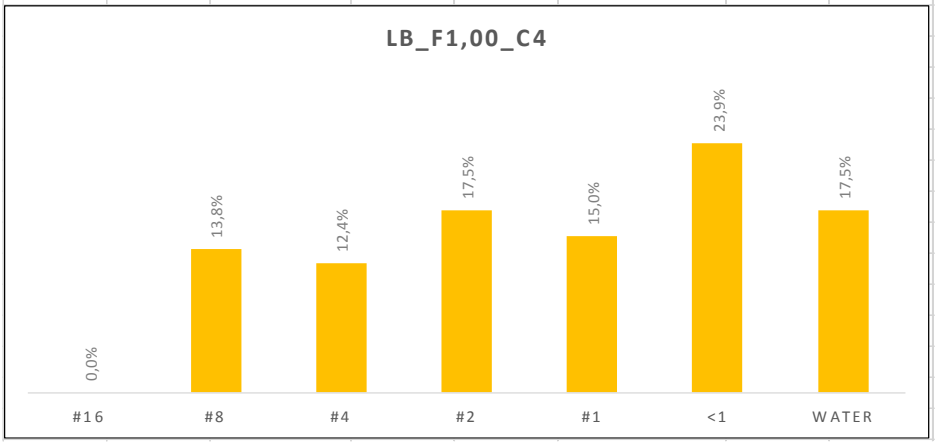

Table 4.6.31

	fraction	Vol [%]	Vol [l]	m [%]	m [kg]	Cv [-]	
LB_F1,25_C4	#16	0,0%	0,00	0,0%	0,00	coarse	0,66
	#8	11,2%	1,40	13,5%	3,62	fine	0,22
	#4	10,1%	1,26	12,2%	3,25	total	0,52
	#2	14,2%	1,78	17,2%	4,59	porosity	0,48
	#1	12,2%	1,52	14,7%	3,93		
	<1	24,3%	3,04	29,4%	7,85	density	[Kg/l]
	water	28,0%	3,50	13,1%	3,50	ρ_t	2,14
	∑	100,0%	16,02	100,00%	26,74	ρ_s	2,58

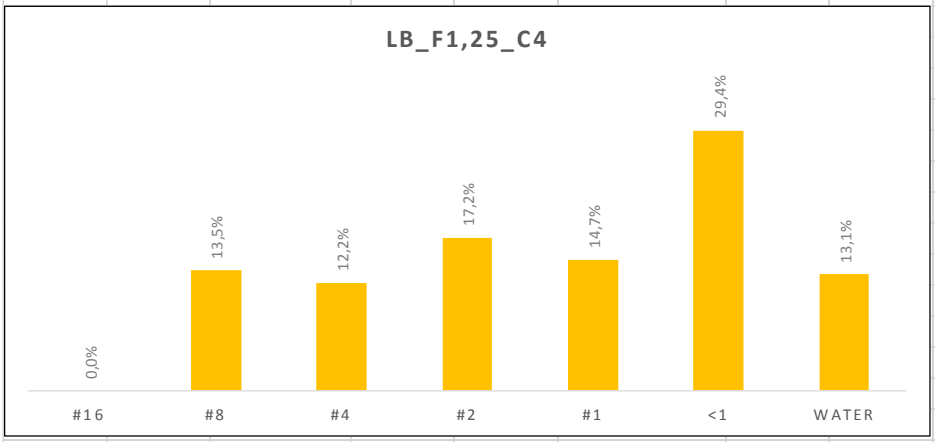

Table 4.6.32

4.7 DATA ARRANGEMENT

In order to calculate the dissipation coefficient D by using Matlab ©, a data arrangement was needed.

4.7.1 Shifting

It was useful to have all the same hydrostatic asymptotic value for each sensor. In some tests, the dumped material was not exactly filling the designed height in the cylinder. This problem was due to little leaking of mixture during mixing and pouring. For that reason, the 50 Hz data series have been shifted to the hydrostatic pressure value, by using a Matlab script designed for that: for each test, I plotted the measured values for the bottom sensor and chose an interval (starting arbitrarily) in which the pressure value was already "hydrostatic" for the considered case. Of this interval, for each sensor, the mean value was calculated and algebraically sum up with the designed hydrostatic values, so the delta vector was calculated. The delta vector was algebraically subtracted to the measured values.

4.7.2 Nip & Tuck

Next step was necessary to correct some involuntary accidents that happened, i.e. when something bumped the cylinder and the vibrations caused a peak of pressure. Another Matlab script was designed to correct the errors, by substituting the perturbed part with a linear data series. Manually I checked those tests needing the correction and chose the interval to change, referring to the bottom sensor. This correction needs just the first and the second x-coordinate as input and automatically take the corresponding y(x)-values to calculate the straight line. This way it was possible to "save" the tests with some problems.

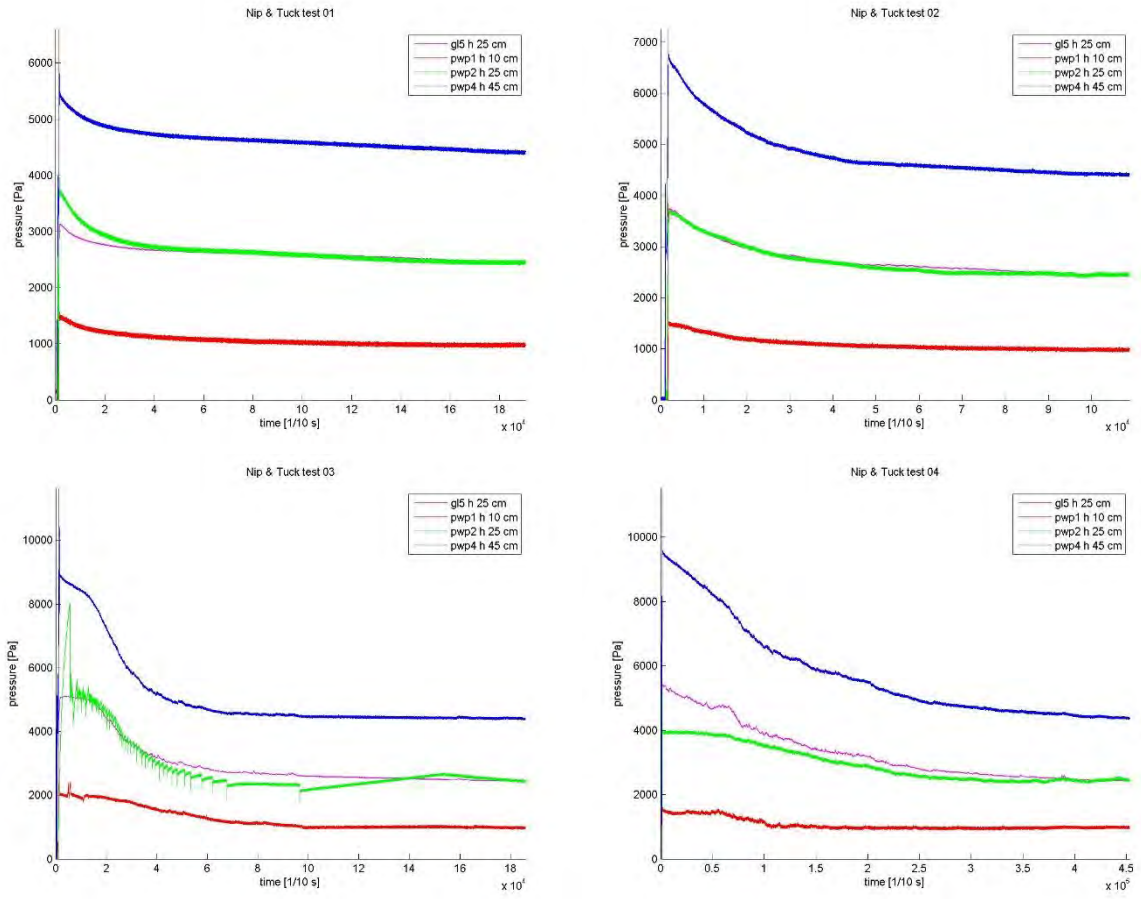

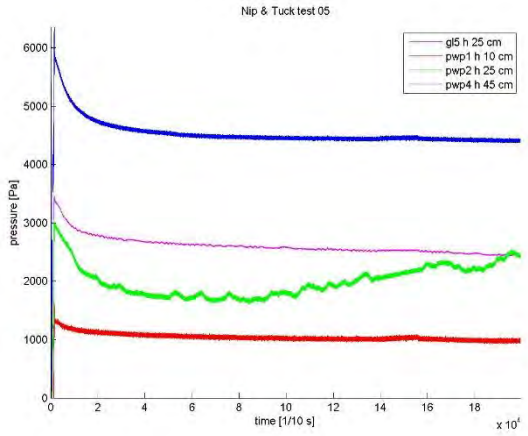
Nip & Tuck test 05
gl5 h 25 cm
pwp1 h 10 cm
pwp2 h 25 cm
pwp4 h 45 cm
pressure [Pa]
time [1/10 s]
x 10^4

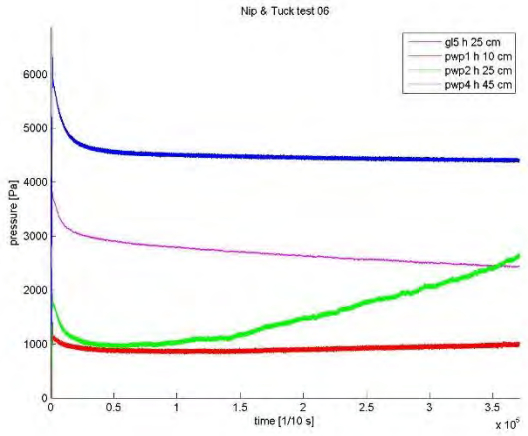
Nip & Tuck test 06
gl5 h 25 cm
pwp1 h 10 cm
pwp2 h 25 cm
pwp4 h 45 cm
pressure [Pa]
time [1/10 s]
x 10^5

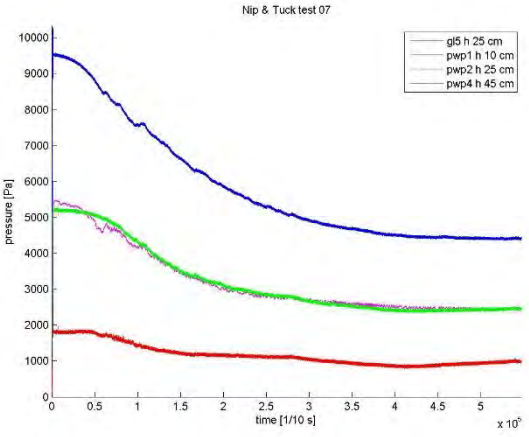
Nip & Tuck test 07
gl5 h 25 cm
pwp1 h 10 cm
pwp2 h 25 cm
pwp4 h 45 cm
pressure [Pa]
time [1/10 s]
x 10^5

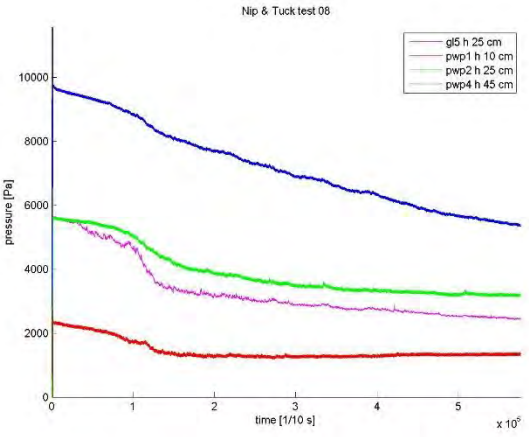
Nip & Tuck test 08
gl5 h 25 cm
pwp1 h 10 cm
pwp2 h 25 cm
pwp4 h 45 cm
pressure [Pa]
time [1/10 s]
x 10^5

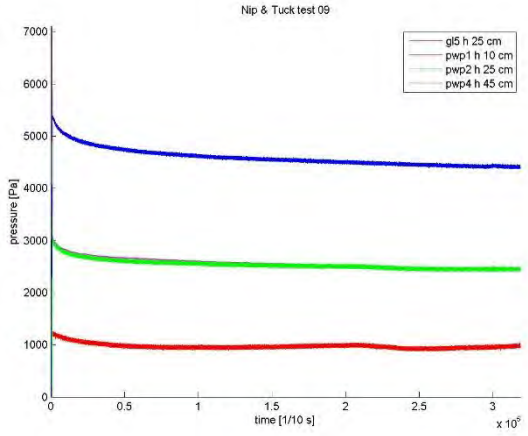
Nip & Tuck test 09
gl5 h 25 cm
pwp1 h 10 cm
pwp2 h 25 cm
pwp4 h 45 cm
pressure [Pa]
time [1/10 s]
x 10^5

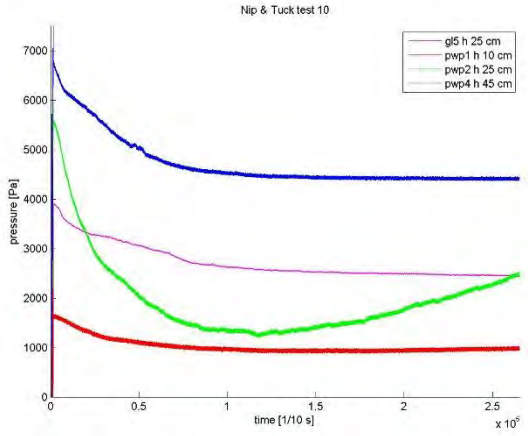
Nip & Tuck test 10
gl5 h 25 cm
pwp1 h 10 cm
pwp2 h 25 cm
pwp4 h 45 cm
pressure [Pa]
time [1/10 s]
x 10^5

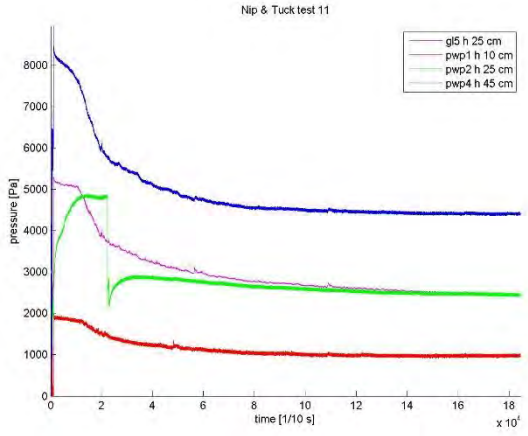
Nip & Tuck test 11
gl5 h 25 cm
pwp1 h 10 cm
pwp2 h 25 cm
pwp4 h 45 cm
pressure [Pa]
time [1/10 s]
x 10^4

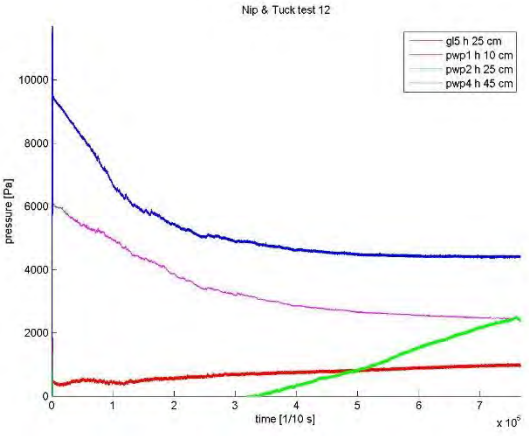
Nip & Tuck test 12
gl5 h 25 cm
pwp1 h 10 cm
pwp2 h 25 cm
pwp4 h 45 cm
pressure [Pa]
time [1/10 s]
x 10^5

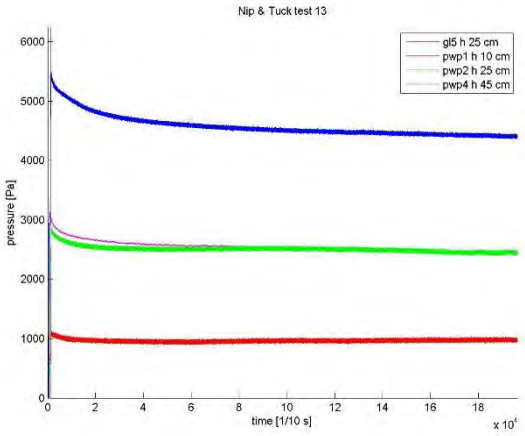
Nip & Tuck test 13
gl5 h 25 cm
pwp1 h 10 cm
pwp2 h 25 cm
pwp4 h 45 cm
pressure [Pa]
time [1/10 s]
x 10^4

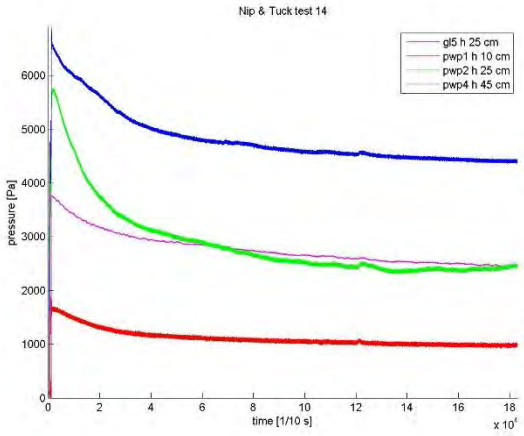
Nip & Tuck test 14
gl5 h 25 cm
pwp1 h 10 cm
pwp2 h 25 cm
pwp4 h 45 cm
pressure [Pa]
time [1/10 s]
x 10^4

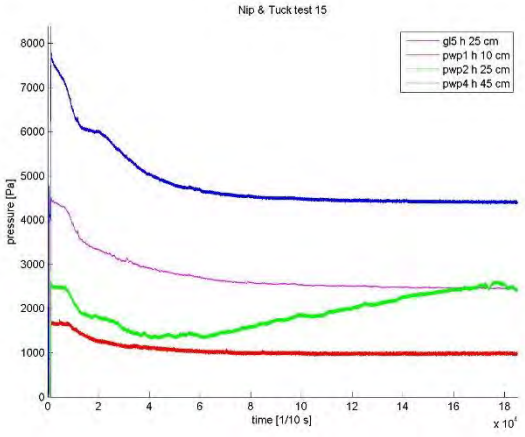
Nip & Tuck test 15
gl5 h 25 cm
pwp1 h 10 cm
pwp2 h 25 cm
pwp4 h 45 cm
pressure [Pa]
time [1/10 s]
x 10^4

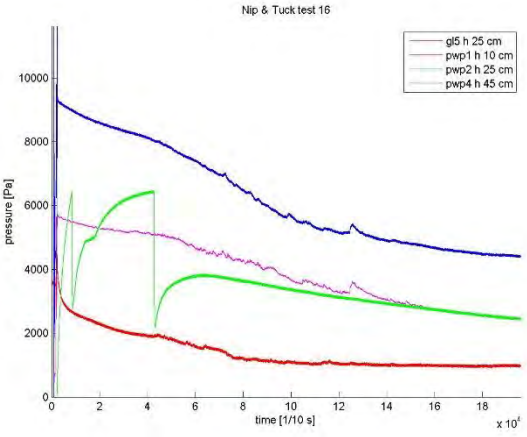
Nip & Tuck test 16
gl5 h 25 cm
pwp1 h 10 cm
pwp2 h 25 cm
pwp4 h 45 cm
pressure [Pa]
time [1/10 s]
x 10^4

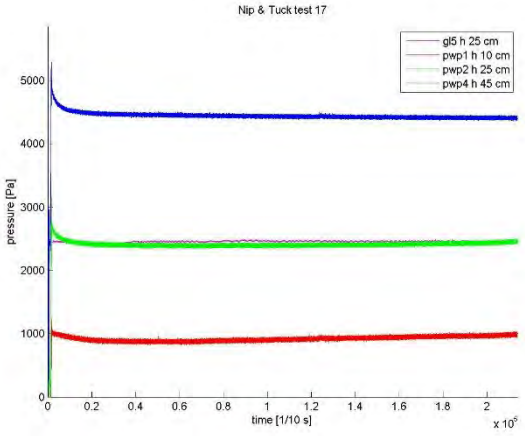
Nip & Tuck test 17
gl5 h 25 cm
pwp1 h 10 cm
pwp2 h 25 cm
pwp4 h 45 cm
pressure [Pa]
time [1/10 s]
x 10^5

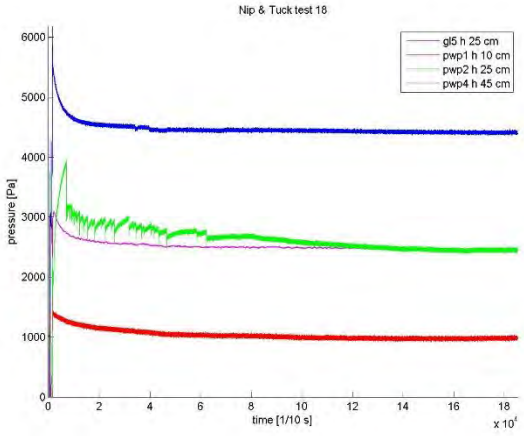
Nip & Tuck test 18
gl5 h 25 cm
pwp1 h 10 cm
pwp2 h 25 cm
pwp4 h 45 cm
pressure [Pa]
time [1/10 s]
x 10^4

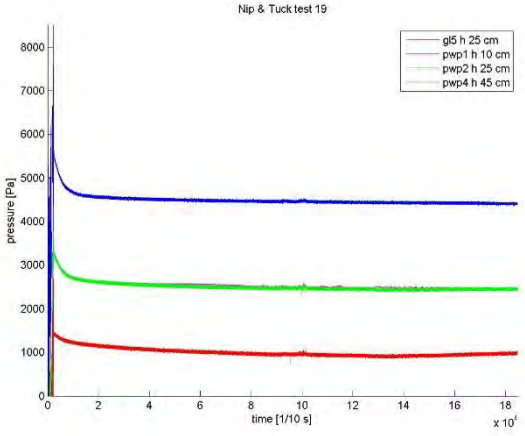
Nip & Tuck test 19
gl5 h 25 cm
pwp1 h 10 cm
pwp2 h 25 cm
pwp4 h 45 cm
pressure [Pa]
time [1/10 s]
x 10^4

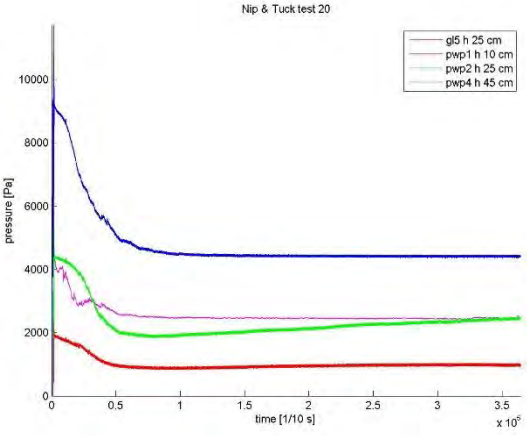
Nip & Tuck test 20
gl5 h 25 cm
pwp1 h 10 cm
pwp2 h 25 cm
pwp4 h 45 cm
pressure [Pa]
time [1/10 s]
x 10^5

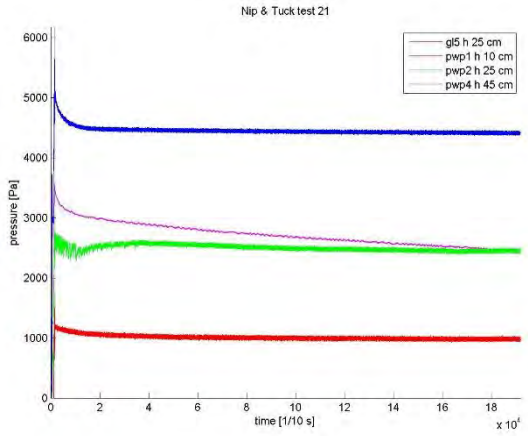
Nip & Tuck test 21
gl5 h 25 cm
pwp1 h 10 cm
pwp2 h 25 cm
pwp4 h 45 cm
pressure [Pa]
time [1/10 s]
x 10^4

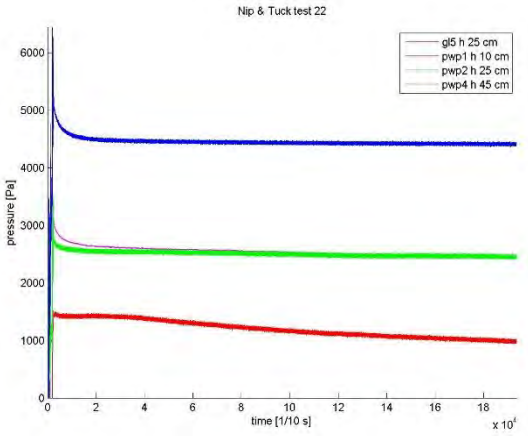
Nip & Tuck test 22
gl5 h 25 cm
pwp1 h 10 cm
pwp2 h 25 cm
pwp4 h 45 cm
pressure [Pa]
time [1/10 s]
x 10^4

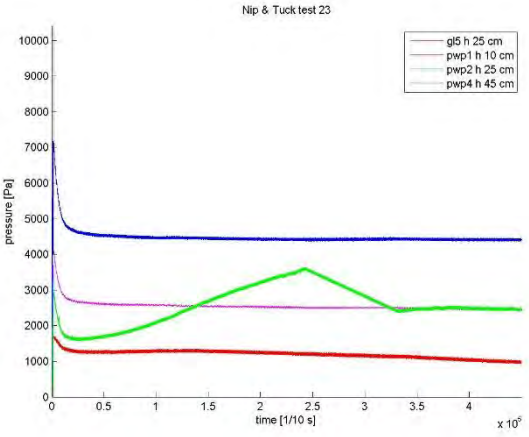
Nip & Tuck test 23
gl5 h 25 cm
pwp1 h 10 cm
pwp2 h 25 cm
pwp4 h 45 cm
pressure [Pa]
time [1/10 s]
x 10^5

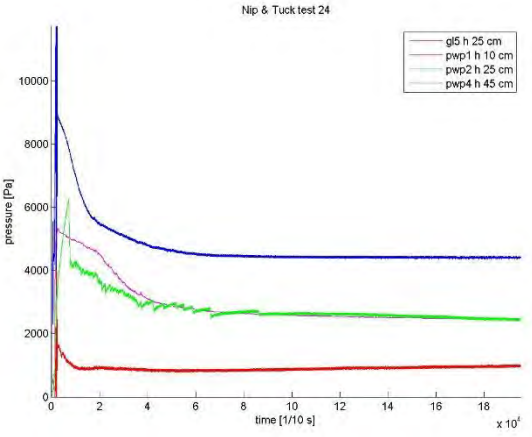
Nip & Tuck test 24
gl5 h 25 cm
pwp1 h 10 cm
pwp2 h 25 cm
pwp4 h 45 cm
pressure [Pa]
time [1/10 s]
x 10^4

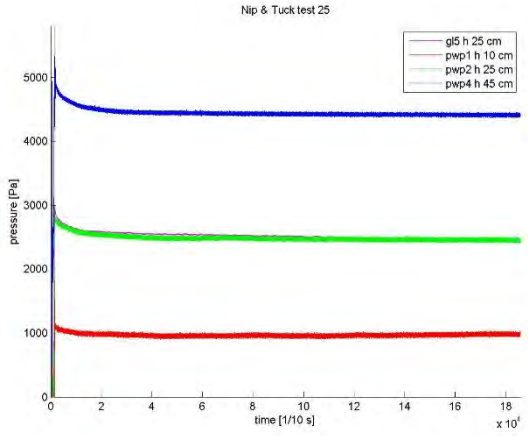
Nip & Tuck test 25
gl5 h 25 cm
pwp1 h 10 cm
pwp2 h 25 cm
pwp4 h 45 cm
pressure [Pa]
time [1/10 s]
x 10^4

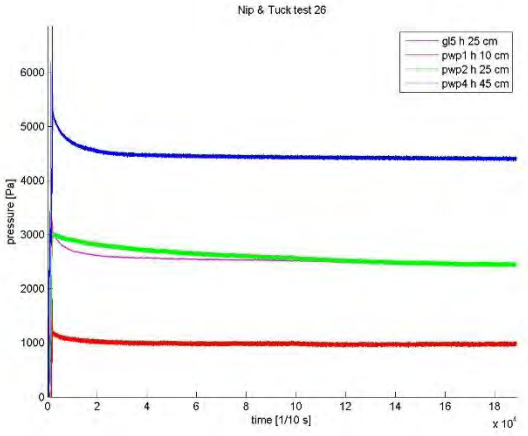
Nip & Tuck test 26
gl5 h 25 cm
pwp1 h 10 cm
pwp2 h 25 cm
pwp4 h 45 cm
pressure [Pa]
time [1/10 s]
x 10^4

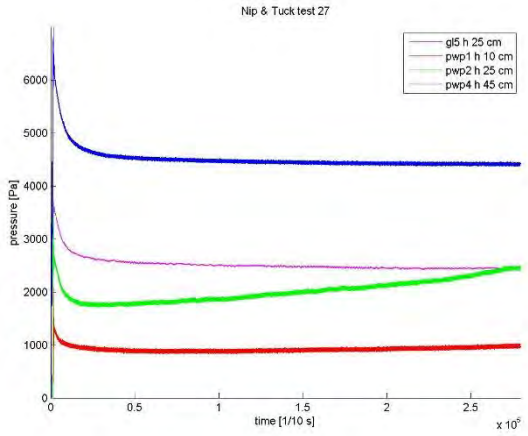
Nip & Tuck test 27
gl5 h 25 cm
pwp1 h 10 cm
pwp2 h 25 cm
pwp4 h 45 cm
pressure [Pa]
time [1/10 s]
x 10^5

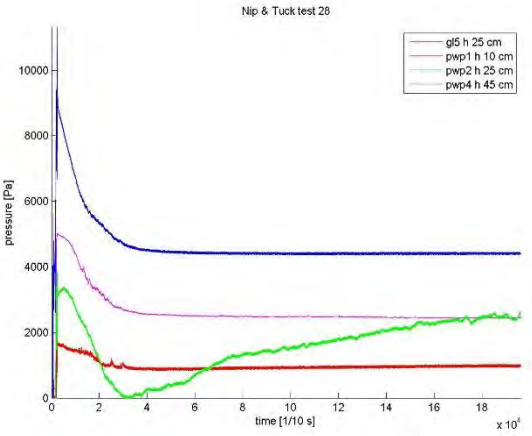
Nip & Tuck test 28
gl5 h 25 cm
pwp1 h 10 cm
pwp2 h 25 cm
pwp4 h 45 cm
pressure [Pa]
time [1/10 s]
x 10^4

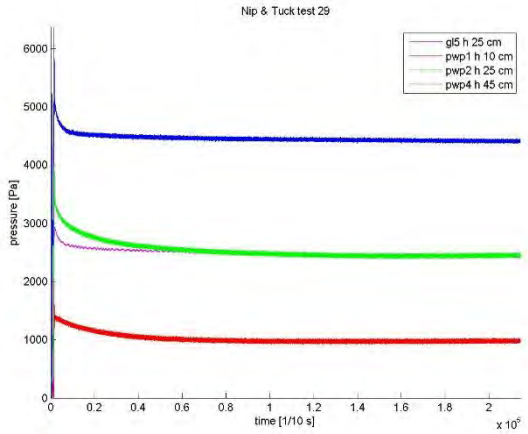
Nip & Tuck test 29
gl5 h 25 cm
pwp1 h 10 cm
pwp2 h 25 cm
pwp4 h 45 cm
pressure [Pa]
time [1/10 s]
x 10^5

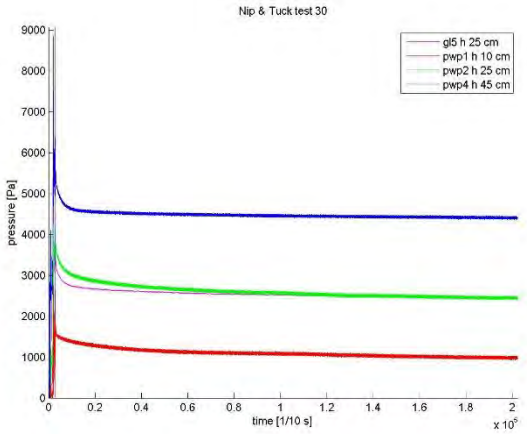
Nip & Tuck test 30
gl5 h 25 cm
pwp1 h 10 cm
pwp2 h 25 cm
pwp4 h 45 cm
pressure [Pa]
time [1/10 s]
x 10^5

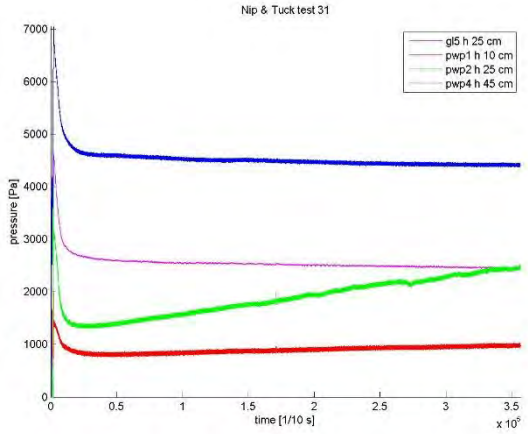
Nip & Tuck test 31
gl5 h 25 cm
pwp1 h 10 cm
pwp2 h 25 cm
pwp4 h 45 cm
pressure [Pa]
time [1/10 s]
x 10^5

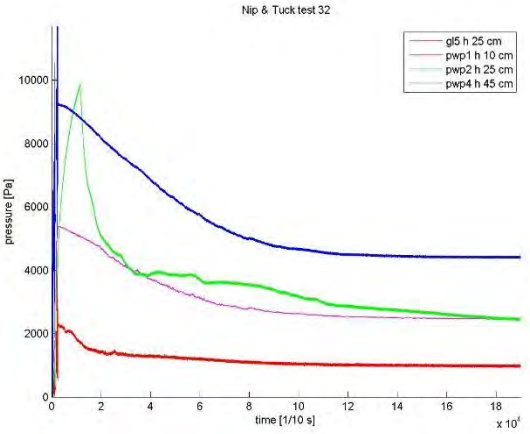
Nip & Tuck test 32
gl5 h 25 cm
pwp1 h 10 cm
pwp2 h 25 cm
pwp4 h 45 cm
pressure [Pa]
time [1/10 s]
x 10^4

4.7.3 Starting Point

Another relevant problem for the data series was to choose a proper starting point, because dumping the mixture in the cylinder usually caused a big peak of pressure (both positive and negative). Consequently, it was paramount to find a valid criterion to clean the initial part of the series. A maximum criterion was adopted: each data series (recorded at 50 Hz frequency) was transformed into a 1 Hz series, so the mean pressure value was calculated. This choice brought to a strong decrease of the series length and a kind of smoothing to the peaks. Then, I assumed the highest value as starting value.

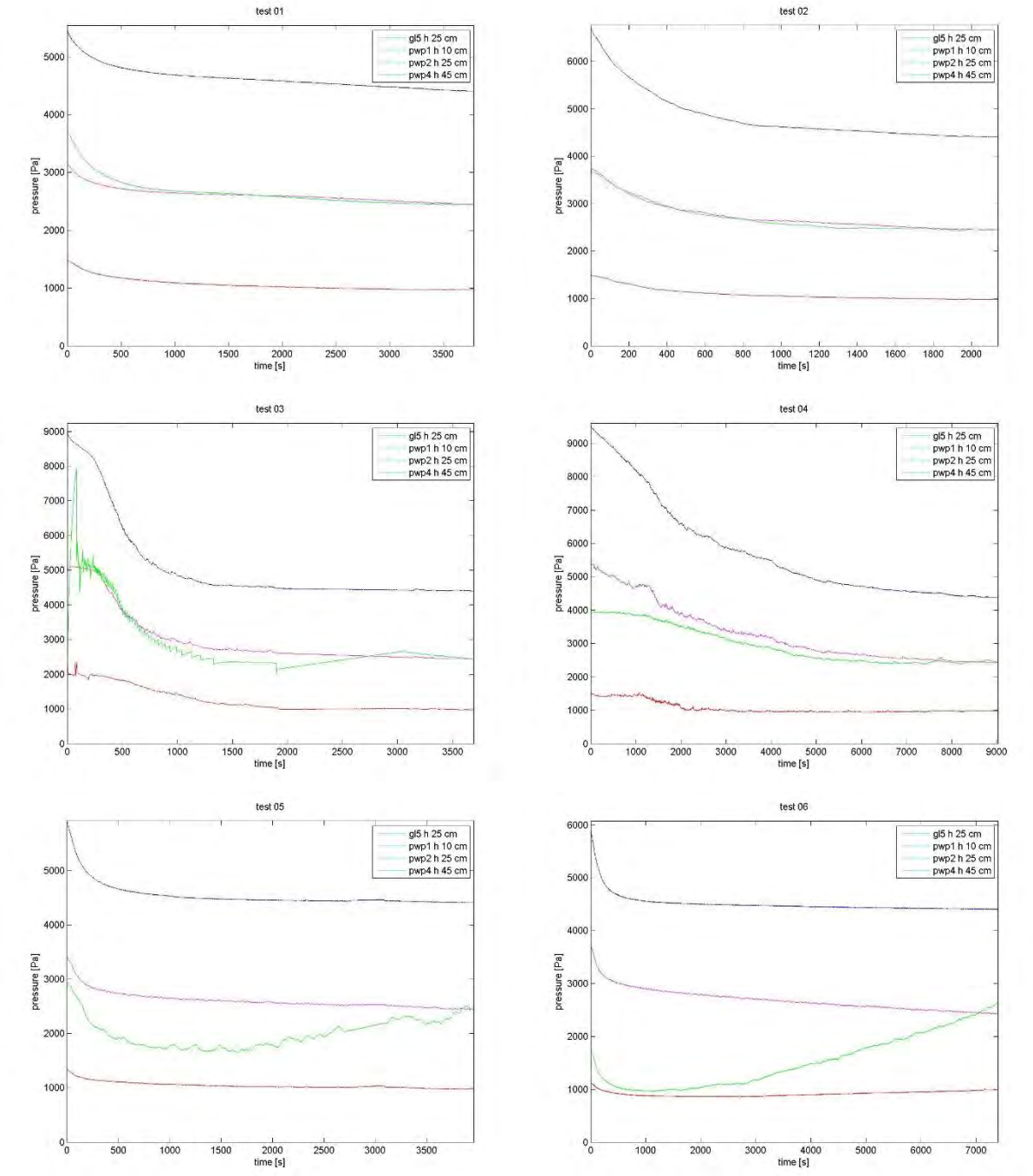

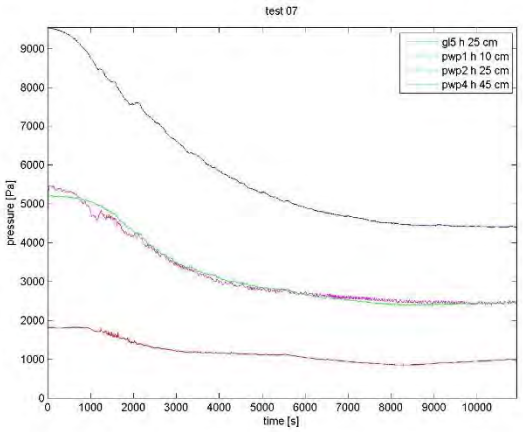
test 07
gl5 h 25 cm
pwp1 h 10 cm
pwp2 h 25 cm
pwp4 h 45 cm
pressure [Pa]
time [s]

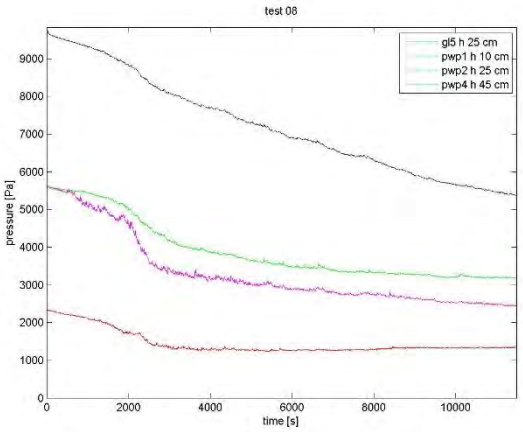
test 08
gl5 h 25 cm
pwp1 h 10 cm
pwp2 h 25 cm
pwp4 h 45 cm
pressure [Pa]
time [s]

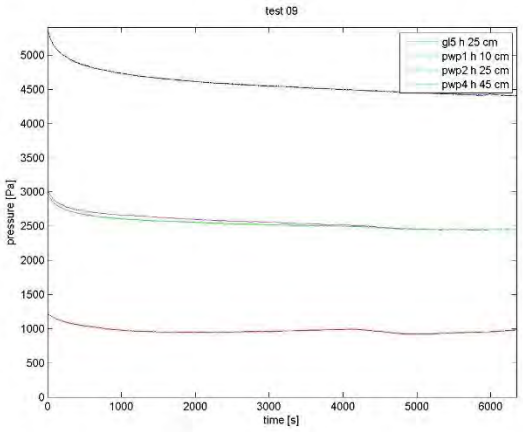
test 09
gl5 h 25 cm
pwp1 h 10 cm
pwp2 h 25 cm
pwp4 h 45 cm
pressure [Pa]
time [s]

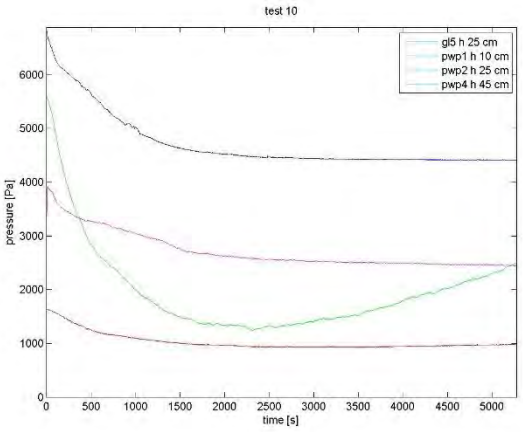
test 10
gl5 h 25 cm
pwp1 h 10 cm
pwp2 h 25 cm
pwp4 h 45 cm
pressure [Pa]
time [s]

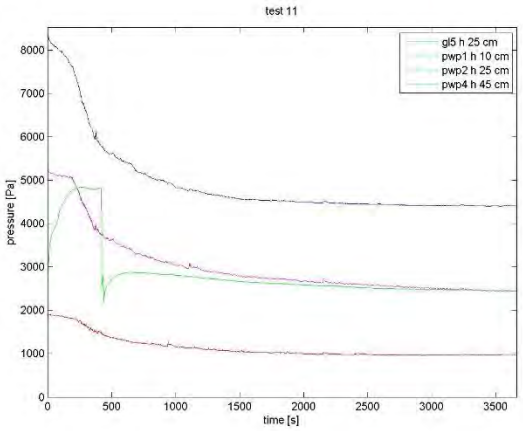
test 11
gl5 h 25 cm
pwp1 h 10 cm
pwp2 h 25 cm
pwp4 h 45 cm
pressure [Pa]
time [s]

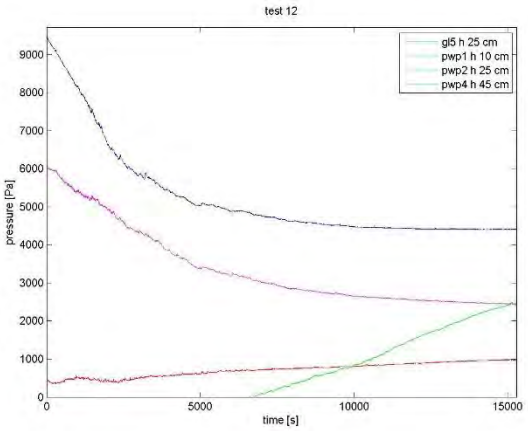
test 12
gl5 h 25 cm
pwp1 h 10 cm
pwp2 h 25 cm
pwp4 h 45 cm
pressure [Pa]
time [s]

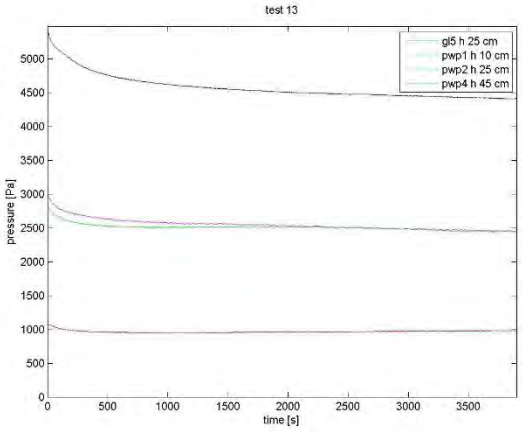
test 13
gl5 h 25 cm
pwp1 h 10 cm
pwp2 h 25 cm
pwp4 h 45 cm
pressure [Pa]
time [s]

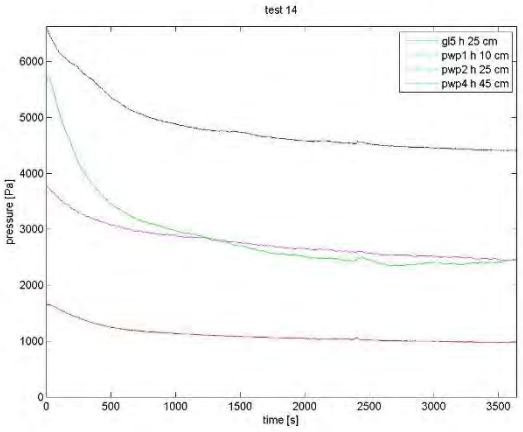
test 14
gl5 h 25 cm
pwp1 h 10 cm
pwp2 h 25 cm
pwp4 h 45 cm
pressure [Pa]
time [s]

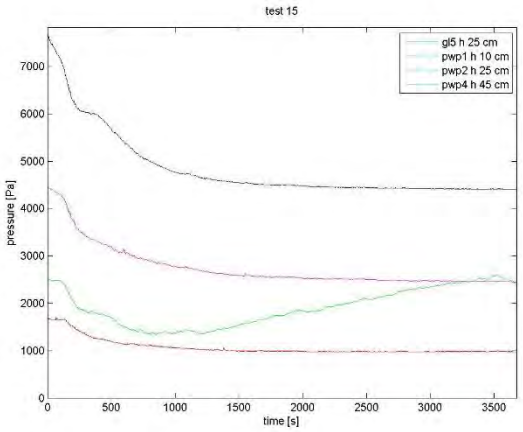
test 15
gl5 h 25 cm
pwp1 h 10 cm
pwp2 h 25 cm
pwp4 h 45 cm
pressure [Pa]
time [s]

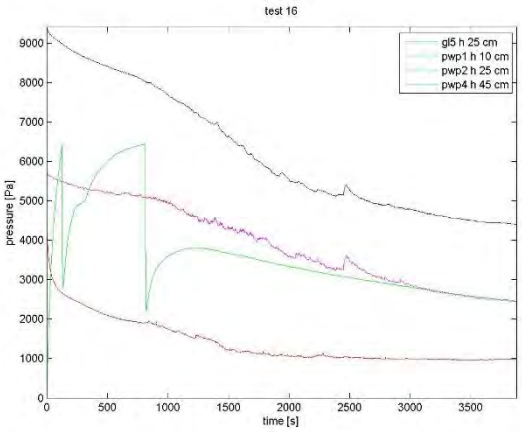
test 16
gl5 h 25 cm
pwp1 h 10 cm
pwp2 h 25 cm
pwp4 h 45 cm
pressure [Pa]
time [s]

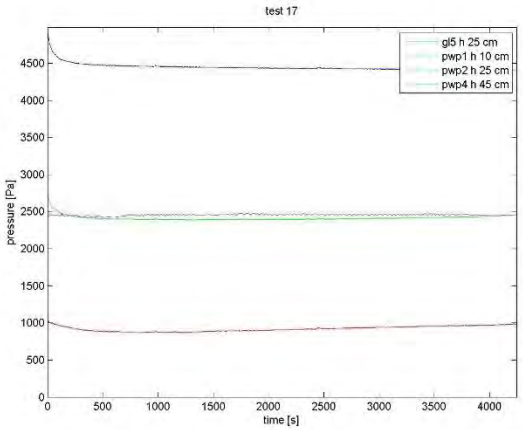
test 17
gl5 h 25 cm
pwp1 h 10 cm
pwp2 h 25 cm
pwp4 h 45 cm
pressure [Pa]
time [s]

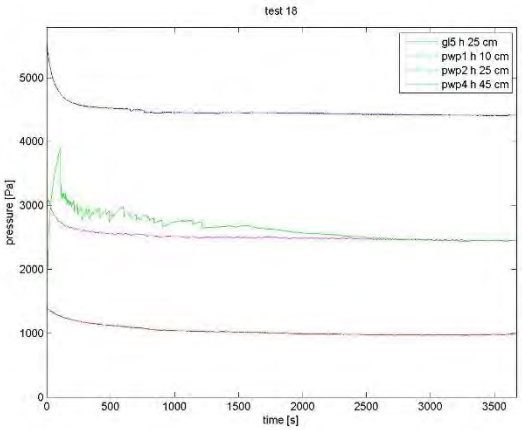
test 18
gl5 h 25 cm
pwp1 h 10 cm
pwp2 h 25 cm
pwp4 h 45 cm
pressure [Pa]
time [s]

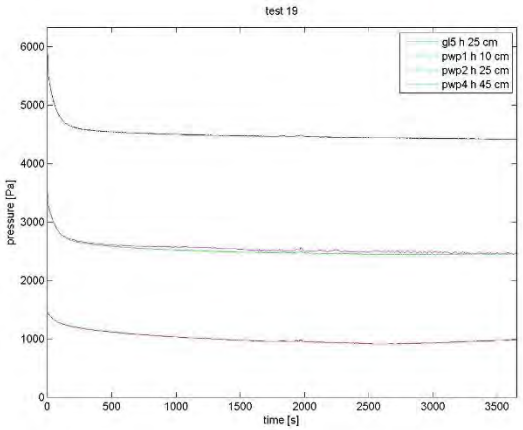
test 19
gl5 h 25 cm
pwp1 h 10 cm
pwp2 h 25 cm
pwp4 h 45 cm
pressure [Pa]
time [s]

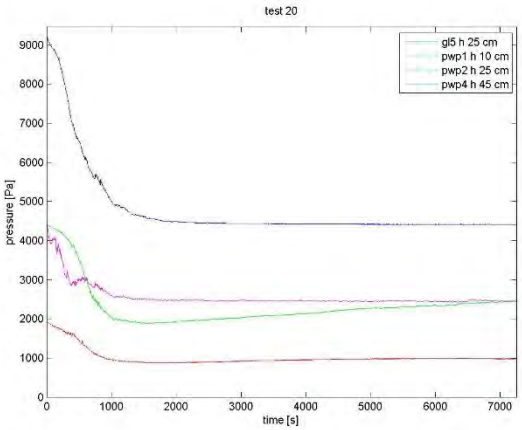
test 20
gl5 h 25 cm
pwp1 h 10 cm
pwp2 h 25 cm
pwp4 h 45 cm
pressure [Pa]
time [s]

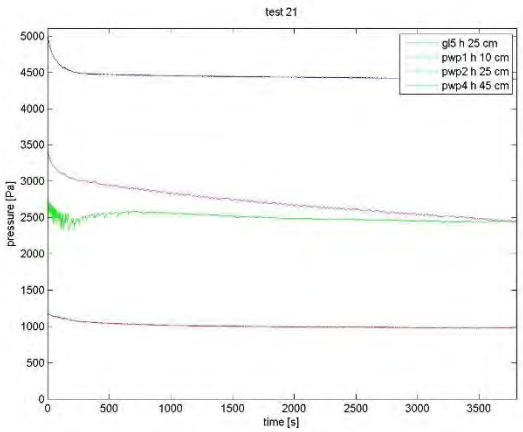
test 21
gl5 h 25 cm
pwp1 h 10 cm
pwp2 h 25 cm
pwp4 h 45 cm
pressure [Pa]
time [s]

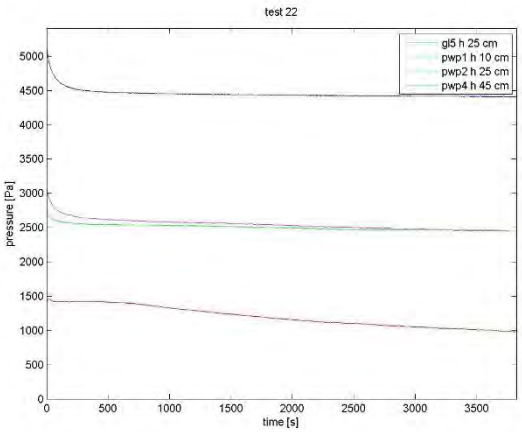
test 22
gl5 h 25 cm
pwp1 h 10 cm
pwp2 h 25 cm
pwp4 h 45 cm
pressure [Pa]
time [s]

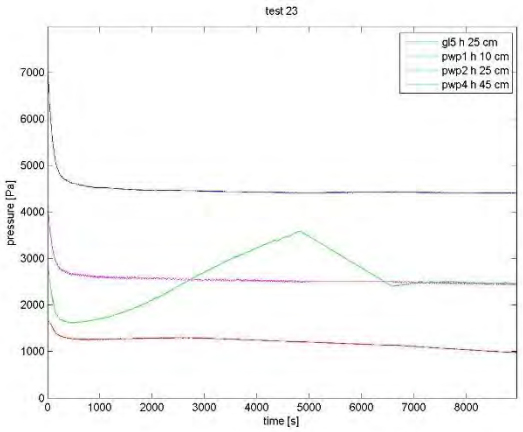
test 23
gl5 h 25 cm
pwp1 h 10 cm
pwp2 h 25 cm
pwp4 h 45 cm
pressure [Pa]
time [s]

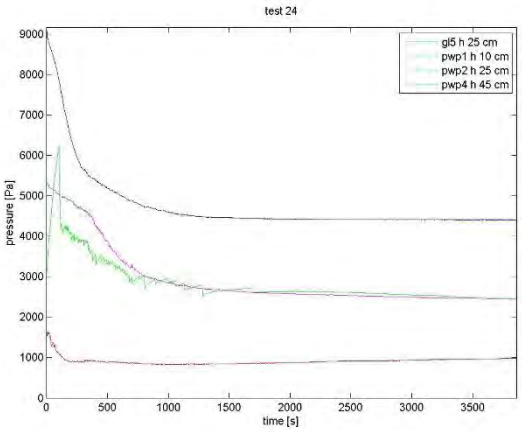
test 24
gl5 h 25 cm
pwp1 h 10 cm
pwp2 h 25 cm
pwp4 h 45 cm
pressure [Pa]
time [s]

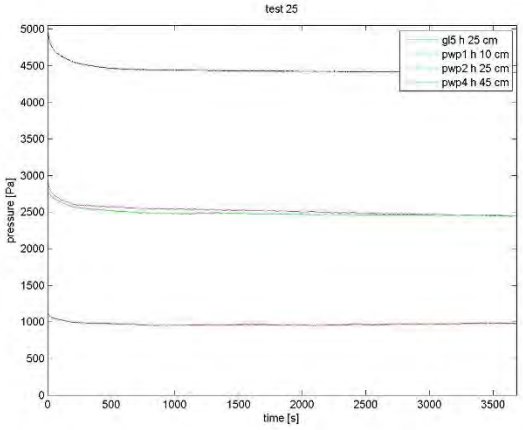
test 25
gl5 h 25 cm
pwp1 h 10 cm
pwp2 h 25 cm
pwp4 h 45 cm
pressure [Pa]
time [s]

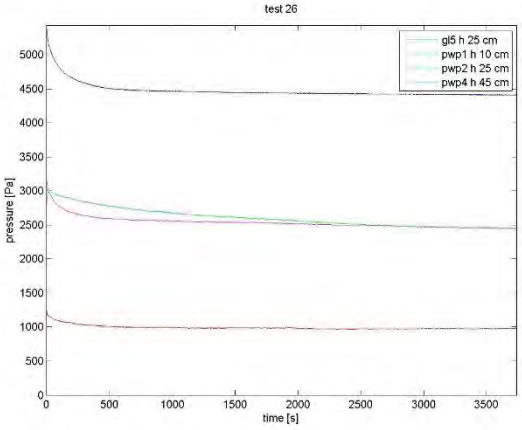
test 26
gl5 h 25 cm
pwp1 h 10 cm
pwp2 h 25 cm
pwp4 h 45 cm
pressure [Pa]
time [s]

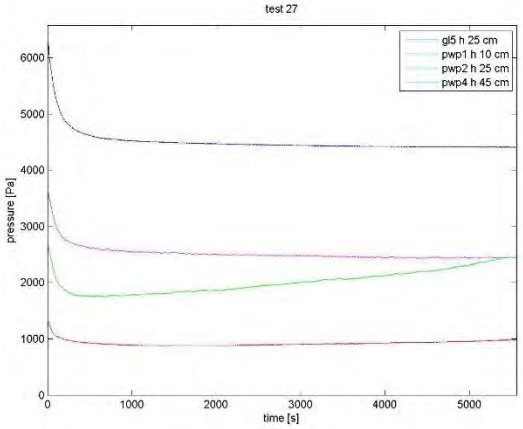
test 27
gl5 h 25 cm
pwp1 h 10 cm
pwp2 h 25 cm
pwp4 h 45 cm
pressure [Pa]
time [s]

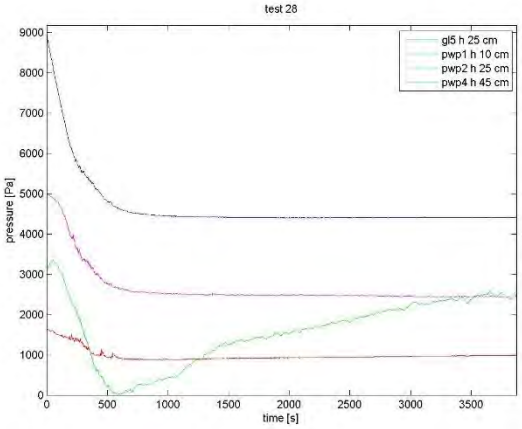
test 28
gl5 h 25 cm
pwp1 h 10 cm
pwp2 h 25 cm
pwp4 h 45 cm
pressure [Pa]
time [s]

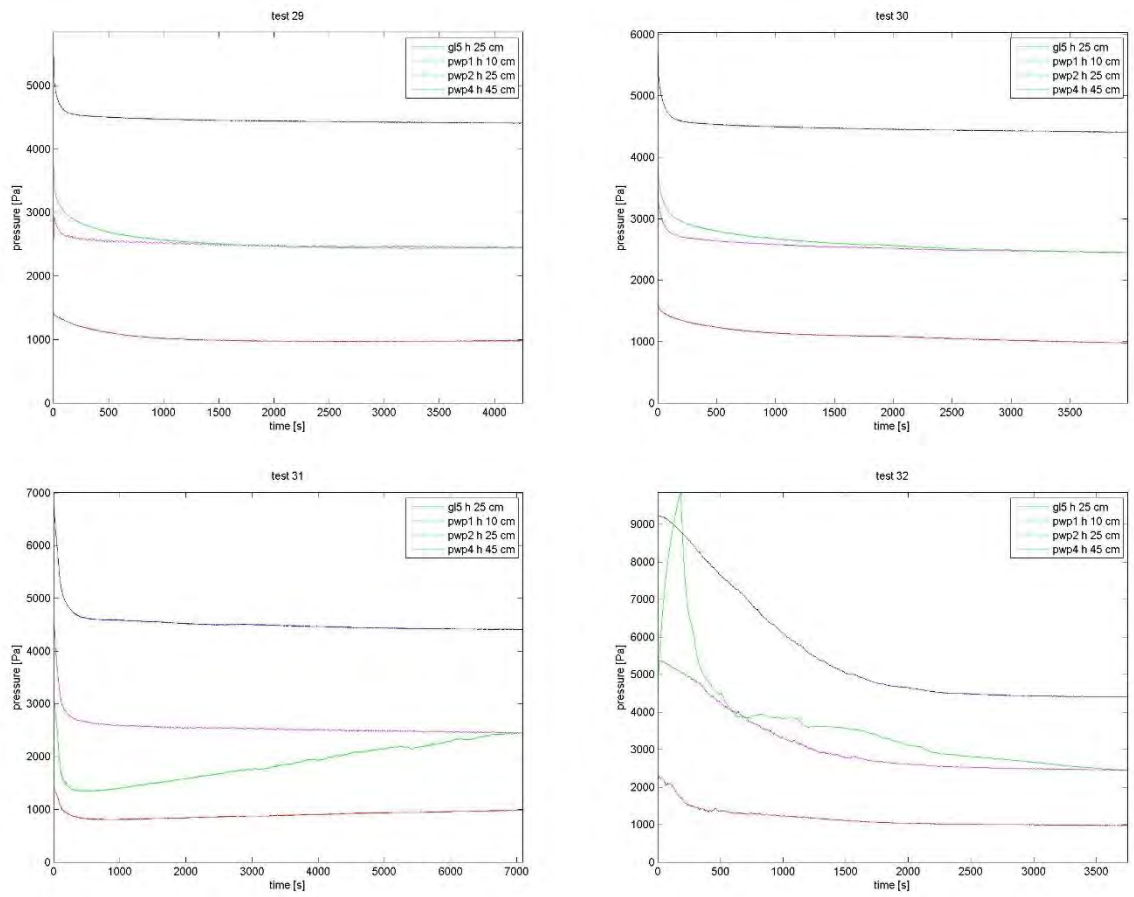

4.8 THE MATLAB SCRIPT OF D-COEFFICIENT CALCULATION

The dissipation coefficient was calculated by using Matlab. A long script was written to automatize and improve the calculation. The basic steps are:

- Data series loading
- Timing to 1 second
- First attempt D values choice
- Input parameters (water weight, solid weight, total density, elevation of sensors from the bottom)
- excess pore pressure equation resolution with first attempt D values
- mean square error and percentage error calculation
- Best fit D value choice, based on minimum percentage error combined sensor calculation
- Fitting calculation with D value
- Output file with test number, C_v value, D_{value} and D_{value} for each sensor.

It may some relevance to underline that the first attempt D value interval has to be manually decided, and the more are the significant figures, the more accurate will be the best D value fitting. In this calculation script I chose to fix the starting point of the fitting series coincident with the first measured value, and to not calculate it as liquefaction pressure value as suggested in (Major, 2000).

To take into account the reliability problems of some sensors (especially pwp1 and pwp2) it was necessary to create a checklist file counting or excluding an unreliable series. Following chapter shows the results, beginning with the error graphics and after with the best fitting plots.

5 RESULTS

5.1 ERROR GRAPHICS

5.1.1 Scalärarüfe

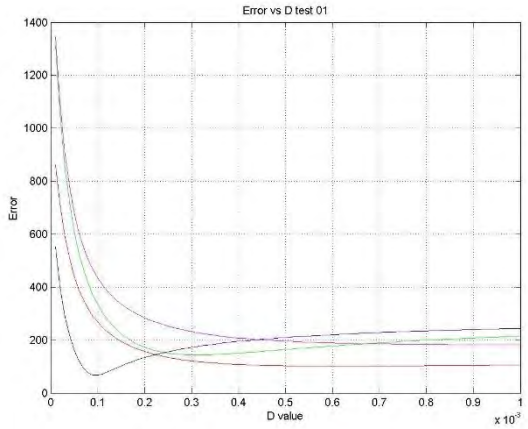

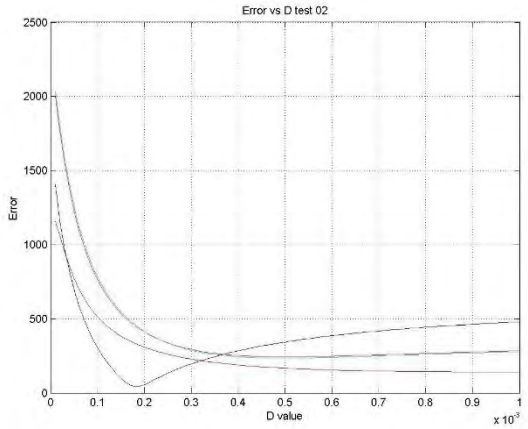

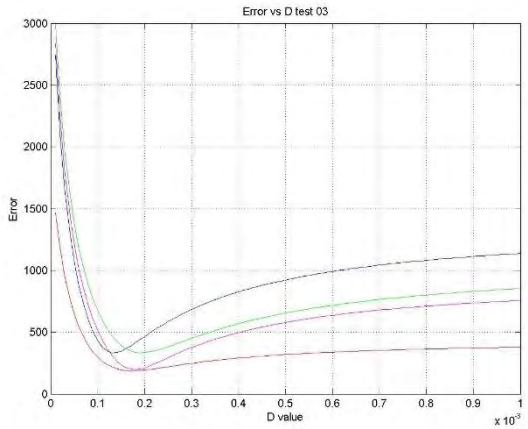

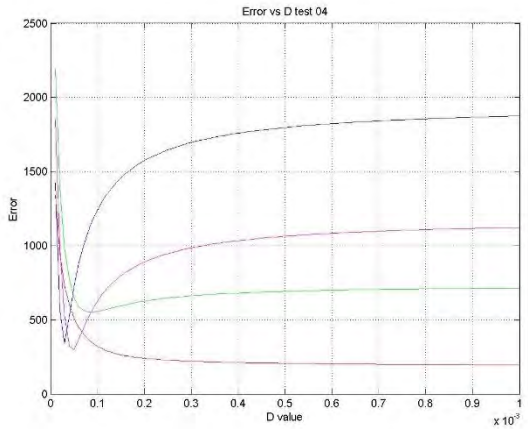

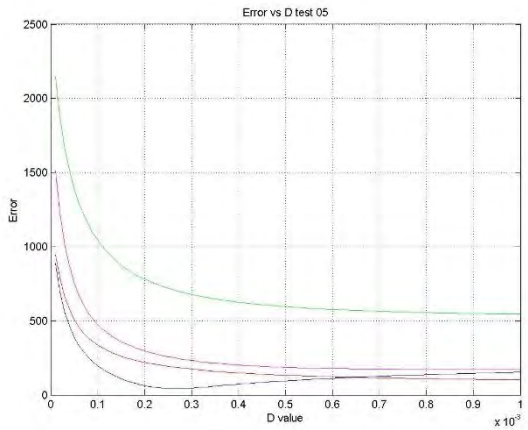

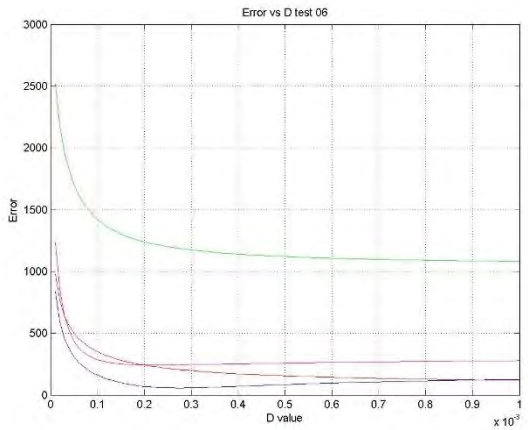

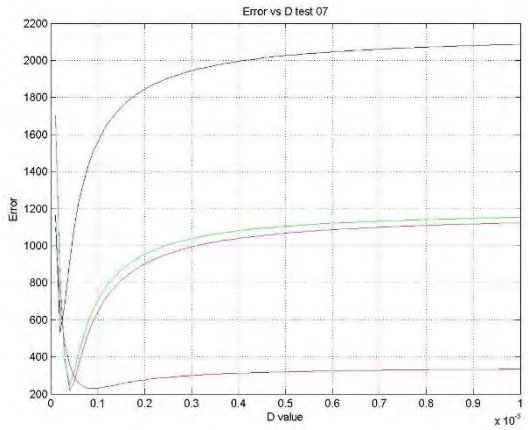
Error vs D test 07
Error
D value
x 10^-3

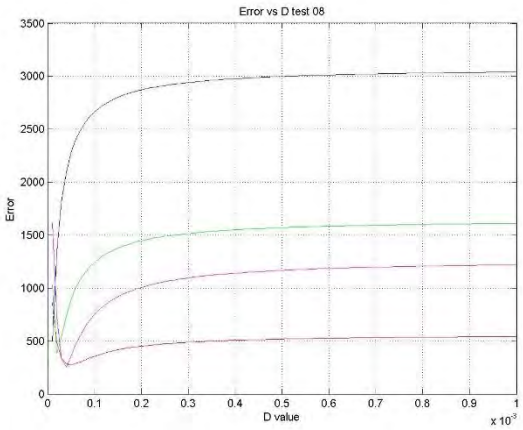
Error vs D test 08
Error
D value
x 10^-3

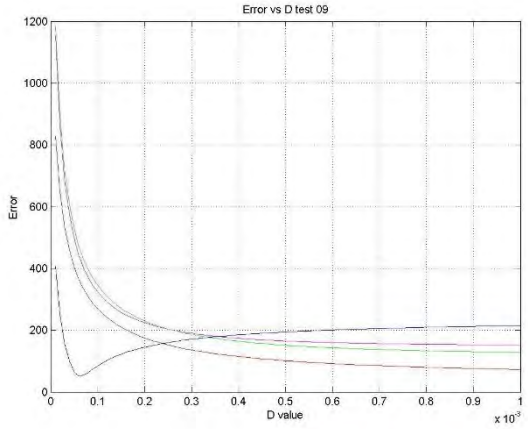
Error vs D test 09
Error
D value
x 10^-3

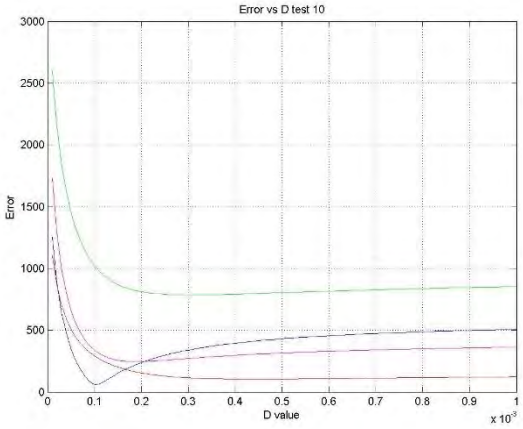
Error vs D test 10
Error
D value
x 10^-3

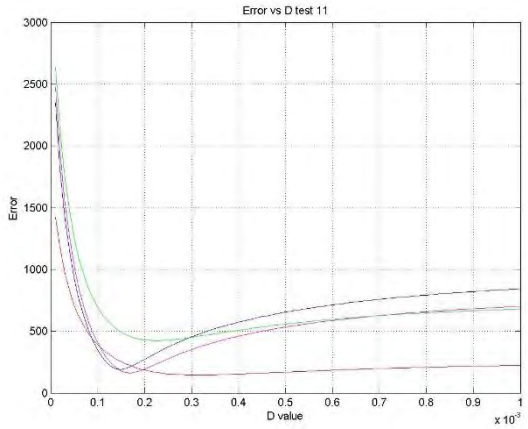
Error vs D test 11
Error
D value
x 10^-3

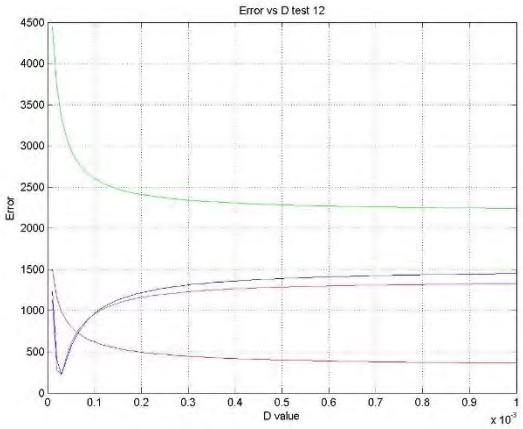
Error vs D test 12
Error
D value
x 10^-3

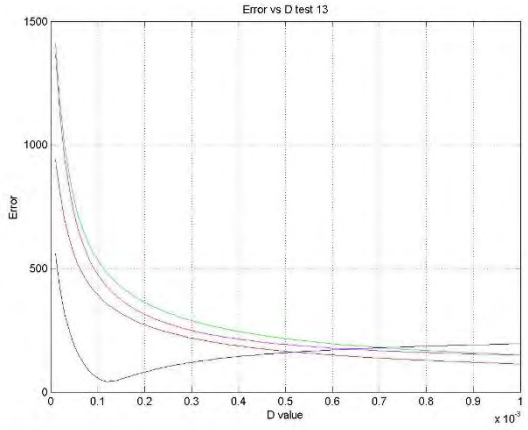
Error vs D test 13
Error
D value
x 10^-3

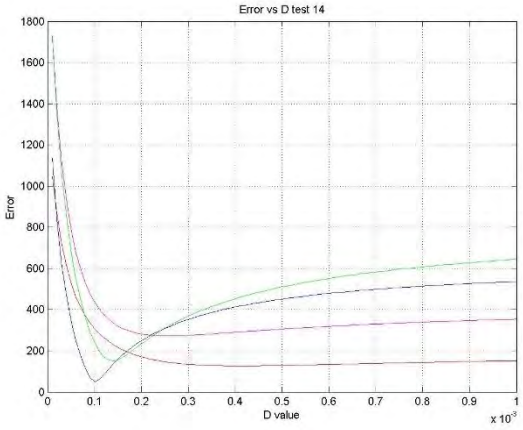
Error vs D test 14
Error
D value
x 10^-3

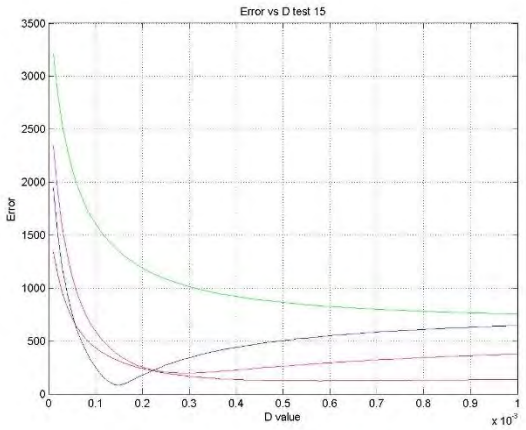

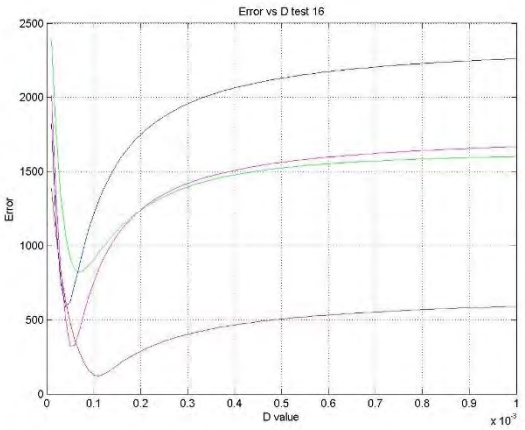

5.1.2 Lorenzerbach

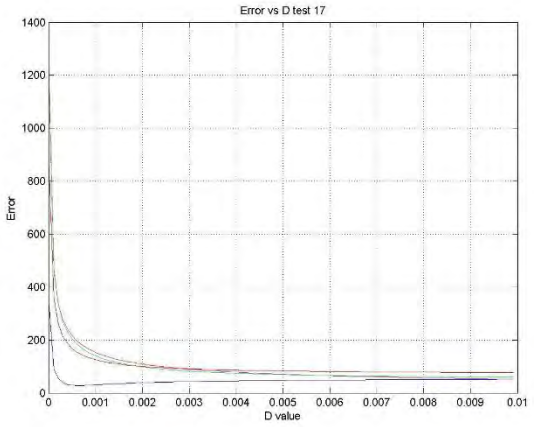

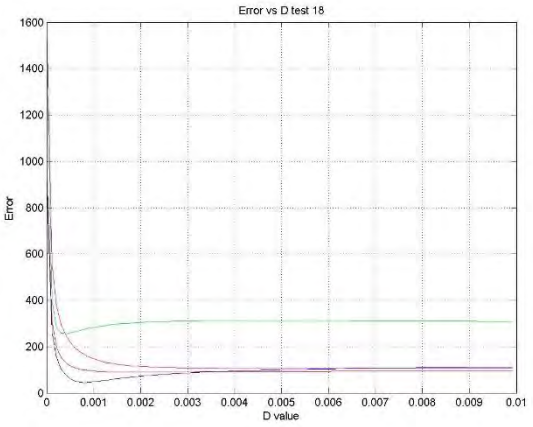

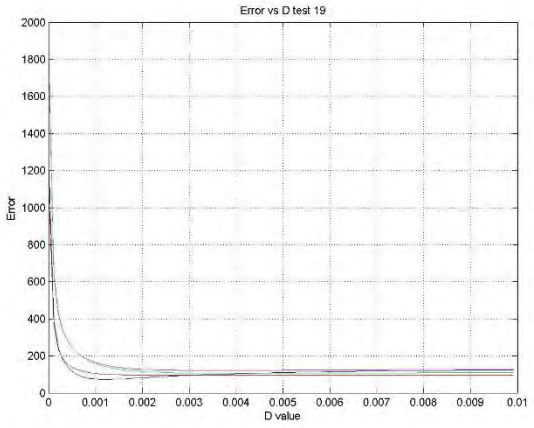

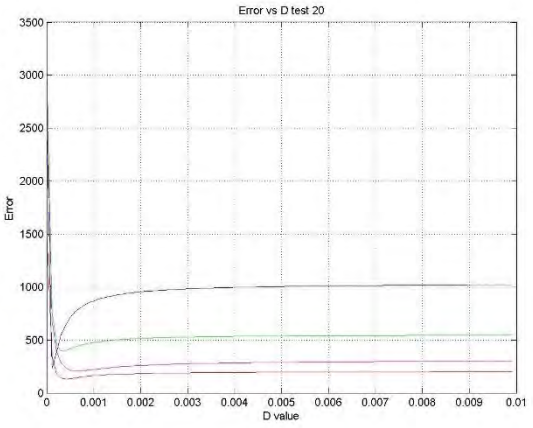

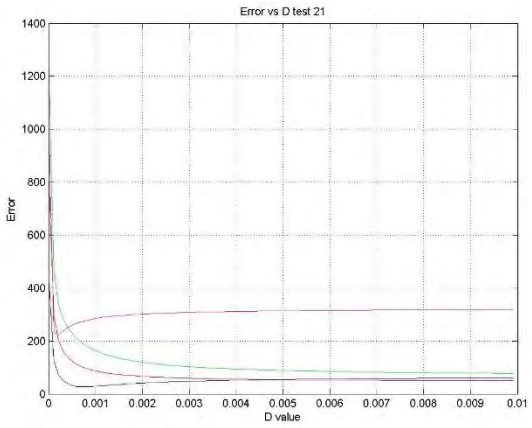
Error vs D test 21
Error
D value

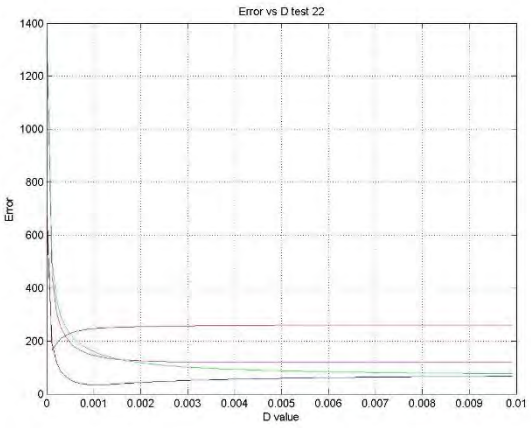
Error vs D test 22
Error
D value

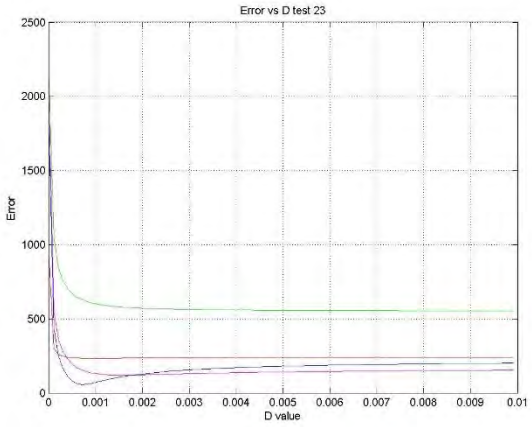
Error vs D test 23
Error
D value

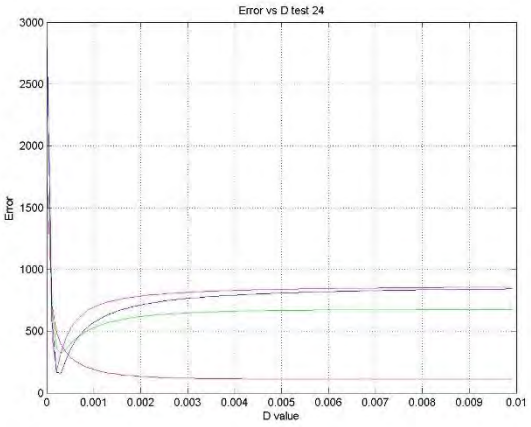
Error vs D test 24
Error
D value

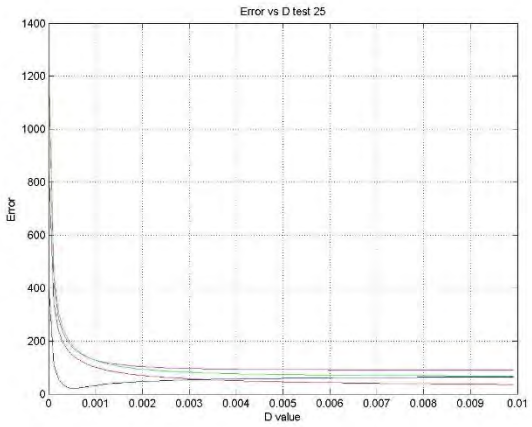
Error vs D test 25
Error
D value

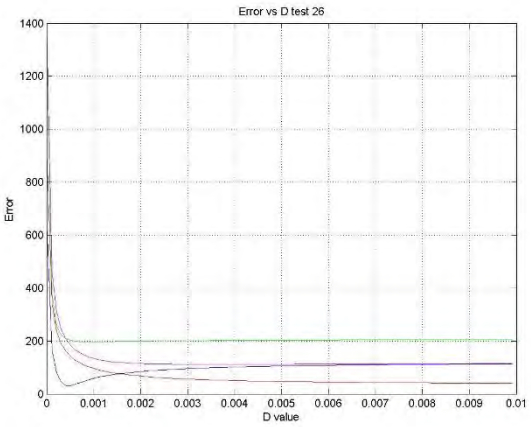
Error vs D test 26
Error
D value

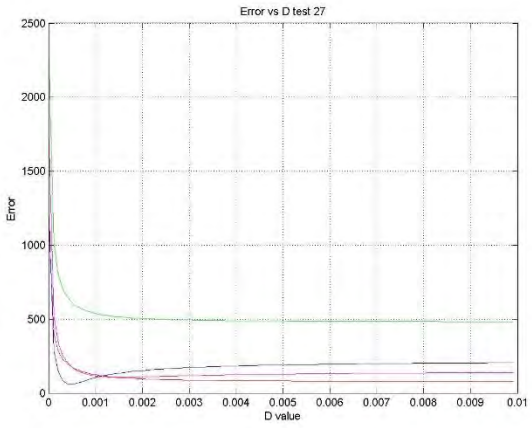
Error vs D test 27
Error
D value

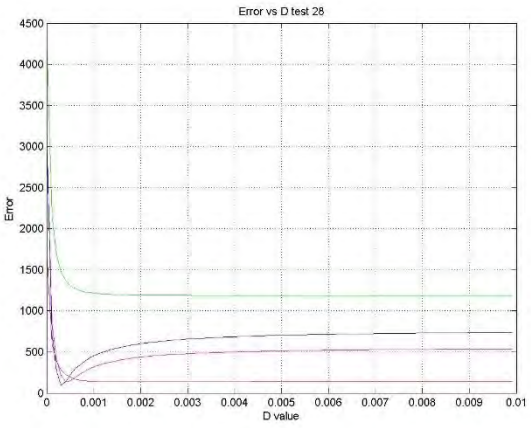
Error vs D test 28
Error
D value

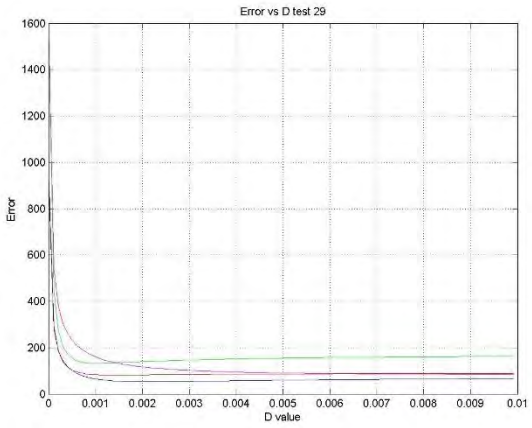
Error vs D test 29
Error
D value
0
200
400
600
800
1000
1200
1400
1600
0.001
0.002
0.003
0.004
0.005
0.006
0.007
0.008
0.009
0.01

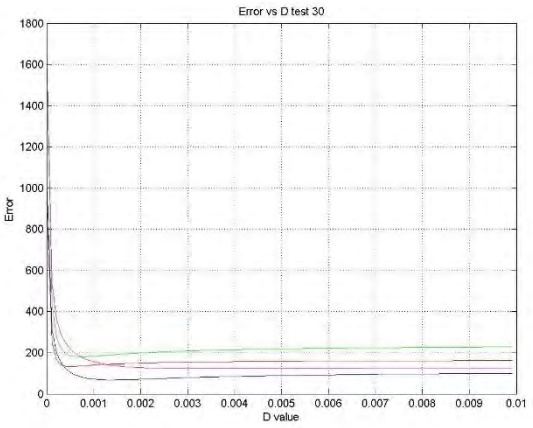
Error vs D test 30
Error
D value
0
200
400
600
800
1000
1200
1400
1600
1800
0.001
0.002
0.003
0.004
0.005
0.006
0.007
0.008
0.009
0.01

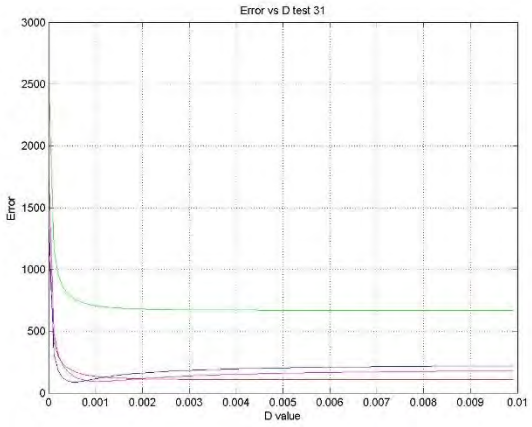
Error vs D test 31
Error
D value
0
500
1000
1500
2000
2500
3000
0.001
0.002
0.003
0.004
0.005
0.006
0.007
0.008
0.009
0.01

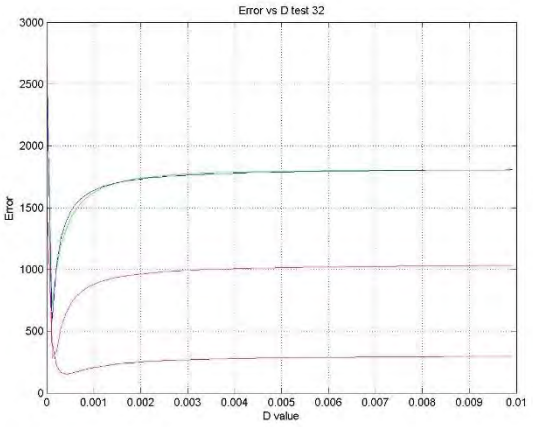
Error vs D test 32
Error
D value
0
500
1000
1500
2000
2500
3000
0.001
0.002
0.003
0.004
0.005
0.006
0.007
0.008
0.009
0.01

5.2 TESTS FITTING

5.2.1 Scalalarufe

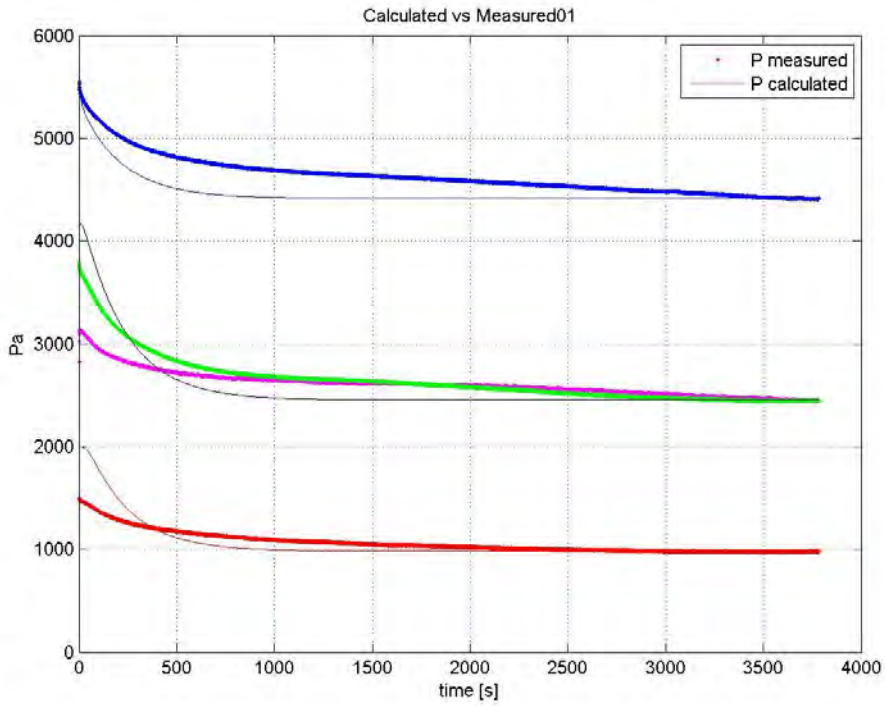

Figure 5.2.a

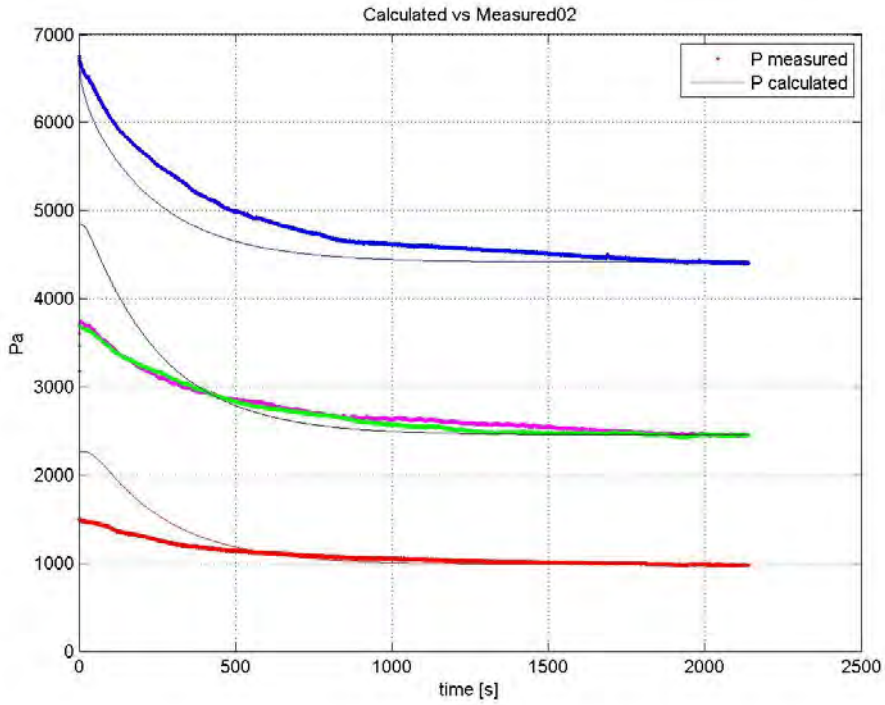

Figure 5.2.b

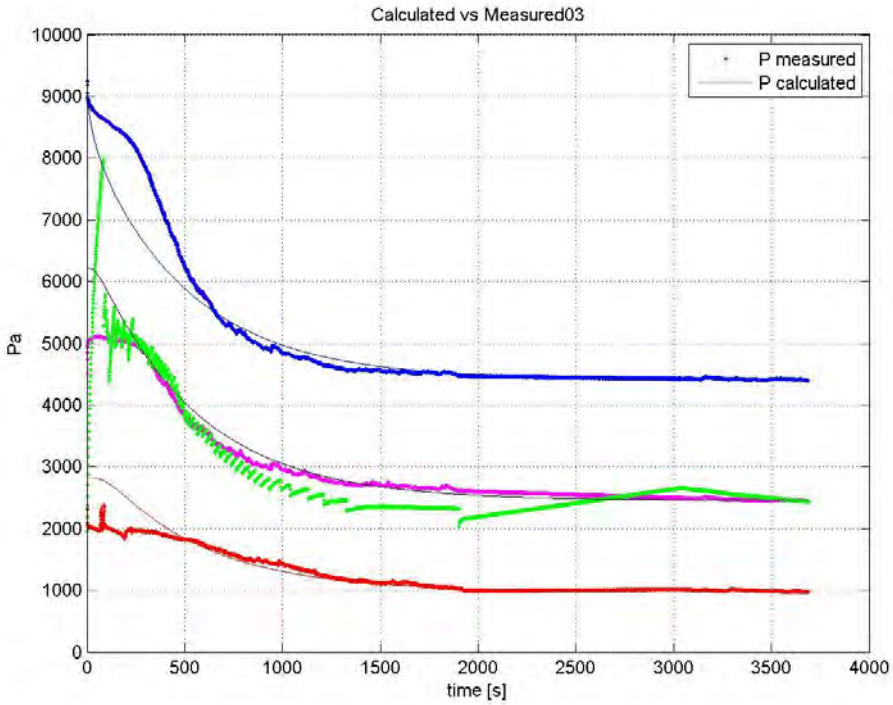

Figure 5.2.c

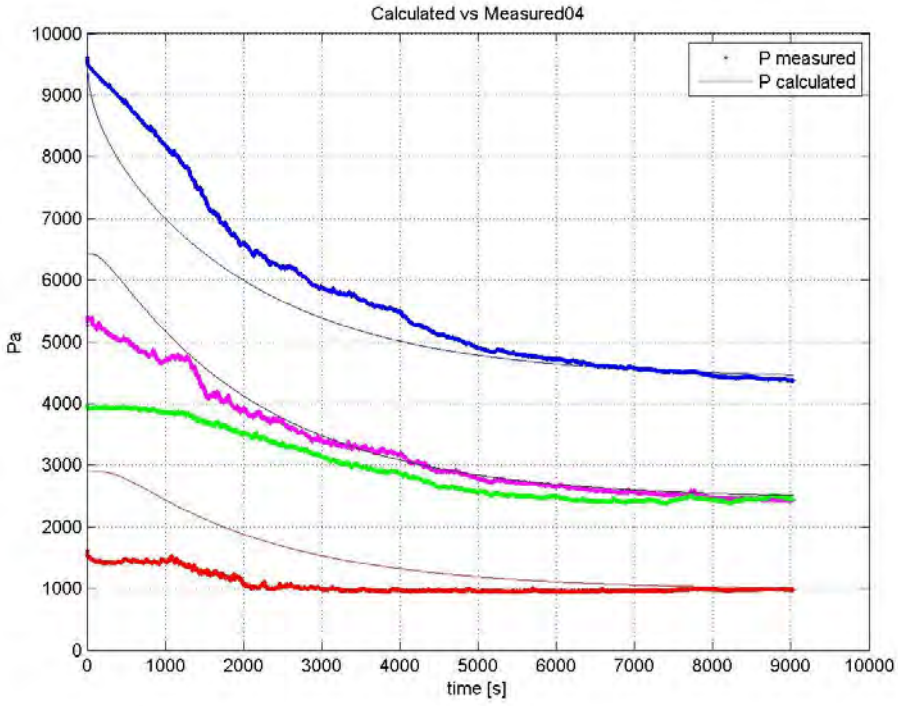

Figure 5.2.d

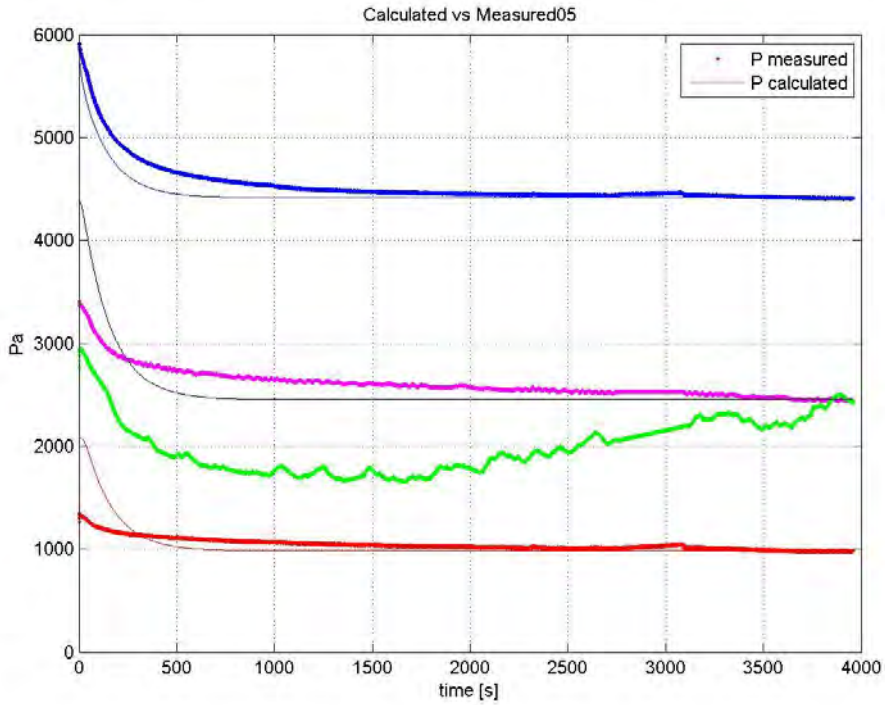

Figure 5.2.e

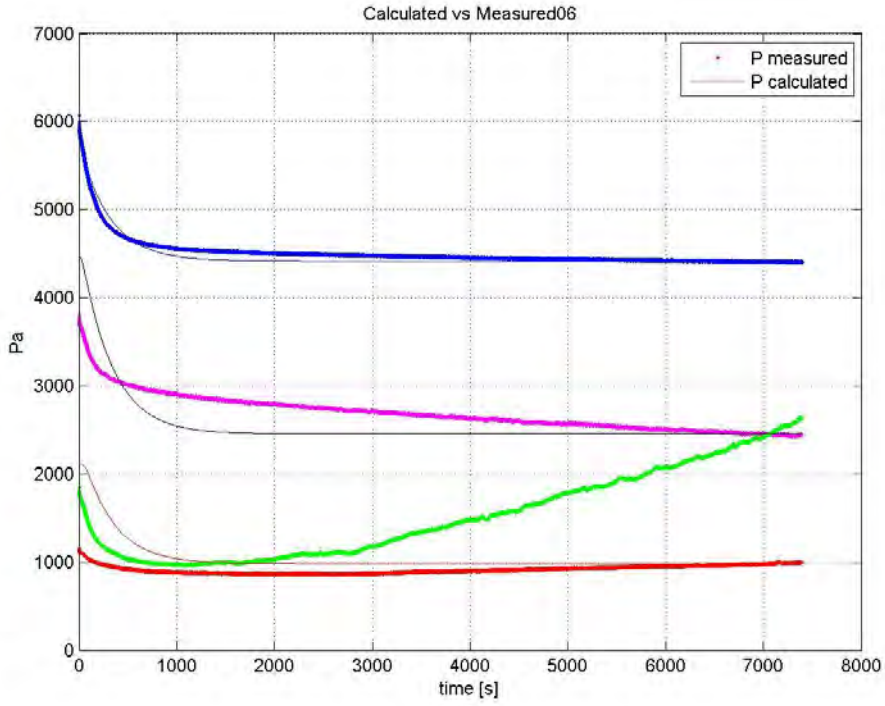

Figure 5.2.f

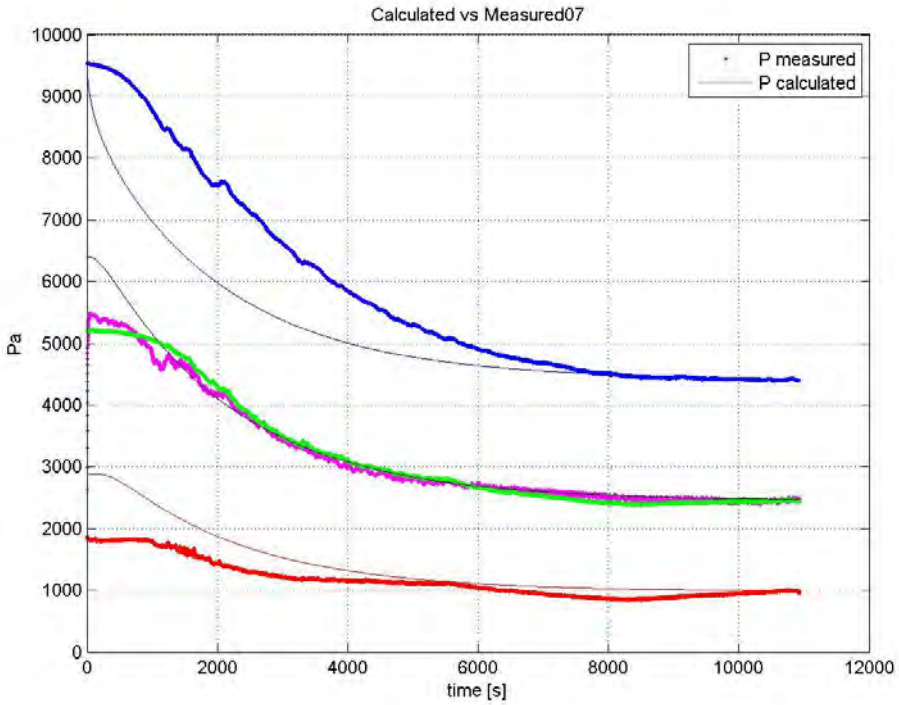

Figure 5.2.g

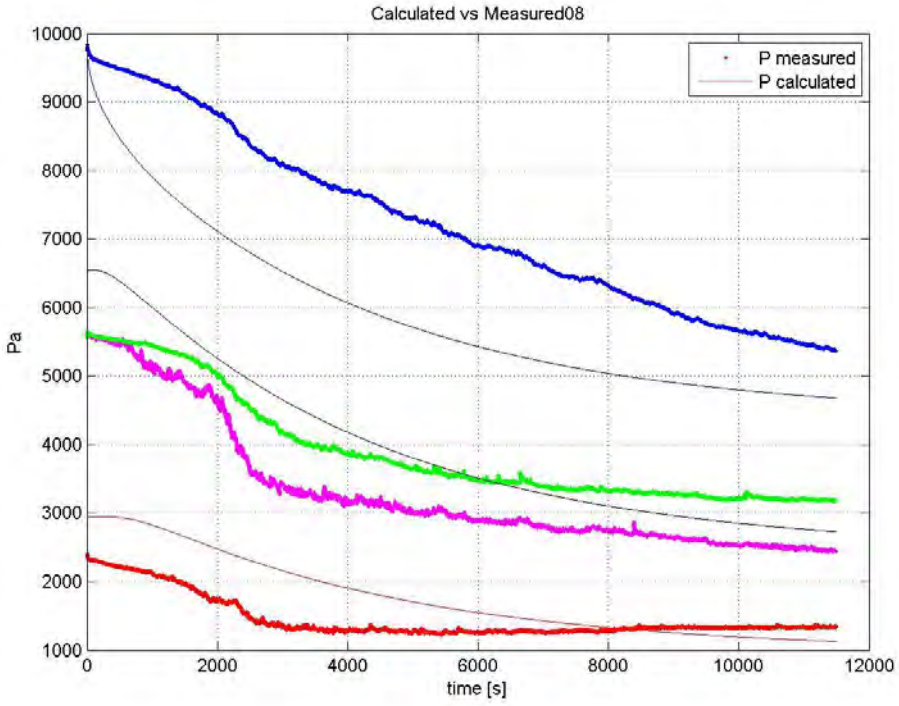

Figure 5.2.h

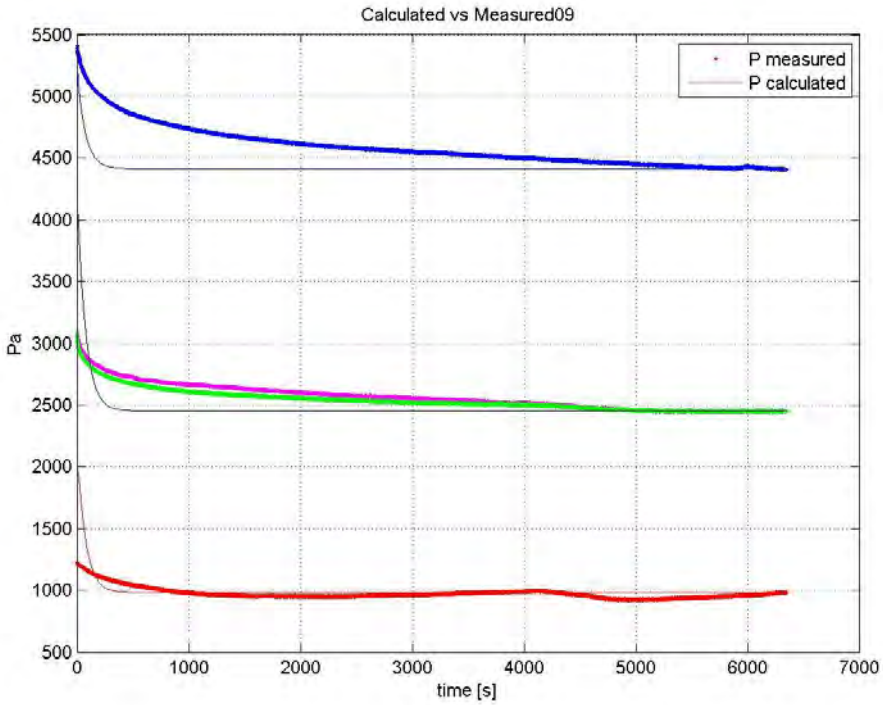

Figure 5.2.i

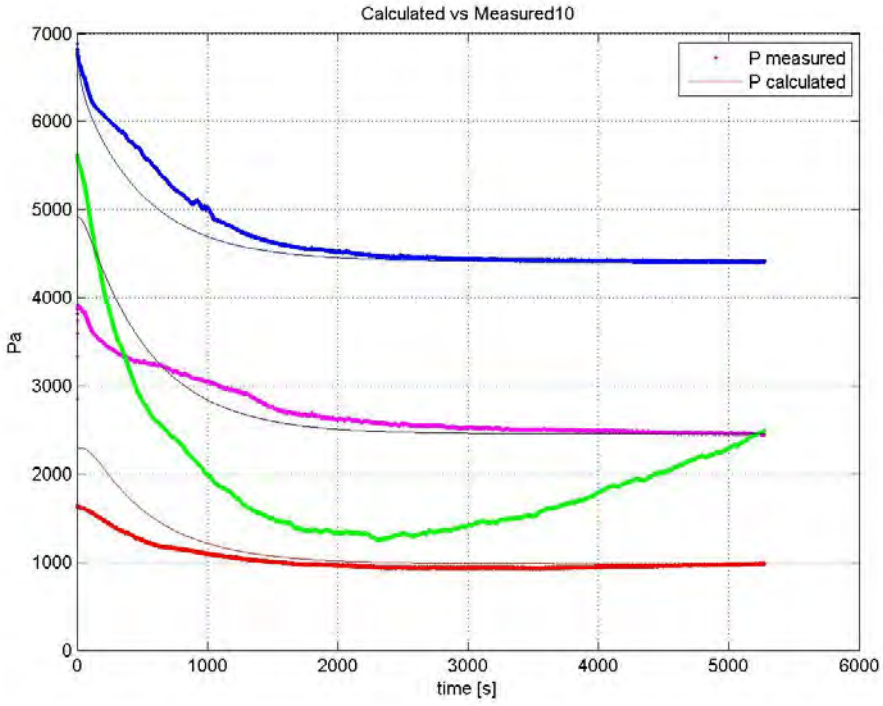

Figure 5.2.j

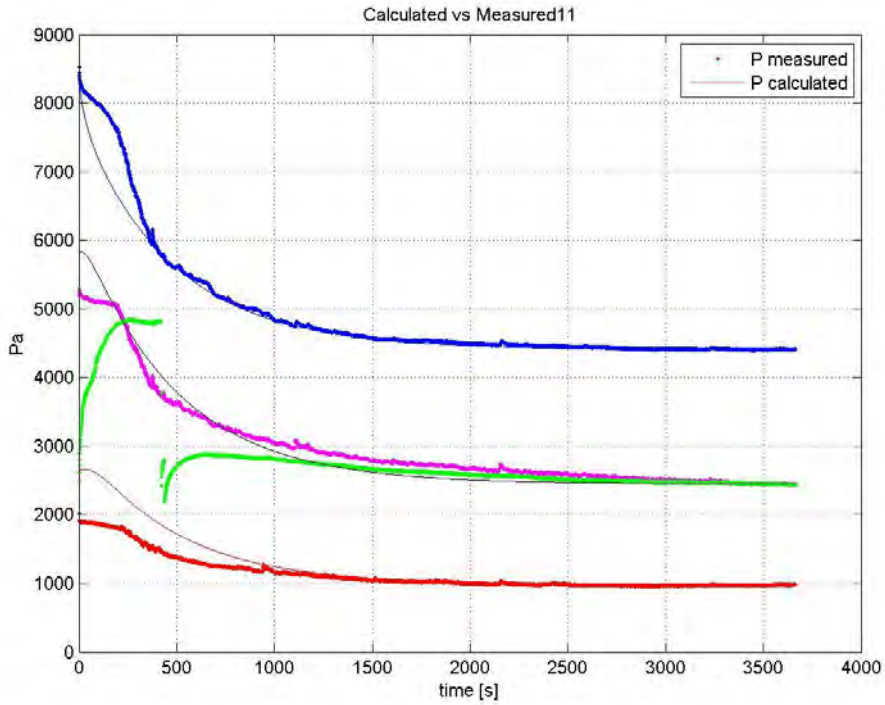

Figure 5.2.k

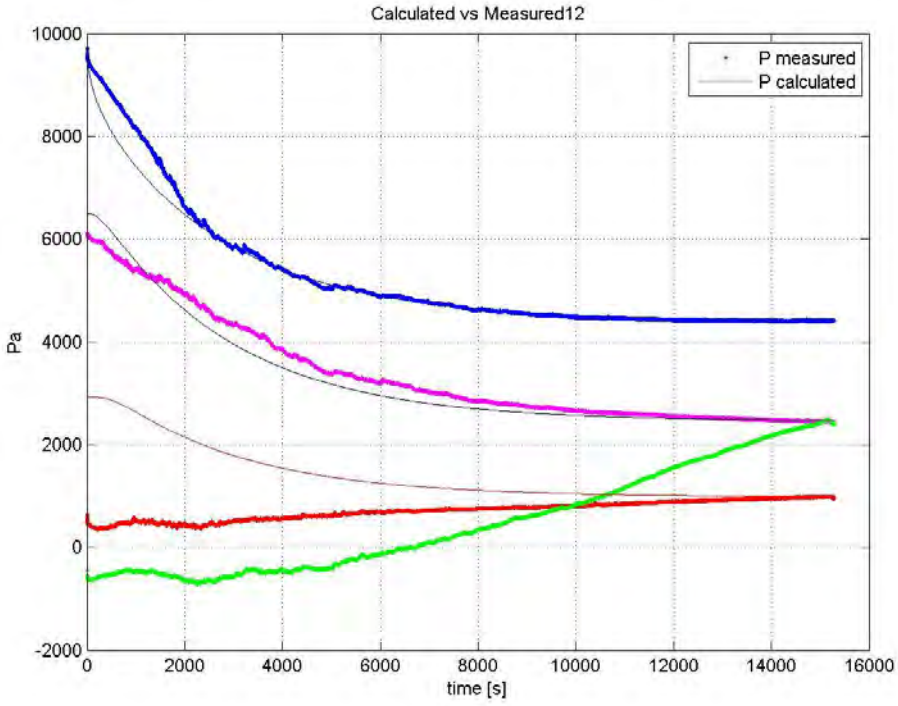

Figure 5.2.l

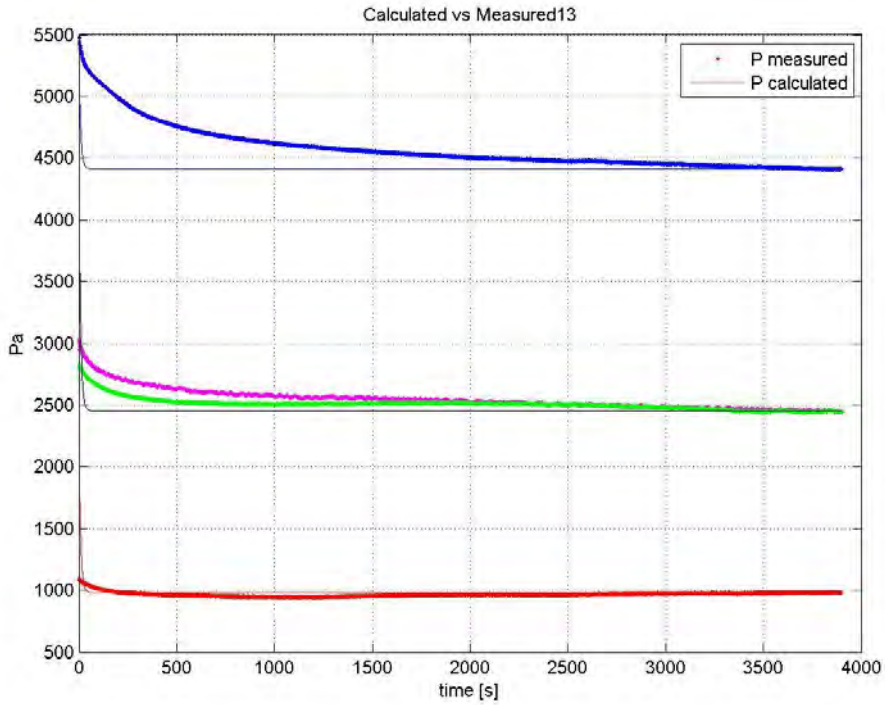

Figure 5.2.m

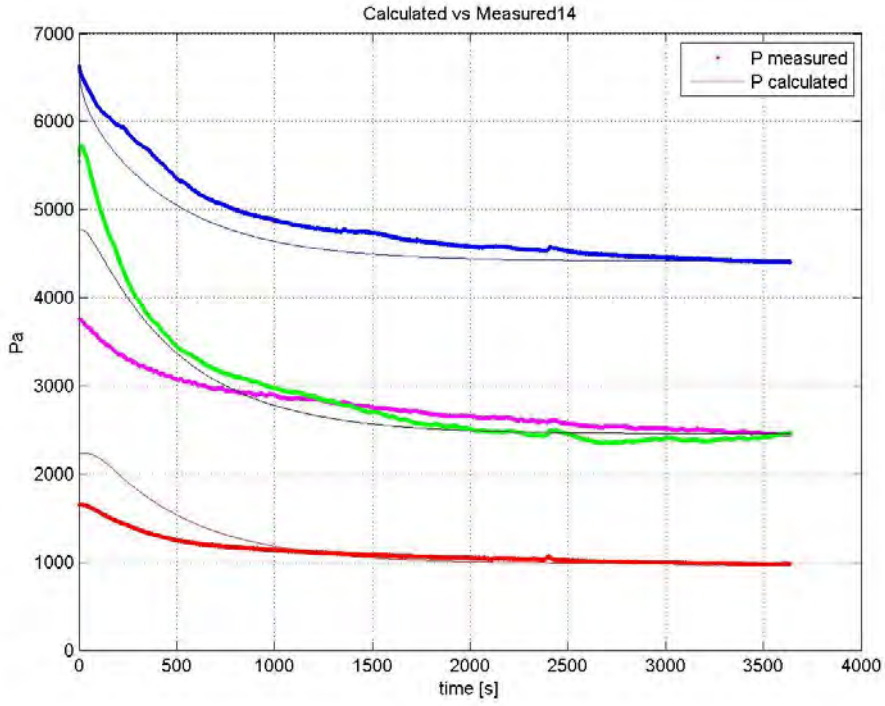

Figure 5.2.n

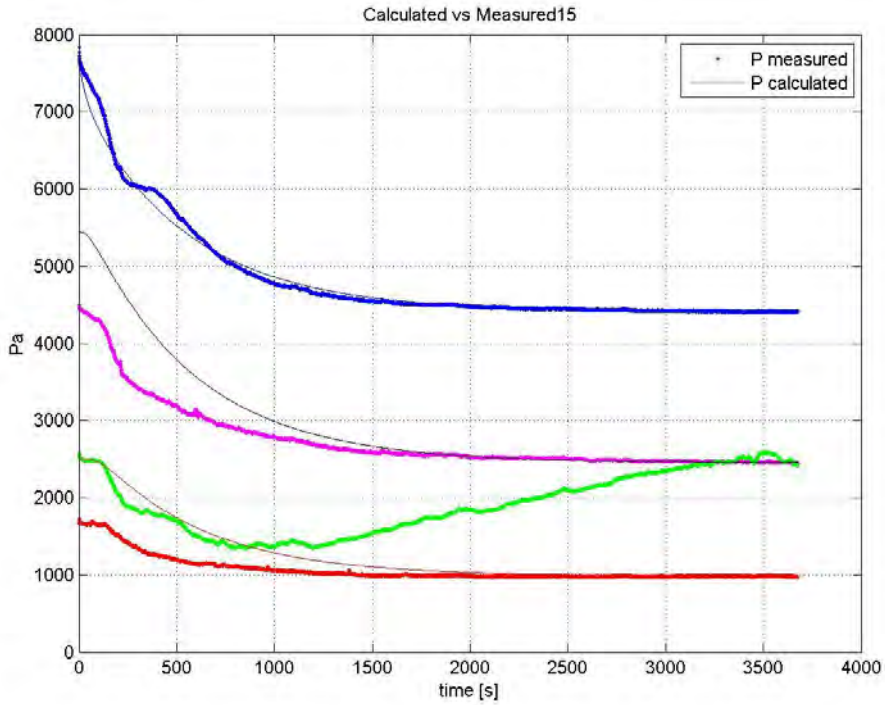

Figure 5.2.o

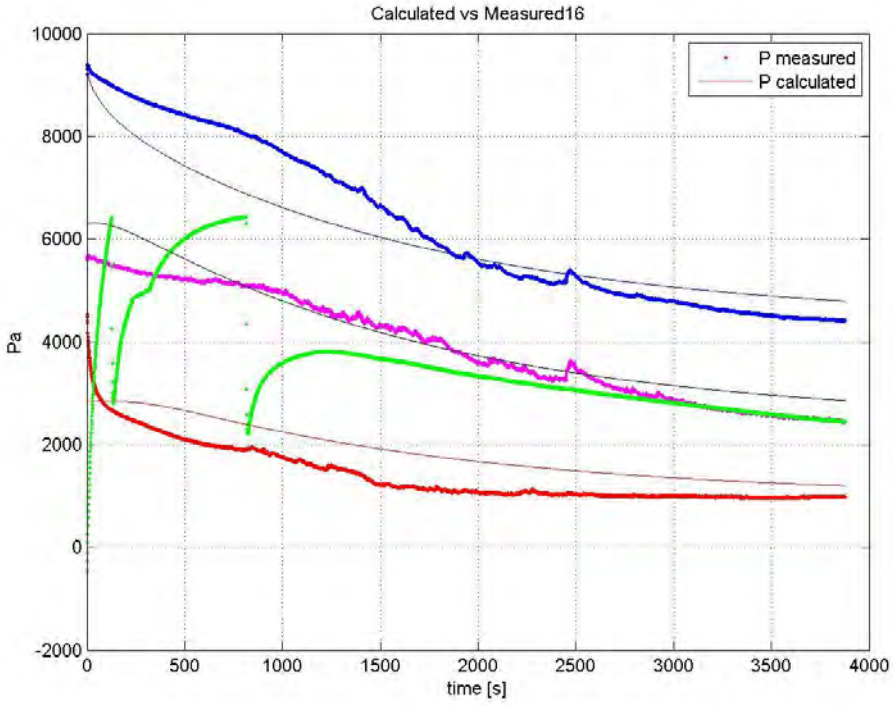

Figure 5.2.p

5.2.2 Lorenzerbach

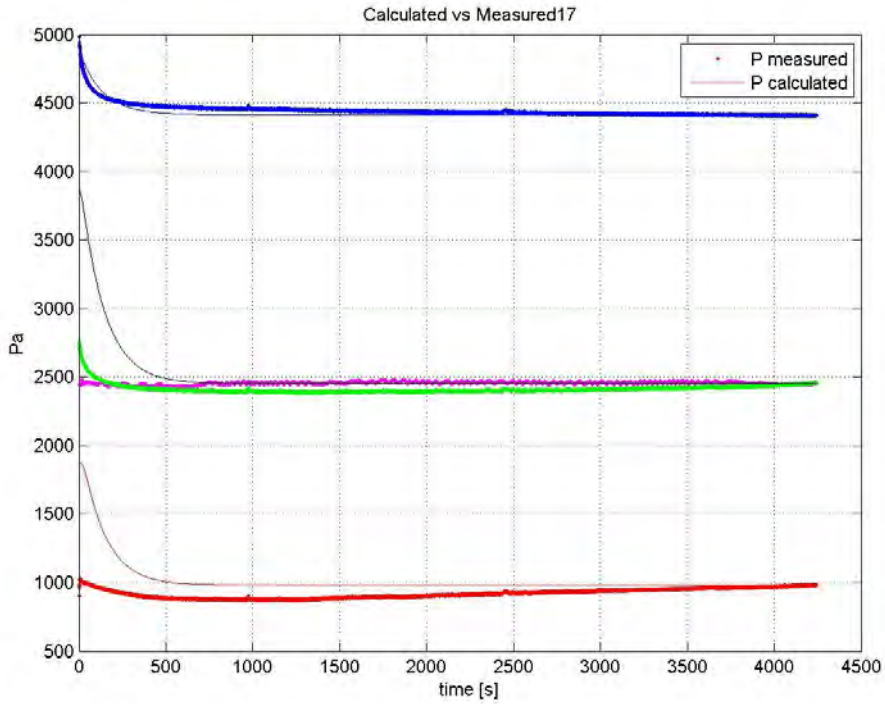

Figure 5.2.q

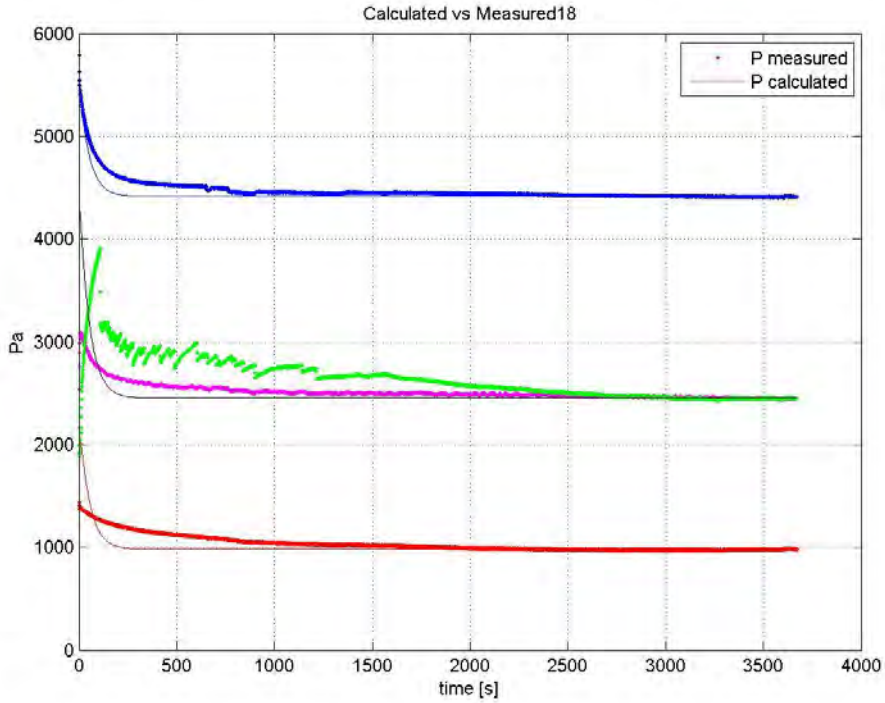

Figure 5.2.r

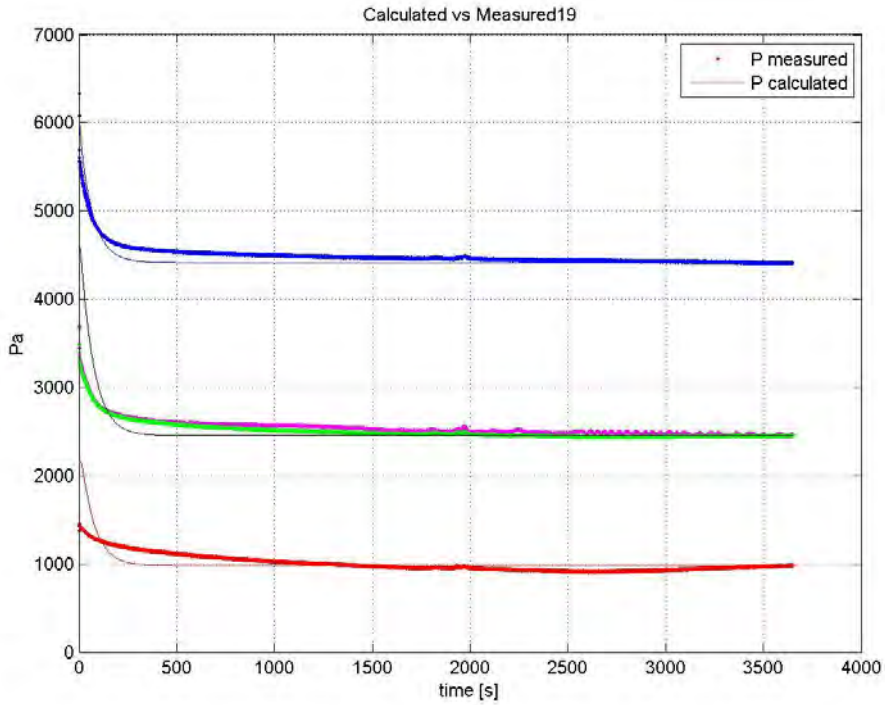

Figure 5.2.s

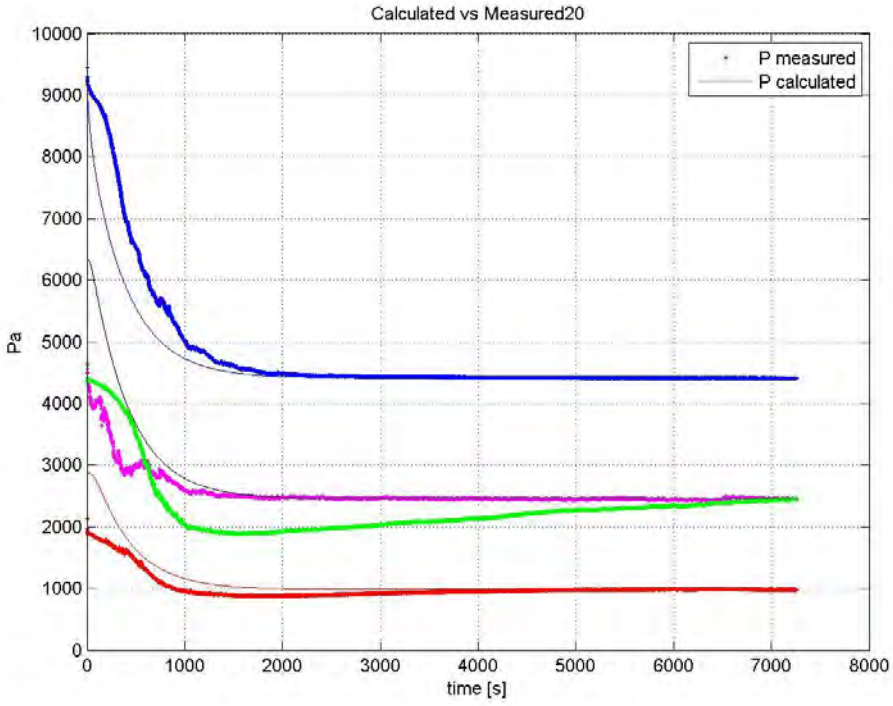

Figure 5.2.t

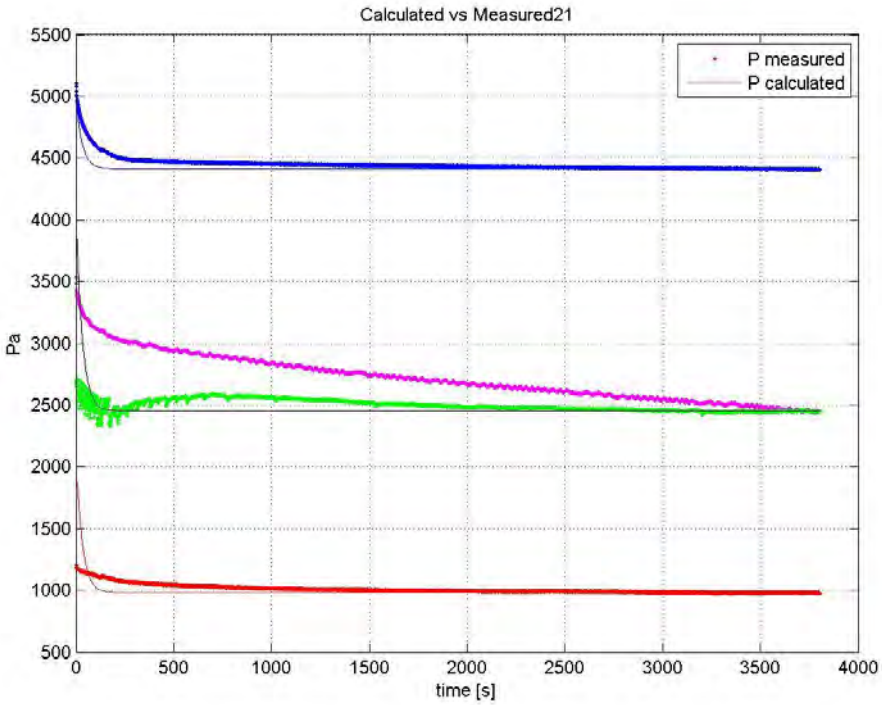

Figure 5.2.u

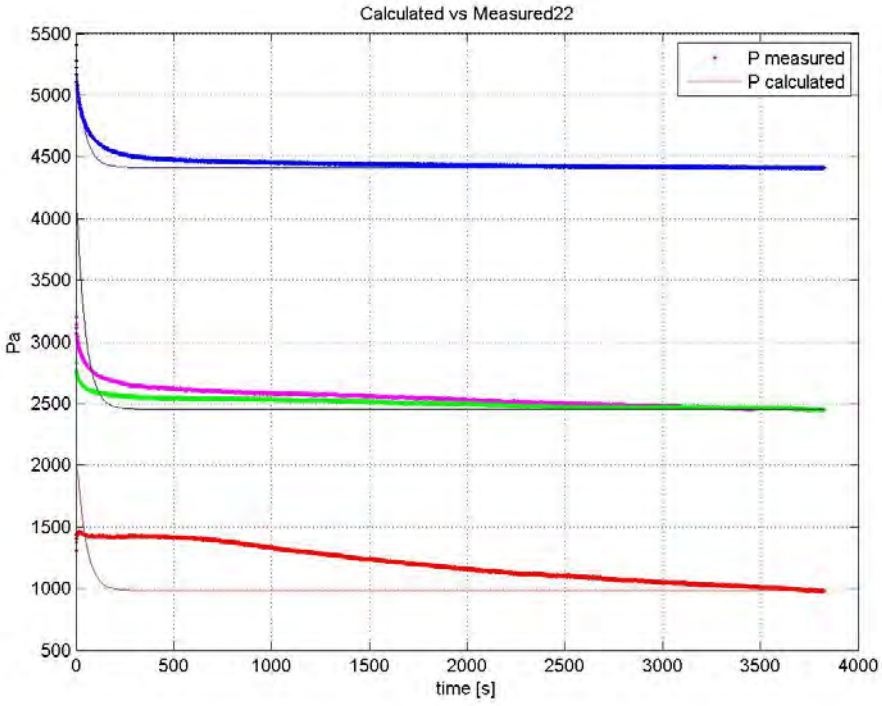

Figure 5.2.v

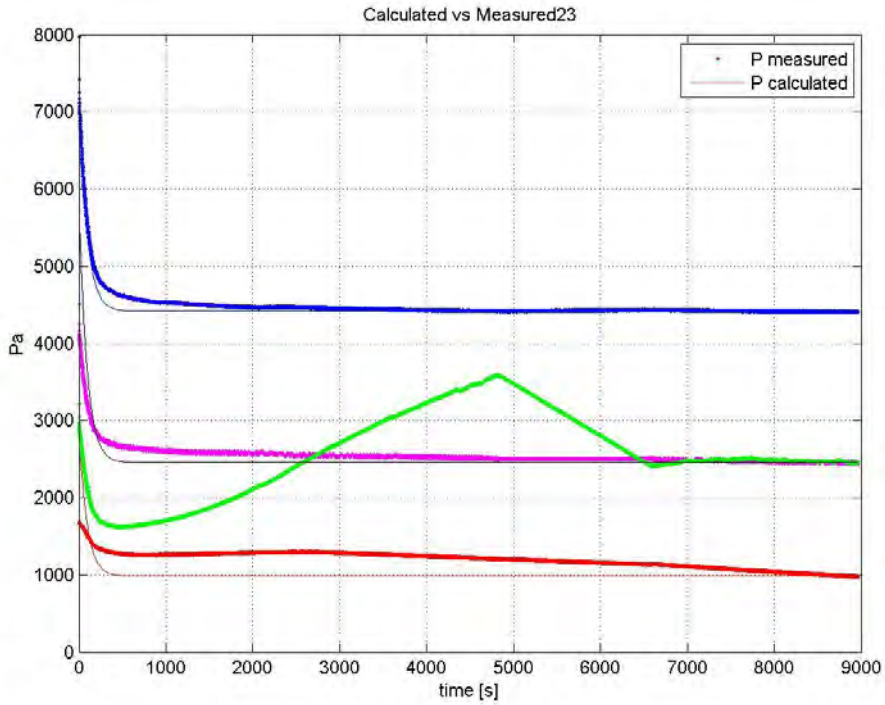

Figure 5.2.w

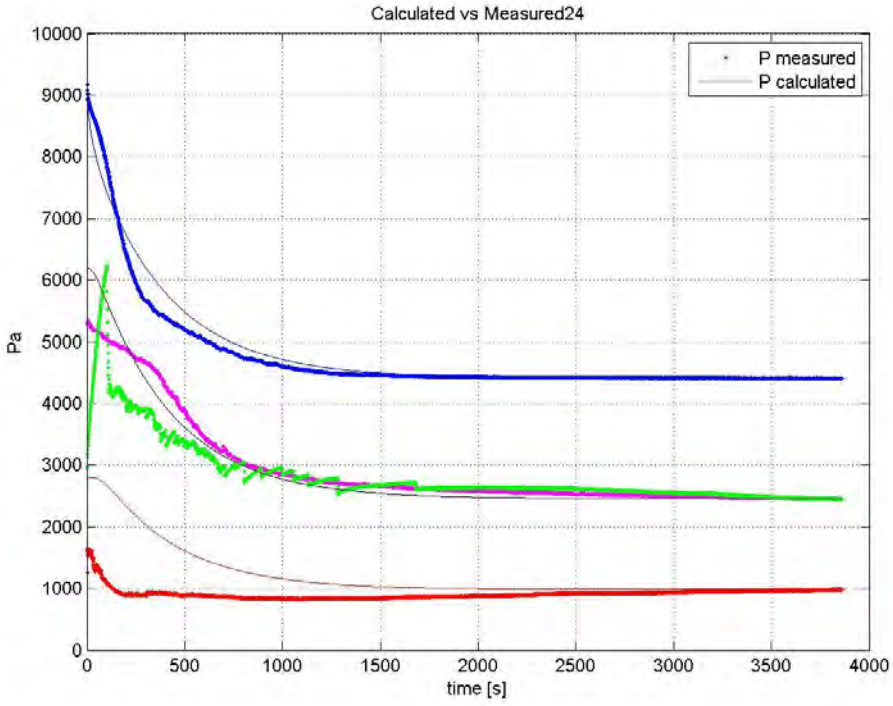

Figure 5.2.x

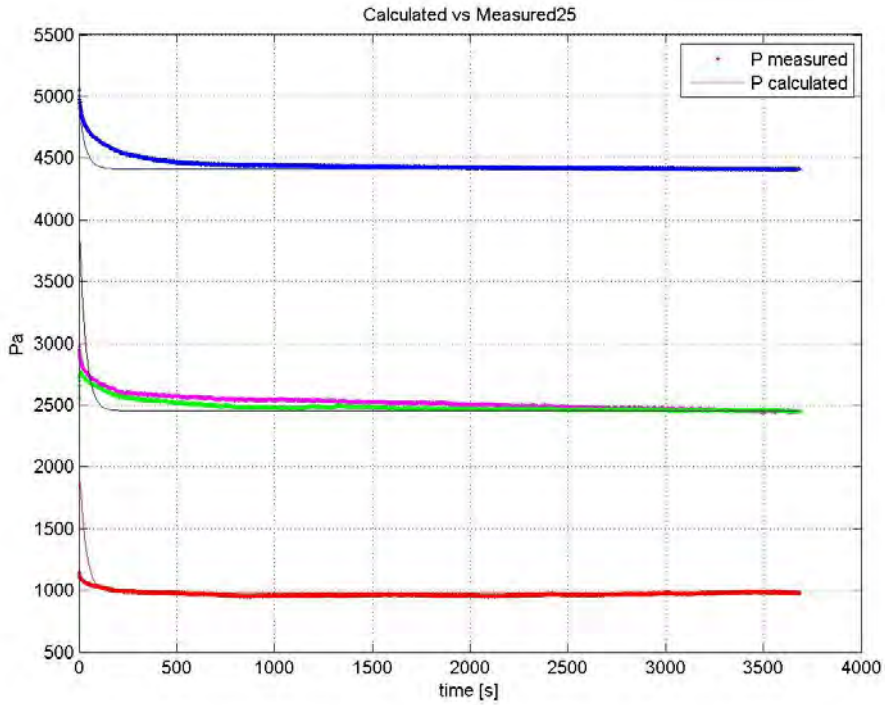

Figure 5.2.y

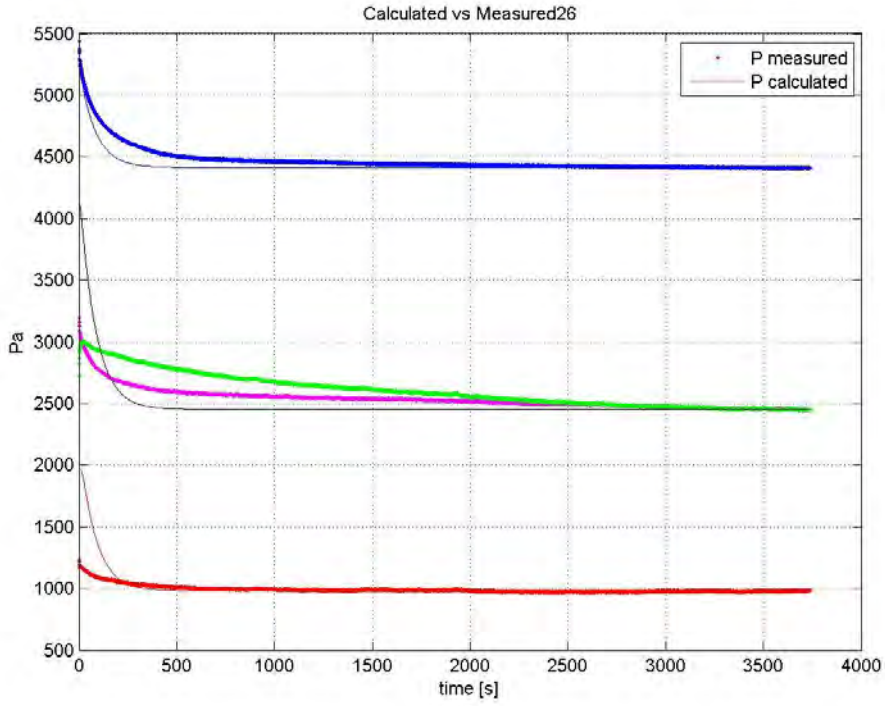

Figure 5.2.z

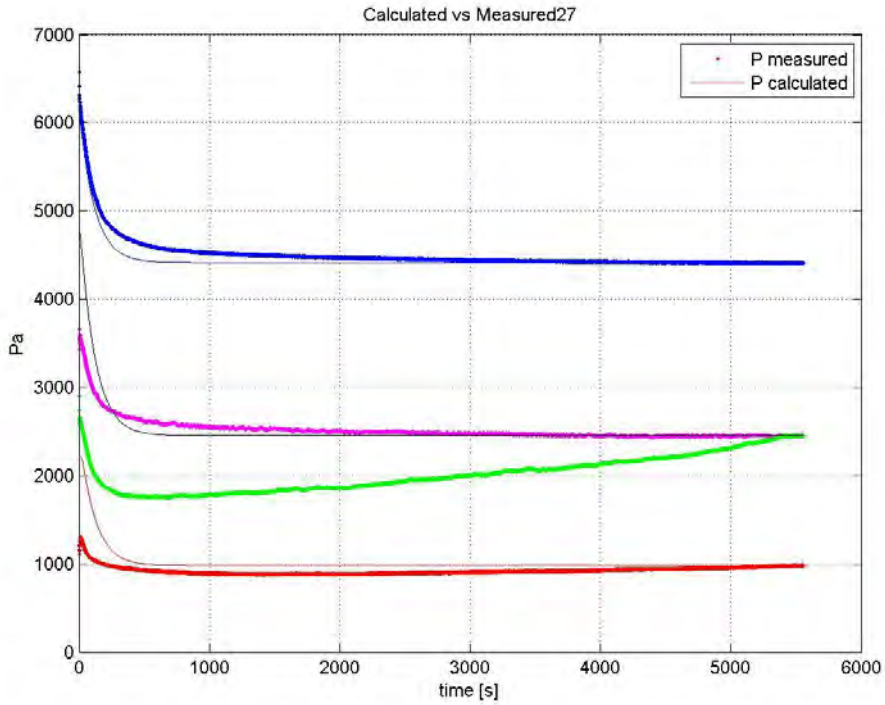

Figure 5.2.aa

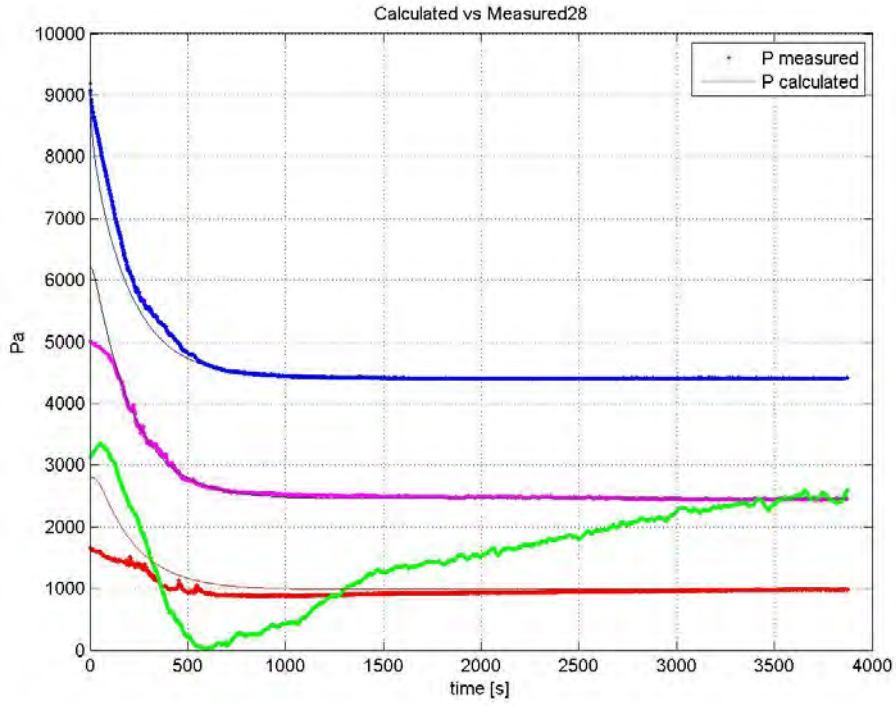

Figure 5.2.bb

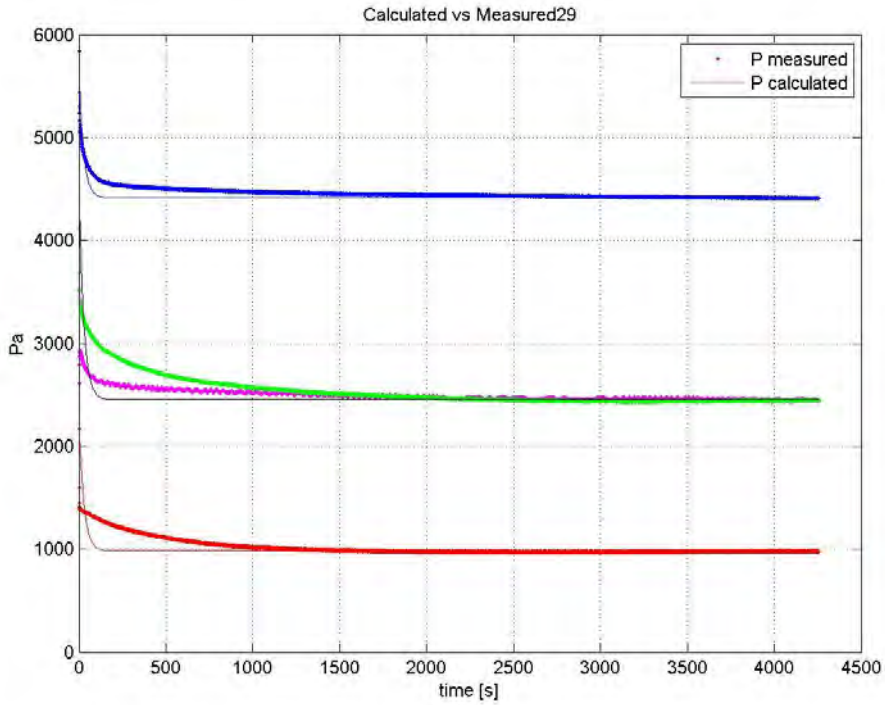

Figure 5.2.cc

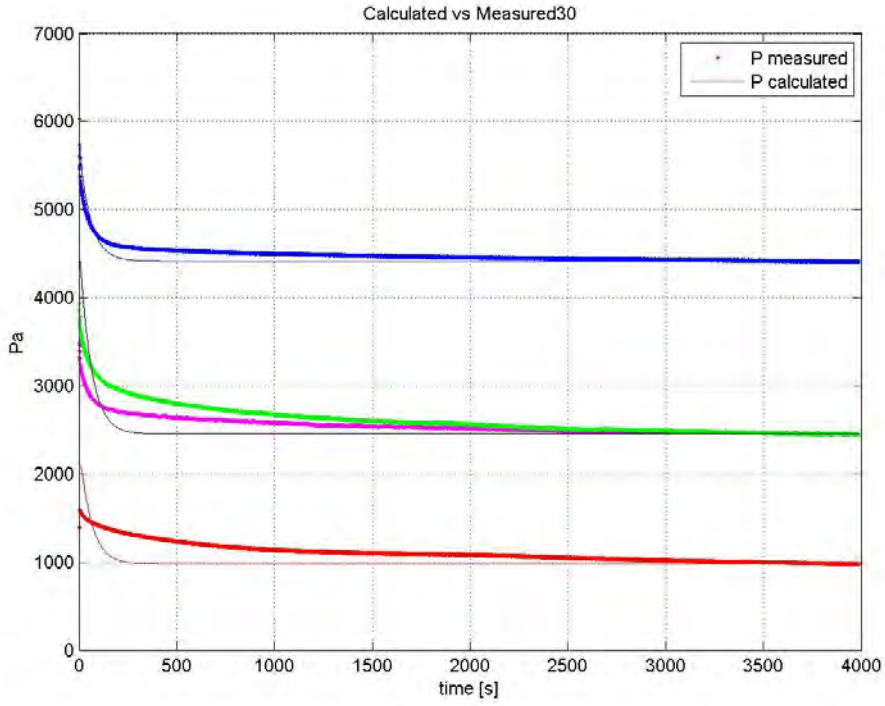

Figure 5.2.dd

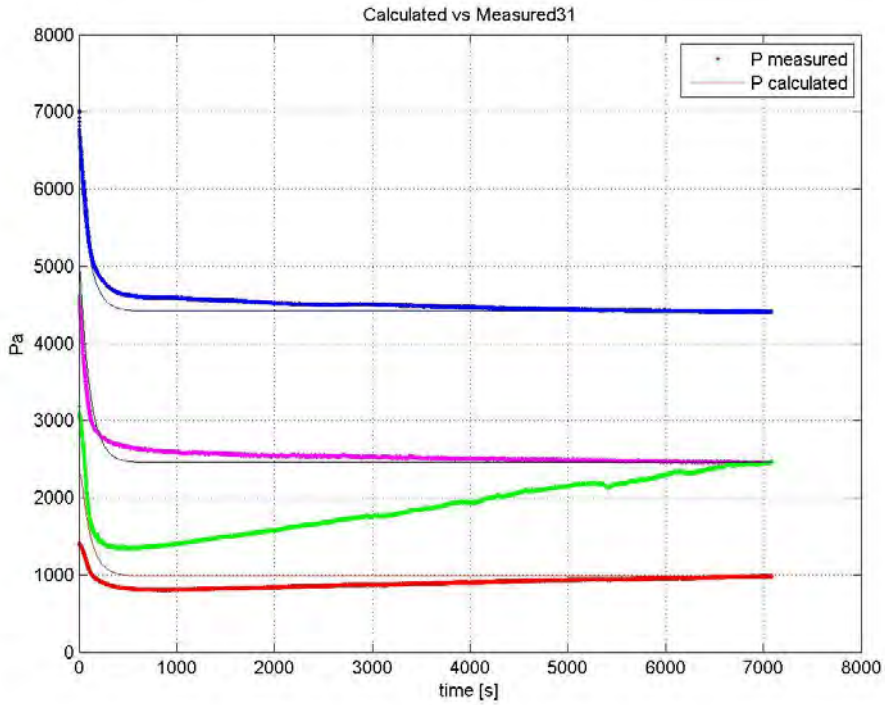

Figure 5.2.ee

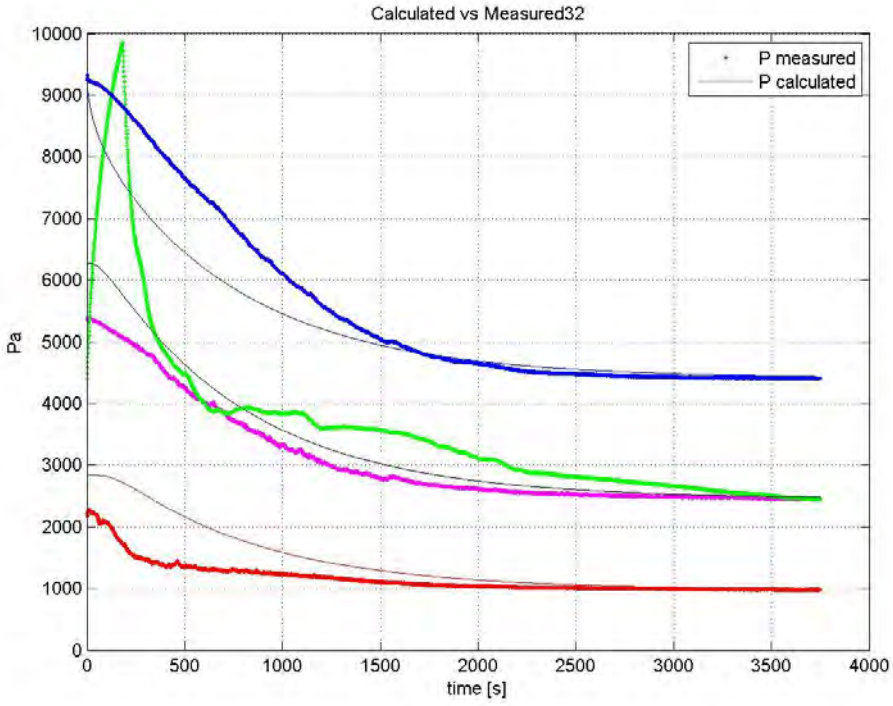

Figure 5.2.ff

5.3 COMPARED GRAPHICS

The following graphics are about the comparison of the bottom sensor series for the 32 test. They are grouped together by four:

- Figure 5.3.a to Figure 5.3.a show the effects of fine-grained particles concentration changes on the different coarse-grained particles composition for the Scalärarüfe samples;
- Figure 5.3.e to Figure 5.3.h show the effects of different coarse composition changes on the different fine particles concentrations for the Scalärarüfe samples;
- Figure 5.3.i to Figure 5.3.l show the effects of fine-grained particles concentration changes on the different coarse-grained particles composition for the Lorenzerbach samples;
- Figure 5.3.m to Figure 5.3.p show the effects of different coarse composition changes on the different fine particles concentrations for the Lorenzerbach samples;

5.3.1 Scalärarüfe

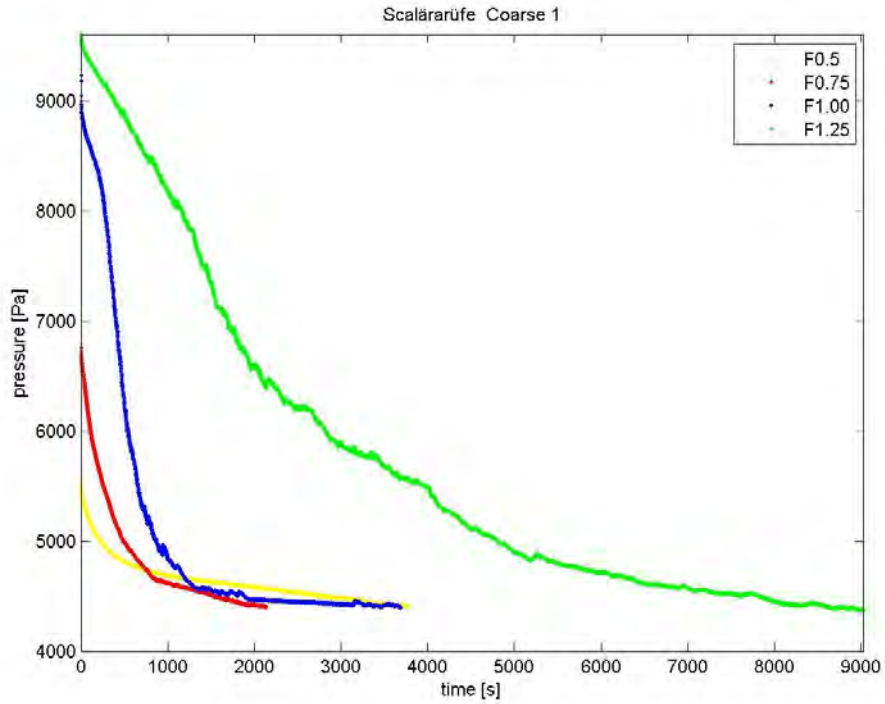

Figure 5.3.a

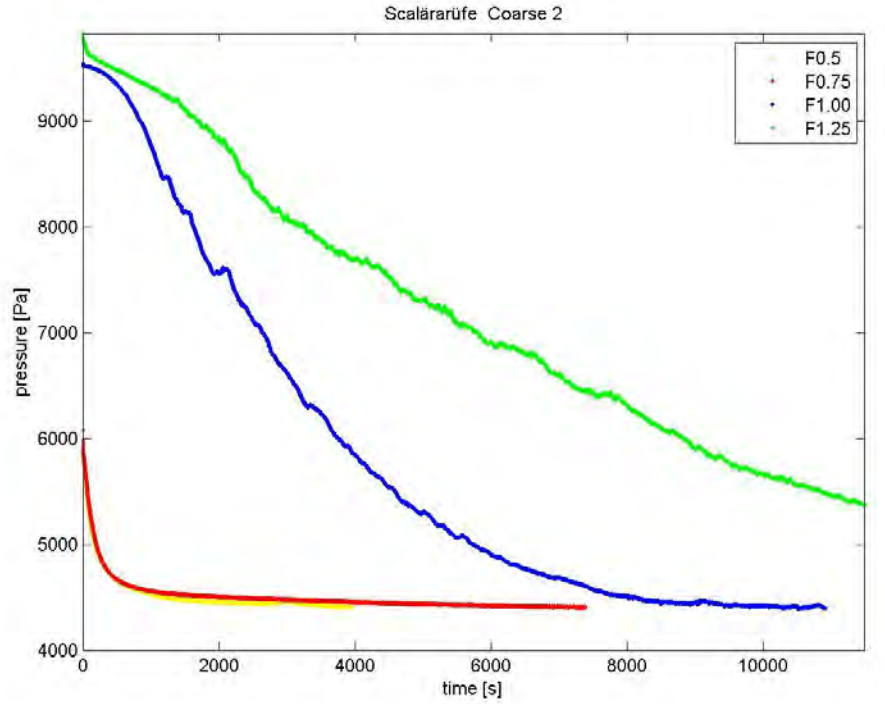

Figure 5.3.b

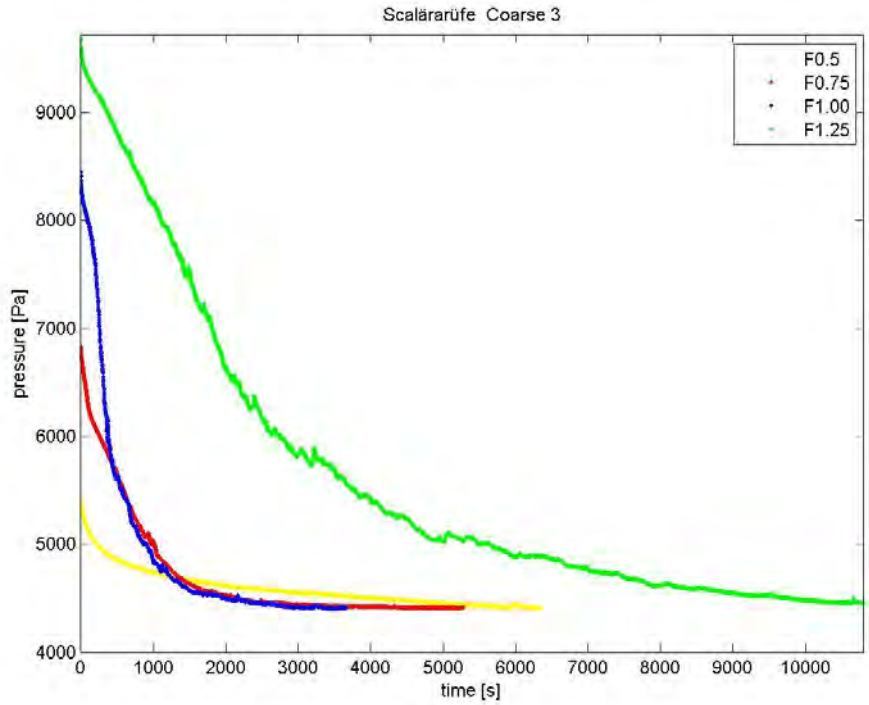

Figure 5.3.c

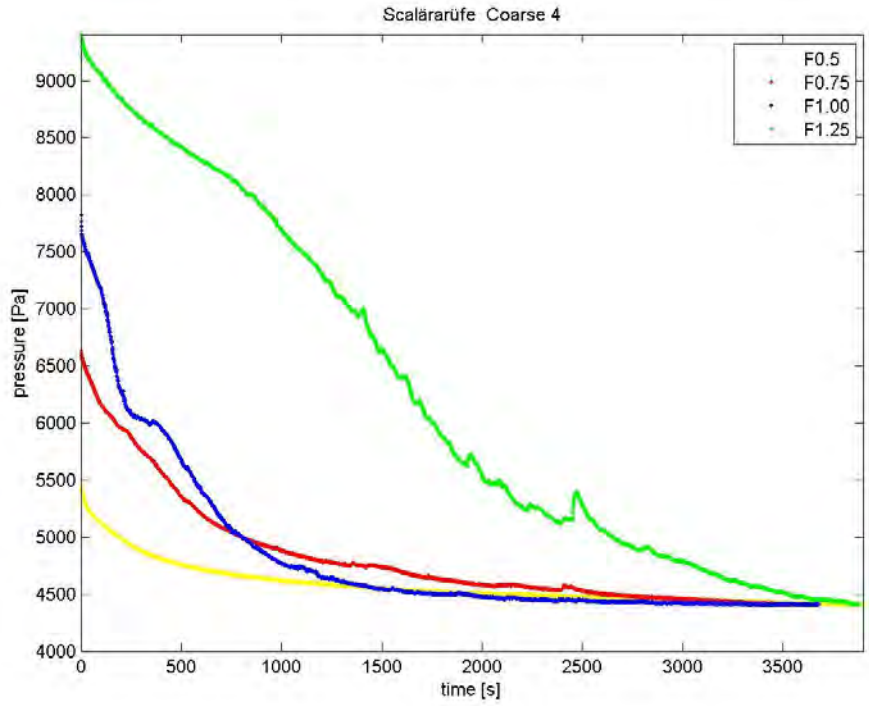

Figure 5.3.d

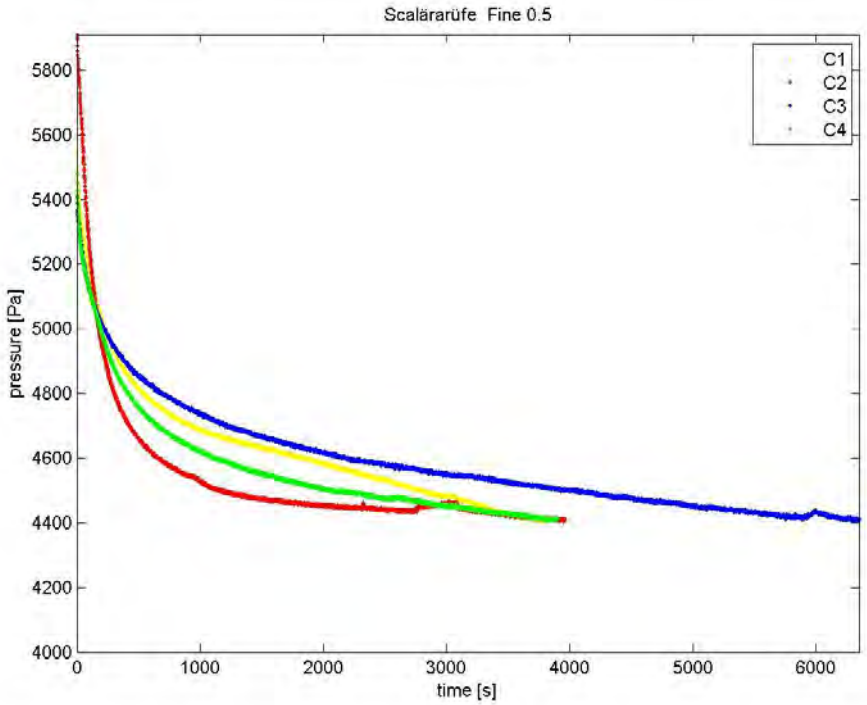

Figure 5.3.e

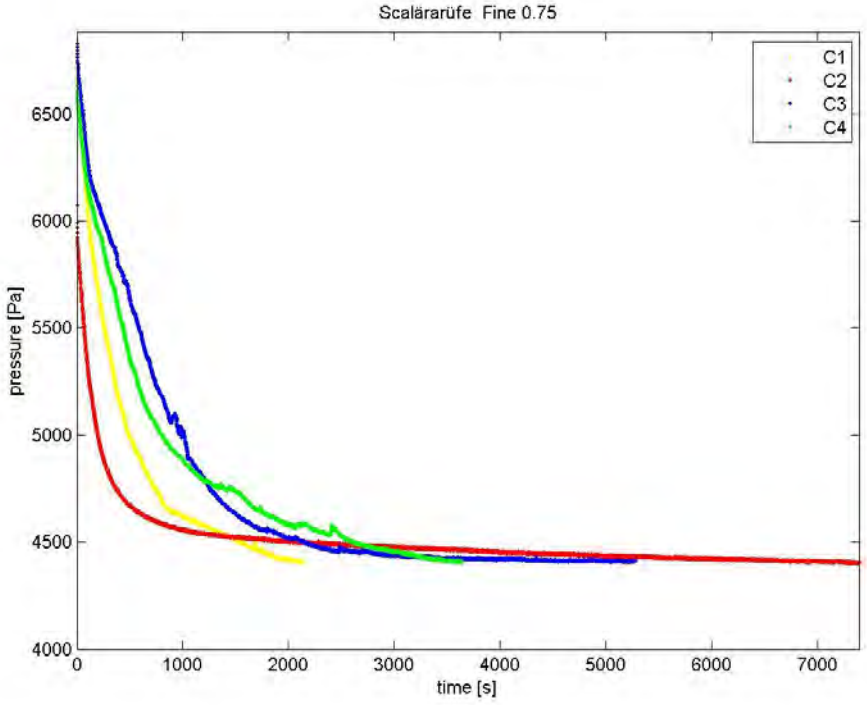

Figure 5.3.f

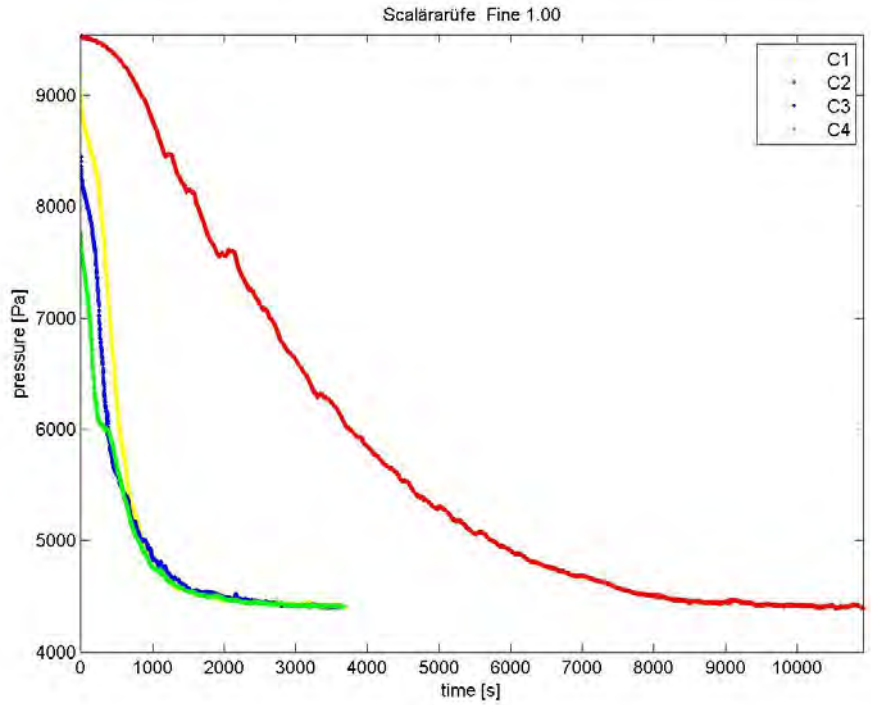

Figure 5.3.g

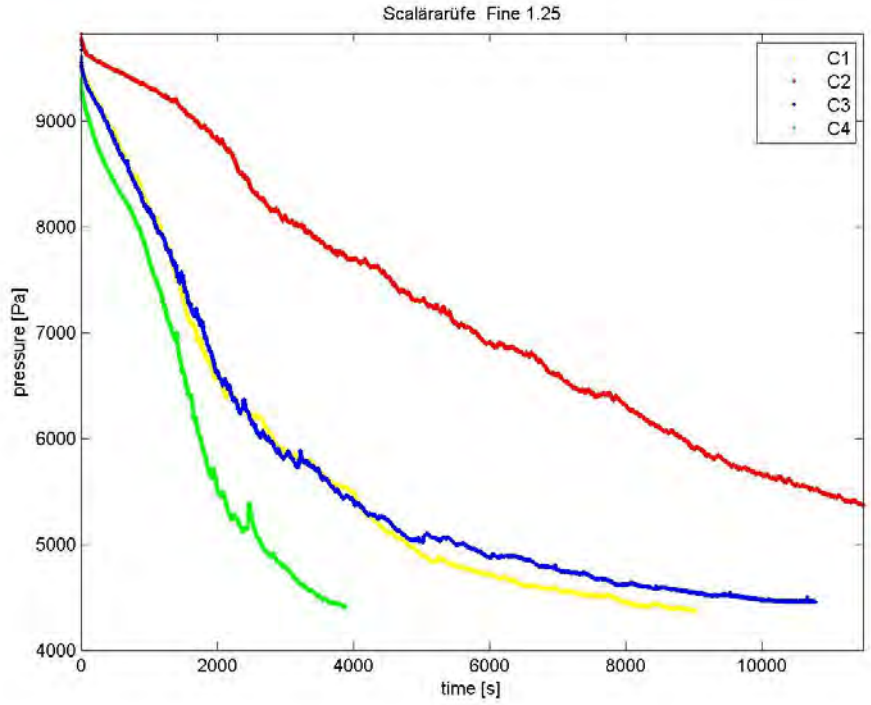

Figure 5.3.h

5.3.2 Lorenzerbach

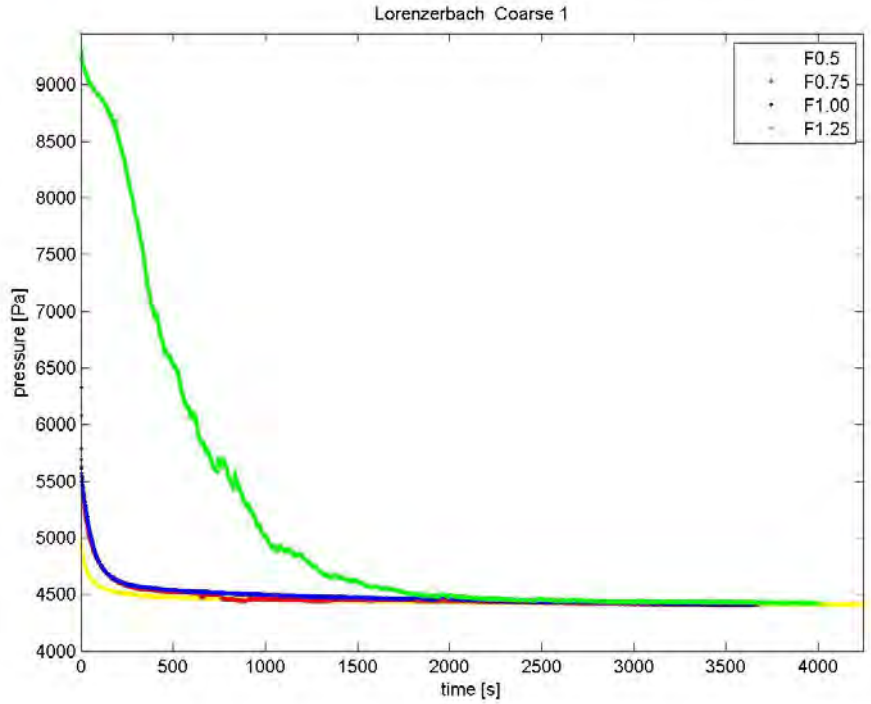

Figure 5.3.i

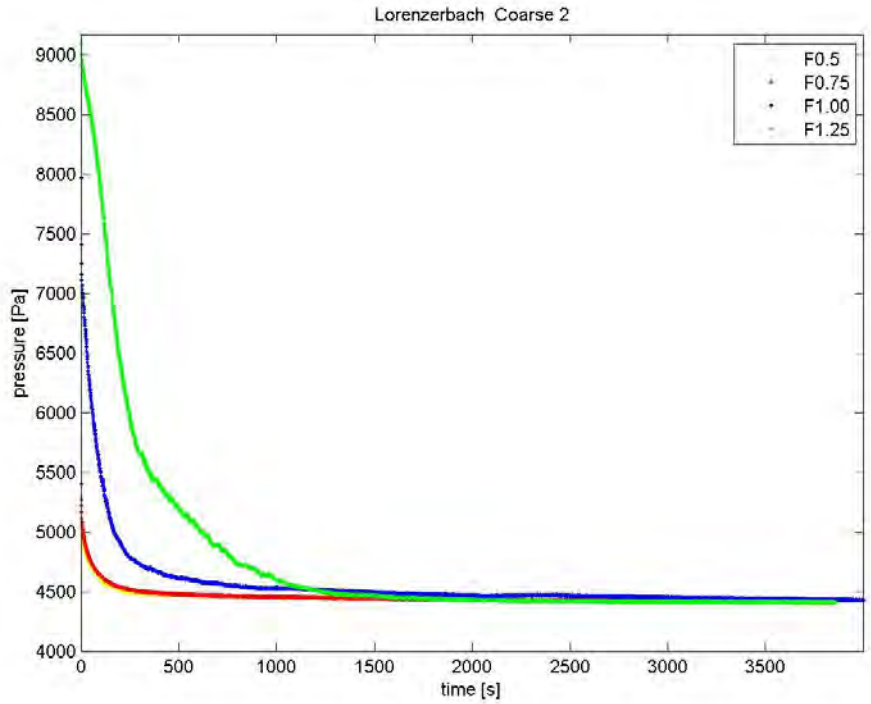

Figure 5.3.j

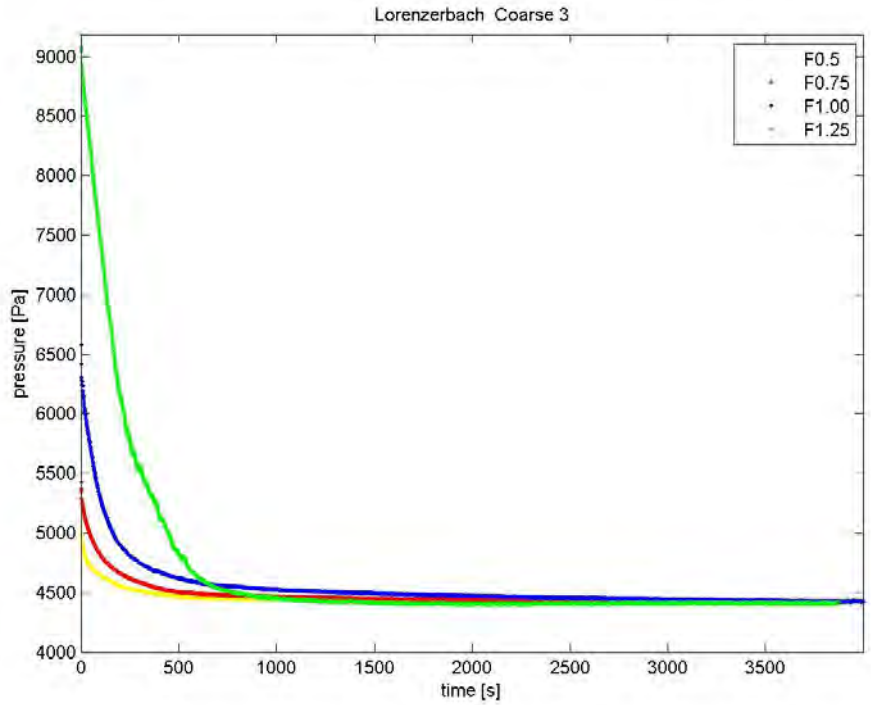

Figure 5.3.k

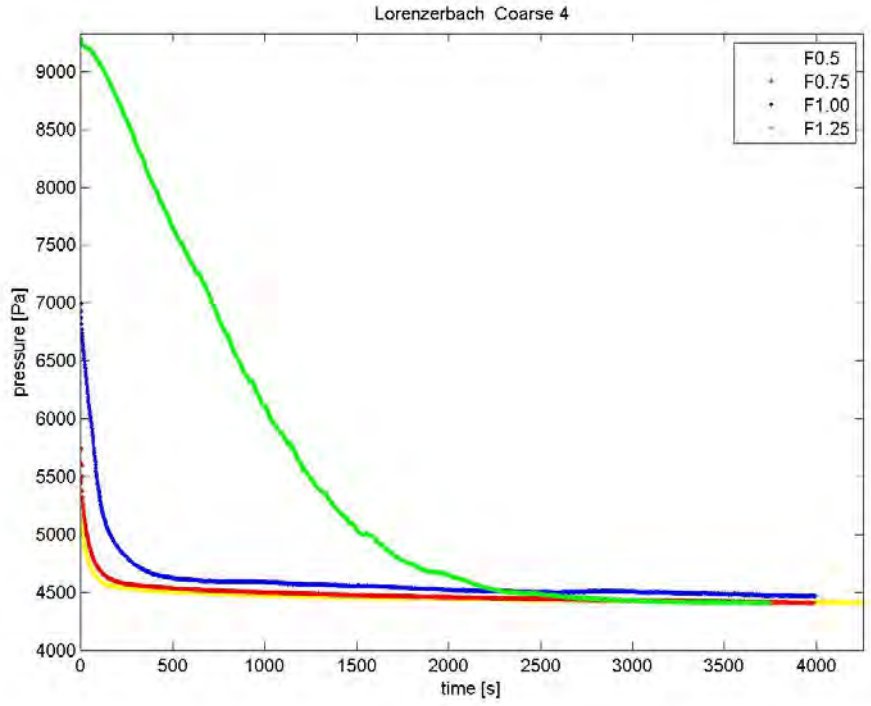

Figure 5.3.l

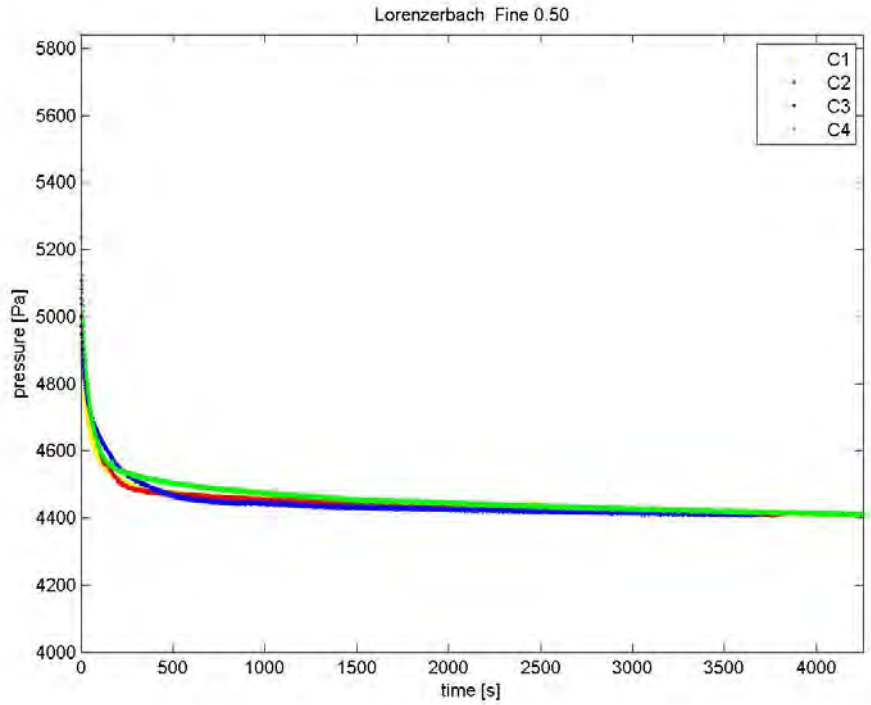

Figure 5.3.m

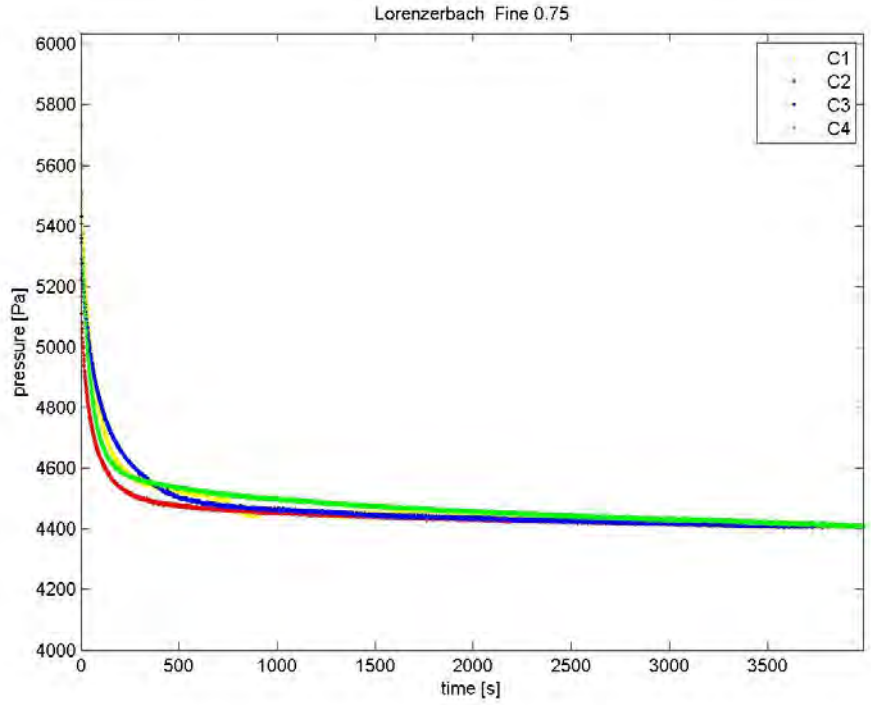

Figure 5.3.n

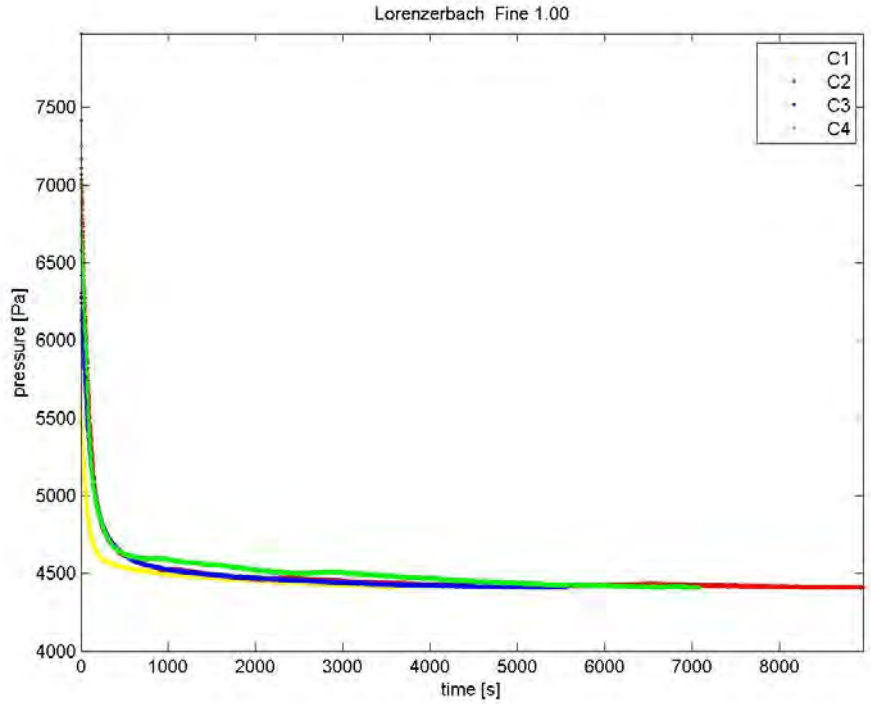

Figure 5.3.o

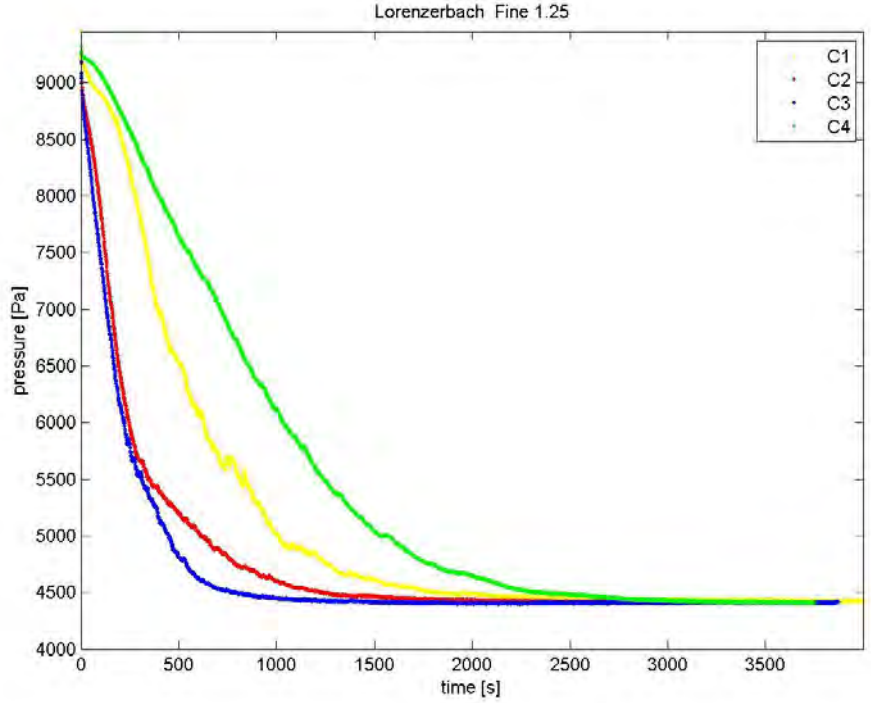

Figure 5.3.p

5.4 D COEFFICIENT VALUES

The tables below show the best fitting D coefficient values for the Scalalarue and Lorenzerbach samples: first two refer to the effects of fine content on coarse composition.

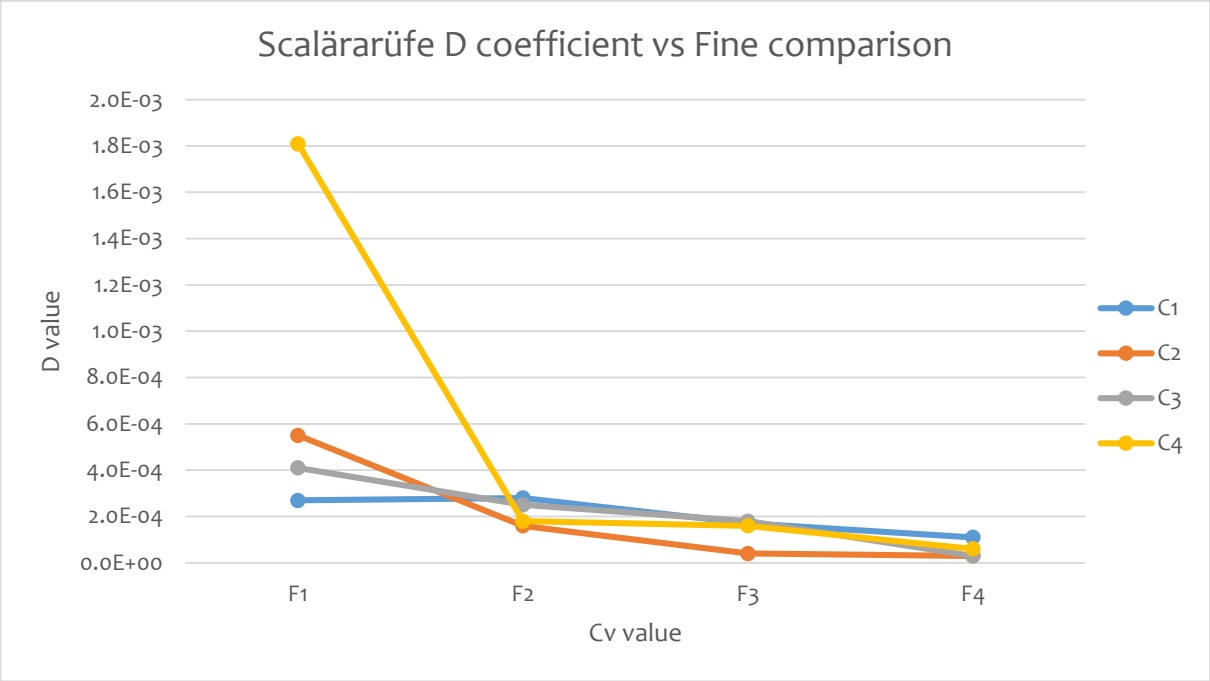

Table 5.4.1

C1 and C2 trends are as expected, whereas C3 and C4 show smaller D value for lower fine content. These tests are T9 and T10 for C3 and T13 and T14 for C4. In all these tests, the only used sensor is the bottom one, and the found D value is quite small. Therefore, it is possible to state these tests are not reliable at all.

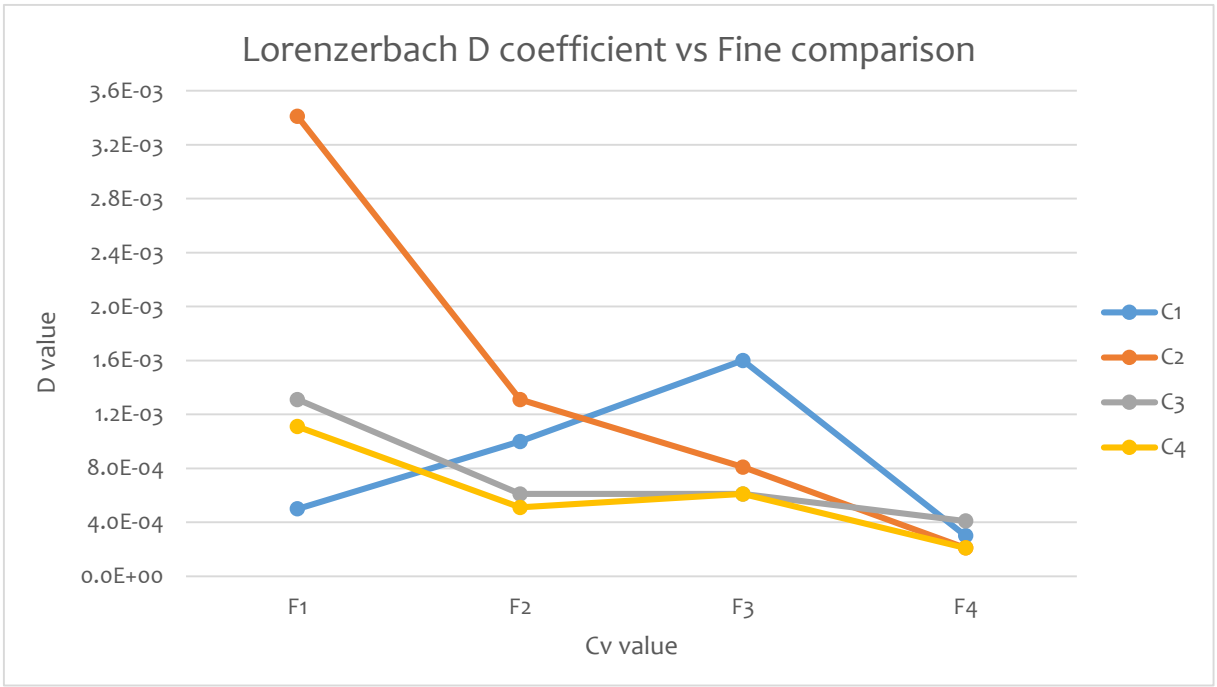

Table 5.4.2

The only "unexpected" D value is the first two from C1. This test shows reliability just for the bottom sensor, so it is possible to state these tests are not significant at all. These tables below refer to coarse effects on fine content: the expected indications after this choice are similar for the Scalärarüfe and Lorenzerbach samples up to C3: D coefficient smaller than C1 for C2, bigger for C3, while it should be bigger for C4 of Scalärarüfe and smaller for C4 of Lorenzerbach. As the table shows, the C1 - F0,5 (blue spot) is quite underestimate (test T1) but, except for that, C2 C3 and C4 present the shape I expected. C3 – F1,25 is smaller than C1 – F1,25 and this is probably due to the fine particles effect that is more relevant than coarse composition for this amount of fine-grained particles.

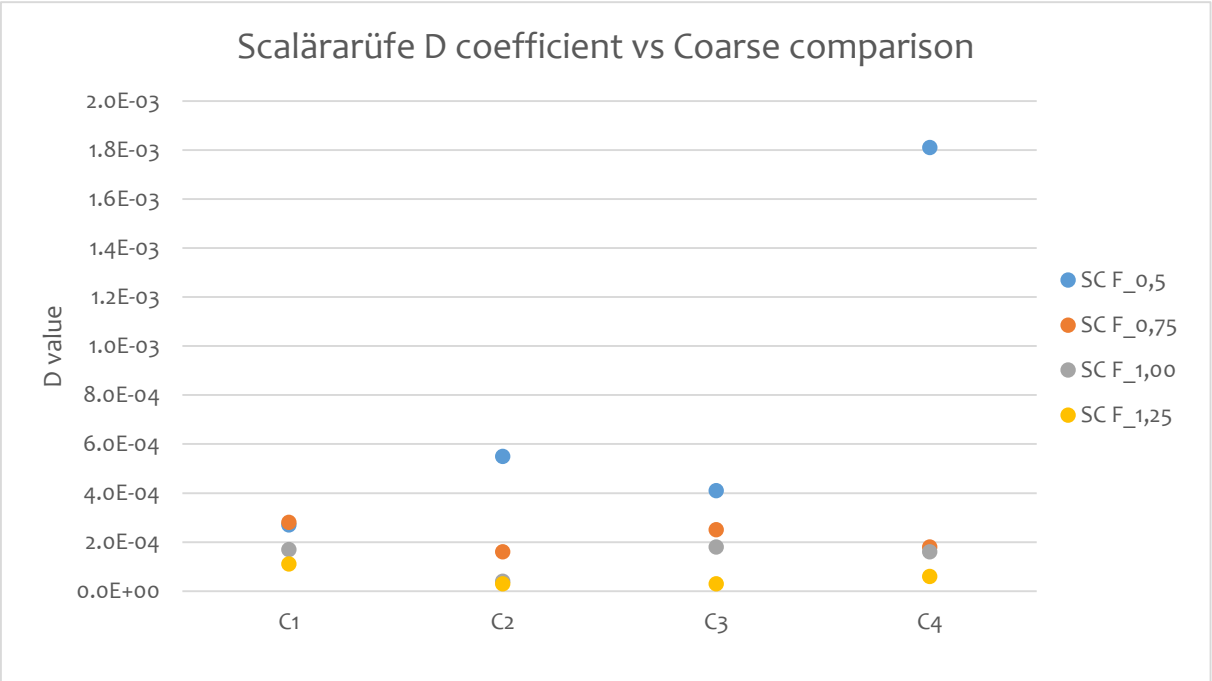

Table 5.4.3

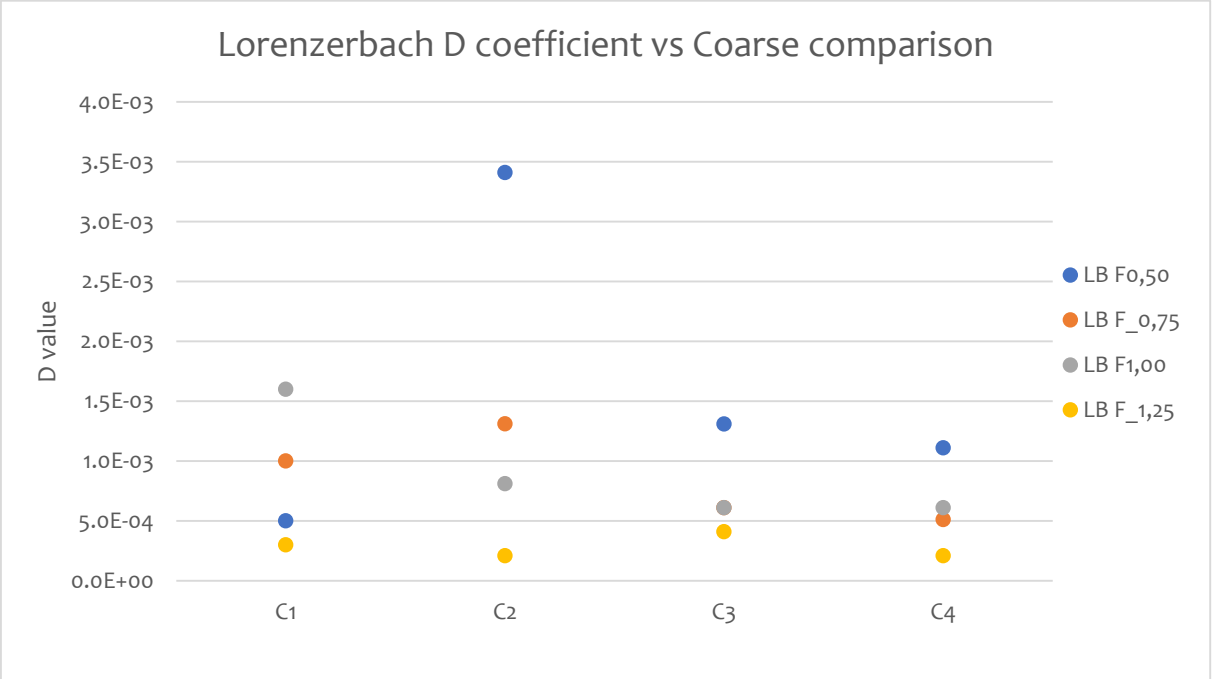

Table 5.4.4

5.5 SENSORS' RELIABILITY

Since I noticed some strange shapes during the tracing of the series, I decided to check item by item for which sensor to use in D coefficient calculation. This choice brought to exclude some sensors from the calculation, and in some cases (i.e. T17) I just used sensor pwp4 (bottom sensor), getting unreliable results. Therefore, it is possible to state that some test are not reliable at all and they should be repeated. On the other hand, I have also cases in which just bottom sensor is used and the results are comparable to expected. In the attachment, the sensor reliability table is added.

5.6 EFFECTS OF FINE PARTICLES

5.6.1 Scalärarüfe

- C_1 serie: fine particles have relevant effect on P_0, initial pressure. Higher concentration of fine particles entails higher P_0 initial pressure.
- C_2 serie: for tests F0,50 and F0,75 changes in C_v have no effects on the data series' shape. For F1,00 and F1,25 P_0 is similar but they have different shape. F1,25 (T8) does not reach the hydrostatic pressure value.
- C_3 serie: fine concentration shows effects on P_0 and settling time so T12 takes 3 hours to reach hydrostatic pressure value.
- C_4 serie: effects on P_0, higher concentration of fine entails higher P_0 value. Strange shape of T15.

5.6.2 Lorenzerbach

- C1 serie: fine concentration causes increase of P_0, but there are no differences in shape of F0,75 and F1,00. All tests need up to 20 min to completely consolidate, except for T20 (F1,25).
- C2 serie: highest P_0 values are for F1,25 and F1,00, instead there are no effects of fine in F0,75 and F0,500. This serie consolidate in less than 20 min as well.
- C3 serie: relevant effects of fine contents on P_0, and clear increasing D values for decreasing fine contents.
- C4 serie: very high P_0 peak for F1,25, but no P0 differences for F0,500 and F0,75. Clear increasing D values for decreasing fine contents.

5.7 EFFECTS OF COARSE PARTICLES

5.7.1 Scalärarüfe

Reduction of #16 fraction (biggest particles) and increase of #1 fraction (C2) entails higher D coefficient values for lower fine content (F0,500 and F0,75), whereas it entails the lowest D values for F1,00 and F1,25, compared to C1 series. So, it is possible to state a correlation between buoyant force and fine particles content. Removing of #1 and #2 fraction and increase of #8 fraction (C4) causes increase of D value for highest fine contents (F1,00 and F1,25). This result confirms on the other side the previous one. Removing of #1 fraction and increase of #8 fraction (C3) has the same effect for all the series: settling time reduces compared to C1 case and D values increase.

5.7.2 Lorenzerbach

Removing of #16 and increase of #4 fraction (C2) causes higher D value, compared to C1 case, for all the fine contents. On the other hand, removing of #1 fraction entails smaller D coefficient values.

Removing of #16 fraction and adding it in weight half to #1 and half to #2 fraction (C4) shows an increase of D coefficient value, confirming that smaller particles have more relevant effect on settling than bigger ones.

6 CONCLUSION

This work focused on the pore pressure dissipation, particularly on the effects of fine-grained particles content and coarse-grained particles composition. The goal of the research was to find, if existent, any correlation among these parameters or, if not existent, to investigate which components are more relevant on the pore pressure decay. I tested 32 different real debris flow mixtures coming from two sources, the first in Switzerland and the latter in Austria. My tests based on the previous work of Jon Major, who tested different mixtures both with drainage allowed from the upper and lower boundary and with drainage allowed just from the upper boundary. I focused on this second condition: my cylinder permitted the drainage just in the upper part. It was equipped with five sensors (with some relevant problems of reliability) to measure the pressure decay with time. Some of the tests are not reliable at all, because the calculation of D coefficient returned values showing around one order of magnitude of difference compared to the others. I looked at the results both from the fine particles side and from the coarse particles side: it was expected to have a decrease of D value increasing the fine content, and this trend is fully respected in all tests (except in those with reliability problems). Similarly, the designed changes in coarse-grained particles composition should have shown the dependence of D value from grain size distribution: in some cases, this is clearly recognizable from the comparison graphics. Therefore, the fundamental goal of the research was reached. Some side-results are important to underline here:

- A very good quality collection of data is needed to obtain reliable and physically significant results in the data analysis.
- The solution of the diffusion equation by Carslaw and Jaeger is adoptable with excellent results to mixture with solid concentration volume up to ~0.65 ÷ 0.68, for higher C_v values the shape of the calculated pressure decay could not fit well the measured one and for this reason the D value could be unreliable.
- A kind of dependence on fine particles content is evident in some data set: the importance of coarse particles changes are irrelevant compared to the fine particles content changes.
- The relation between coarse and fine particles, if exist, is not so clearly predicable.
- Further different results could be found with another set of tests and more experiments should be carry out with the same materials to investigate the behavior for higher and lower fine content and different coarse compositions.

Apart from this kind of "static" tests, would be interesting to conduct flume and rheology tests to fill in the table with "dynamic" parameters, verifying the agreement between the two kinds of result.

REFERENCES

Alcàntara_Ayala, I. (2002, October 1). Geomorphology, natural hazards, vulnerability and prevention of natural disasters in developing countries. *Geomorphology*, p. 107-110.

Dietrich, W. E. (1987). Settling Velocity of Natural Particles. *Water Resources Research*, 1615-1626.

Fox, P. J., & Baxter, C. D. (1997). *Consolidation Properties of Soil Slurries.*

King, H. (2006). Debris Flow Hazards in the United States. *United States Geological Survey Fact*, 176-197. Tratto da geology.com.

Major, J. (2000). *Gravity-driven consolidation of granular slurries — Implications for debris flow.*

Major, J. (2013). Stress, Deformation, Conservation, and Rheology: A Survey of Key Concepts in Continuum Mechanics. In M. R. John F. Shroder, *Treatise on Geomorphology.* San Diego: John F. Shroder.

N. Hotta, T. O. (2000). *Pore water pressure of Debris Flow.* Tokio.

Pierson, T. C. (1981). *Dominant particle support mechanisms in debris flows at Mt Thomas,.* Christchurch, New Zealand.

R. M. Iverson, M. E. (2000). *Acute Sensitivity of Landslide.*

S. Janu, S. M. (2015). *Engineering Geology for Society and Territory - Volume 2.*

Schatzmann, M. (2005). *Rheometry for large particles fluids and debris flows.* Zurich.

Swan, C. C. (s.d.). Grain Size Distributions and Soil. Iowa City.

ATTACHEMENTS

A. MATLAB SCRIPTS

I. DATA SERIES PREPARATION

```
% -----Università degli Studi di Padova-----
% -----Universität für Bodenkultur Vienna-----
% Corso di laurea in Ingegneria Civile Geotecnica
% Anno Accademico 2013-2014
% Studente Stefano Canto matr 103960
% Script to modify input data from lab tests

%% STARTING COMMANDS

clc % clear command window
clear all % clear all variables
close all % close all windows

root='C:/Users/Stefano/Documents/Tesi/Matlab'; %load saved path for the folders
%--------------------------------------------------------------------------
% input files in xls
%--------------------------------------------------------------------------

name_xls={'01_07_15_M1';'01_07_15_M2';'17_06_15_M0';'01_07_15_M3';
   '08_06_15_M11';'12_06_15_M14';'28_05_15_M6';'30_06_15_M9';
   '27_05_15_M5';'03_07_15_M7';'08_06_15_M4';'03_07_15_M8';
   '15_06_15_M15';'08_06_15_M13';'12_06_15_M10';'30_06_15_M12';
   '09_06_15_M17';'10_06_15_M22';'19_06_15_M16';'05_06_15_M21';
   '05_06_15_M19';'19_06_15_M31';'03_06_15_M18';'19_06_15_M30';
   '17_06_15_M29';'17_06_15_M28';'09_06_15_M20';'12_06_15_M25';
   '10_06_15_M24';'15_06_15_M27';'10_06_15_M23';'15_06_15_M26'};

mkdir([root,'/2_txt_acquired']); %create acquisition folder

%--------------------------------------------------------------------------
% read .xls files and print out the values for the four sensors in .txt
%--------------------------------------------------------------------------

for i=1:size(name_xls,1)
filename=[root,'/1_xls_acquisiti/',name_xls{i},'.XLSX'];
disp(['reading ',num2str(i,'%02d'),' xls file'])
mis = xlsread(filename, 'Tabelle1', 'A50:D1048576');
file_out_txt=[root,'/2_txt_acquired/test_',num2str(i,'%02d'),'.txt'];
disp(['printing ',num2str(i,'%02d'),' txt file'])
dlmwrite(file_out_txt, mis, 'delimiter', '\t','precision', '%.8f','newline', 'pc');
end

%% SHIFTING TO THE HYD PRESSURE VALUES

mkdir([root,'/3_shifted']);
mkdir([root,'/3_shifted/Tests']);
mkdir([root,'/3_shifted/Graphics']);

i=9 % to change for each test
file_in_txt=[root,'/2_txt_acquired/test_',num2str(i,'%02d'),'.txt'];
```

```
Press=dlmread(file_in_txt);
figure
plot(Press(:,4));  %plot the graph for the bottom sensor, then manually take the value for the mean

for j=1:4 % for each sensor
med(1,j)= mean(Press(3.146*10^5:size(Press,1),j))
end

Delta1= -(med(1,1)-0.245*10^4); % shift value for each sensor
Delta2= -(med(1,2)-0.098*10^4);
Delta3= -(med(1,3)-0.245*10^4);
Delta4= -(med(1,4)-0.441*10^4);

test= i; % test to be modified
shift=[Delta1,Delta2,Delta3,Delta4] % shift vector

% use this for tests that completely consolidate in 3 hrs
p1=Press(:,1)+shift(1);  %valore di pressione shiftato
p2=Press(:,2)+shift(2);  %valore di pressione shiftato
p3=Press(:,3)+shift(3);  %valore di pressione shiftato
p4=Press(:,4)+shift(4);  %valore di pressione shiftato

% use this for test that do not consolidate in 3 hrs
p1=Press(:,1);  %valore di pressione shiftato
p2=Press(:,2);  %valore di pressione shiftato
p3=Press(:,3);  %valore di pressione shiftato
p4=Press(:,4);  %valore di pressione shiftato

Press_Sh=[p1,p2,p3,p4];    % shifted pressure vector

% print out .txt file

file_out1_txt=[root,'/3_shifted/Tests/test_Sh_',num2str(test,'%02d'),'.txt'];
dlmwrite(file_out1_txt,Press_Sh, 'delimiter', '\t','precision', '%.8f','newline', 'pc');

% draw .jpg file

h1=figure('Visible','off');
hold on
plot(Press_Sh(:,1),'m');
plot(Press_Sh(:,2),'r');
plot(Press_Sh(:,3),'g');
plot(Press_Sh(:,4),'b');
hold off

saveas(h1,[root,'/3_shifted/Graphics/shifted_',num2str(i,'%02d'),'.jpg'])

%% NIP AND TUCK

mkdir([root,'/4_nip&tuck']);
mkdir([root,'/4_nip&tuck/Graphics']);
mkdir([root,'/4_nip&tuck/Tests']);

i=10   % to change for each test
clear Press_NP Press_Sm
file_in_txt_NT = [root,'/3_shifted/Graphics/shifted_',num2str(i,'%02d'),'.txt'];
Press_Sm  = dlmread(file_in_txt_NT);
h=figure
plot(Press_Sm(:,4),'b');
```

```
% use this part for test without changes

Press_NP = Press_Sm;
file_out3_txt=[root,'/4_nip&tuck/Tests/test_NT_',num2str(i,'%02d'),'.txt'];
dlmwrite(file_out3_txt, Press_NP, 'delimiter', '\t','precision', '%.8f','newline', 'pc');

% print out all the corrected sensor together

h2=figure('Visible','off');
hold on
plot(Press_NP(:,1),'m');
plot(Press_NP(:,2),'r');
plot(Press_NP(:,3),'g');
plot(Press_NP(:,4),'b');
hold off

saveas(h2,[root,'/4_nip&tuck/Graphics/N&T_',num2str(i,'%02d'),'.jpg'])

% use this part for test to be changed

% change first segment

x1 =...;       % graphic-based first point coordinate
x2 =...;      % graphic-based second point coordinate

% sensor #1

x1_1 = x1;    % graphic-based first point coordinate
x1_2 = x2;   % graphic-based second point coordinate
y1_1=Press_Sm(x1_1,1);        % first point ordinate
y1_2=Press_Sm(x1_2,1);       % second point ordinate

% adjustment line

x=transpose(x1_1:1:x1_2); % new calculated pressure vector
m=(y1_2-y1_1)/(x1_2-x1_1); % interpolating line parameters
q=y1_1-x1_1*m;
y1_mod=m*x+q+(1.8^2)*randn(size(x)); % add statistical noise to values

Press_NP(:,1)=[Press_Sm(1:x1_1-1,1);y1_mod;Press_Sm(x1_2+1:size(Press_Sm,1),1)];
h=figure ('Visible','off');
plot(Press_NP(:,1),'m')

%  sensor #2

x2_1= x1;     % graphic-based first point coordinate
x2_2= x2;    % graphic-based second point coordinate
y2_1=Press_Sm(x2_1,2);        % first point ordinate
y2_2=Press_Sm(x2_2,2);       % second point ordinate

% adjustment line

x=transpose(x2_1:1:x2_2); % new calculated pressure vector
m=(y2_2-y2_1)/(x2_2-x2_1); % interpolating line parameters
q=y2_1-x2_1*m;
y2_mod=m*x+q+(3.8^2)*randn(size(x)); % add statistical noise to values

Press_NP(:,2)=[Press_Sm(1:x2_1-1,2);y2_mod;Press_Sm(x2_2+1:size(Press_Sm,1),2)];
```

```
h=figure %('Visible','off');
plot(Press_NP(:,2),'r')

%  sensor #3

x3_1= x1;     % graphic-based first point coordinate
x3_2= x2;    % graphic-based second point coordinate
y3_1=Press_Sm(x3_1,3);        % first point ordinate
y3_2=Press_Sm(x3_2,3);       % second point ordinate

% adjustment line

x=transpose(x3_1:1:x3_2); % new calculated pressure vector
m=(y3_2-y3_1)/(x3_2-x3_1); % interpolating line parameters
q=y3_1-x3_1*m;
y3_mod=m*x+q+(3.5^2)*randn(size(x)); % add statistical noise to values

Press_NP(:,3)=[Press_Sm(1:x3_1-1,3);y3_mod;Press_Sm(x3_2+1:size(Press_Sm,1),3)];
h=figure %('Visible','off');
plot(Press_NP(:,3),'g')

%  sensor #4

x4_1= x1;           % graphic-based first point coordinate
x4_2= x2;    % graphic-based second point coordinate
y4_1=Press_Sm(x4_1,4);                % first point ordinate
y4_2=Press_Sm(x4_2,4);          % second point ordinate

% adjustment line

x=transpose(x4_1:1:x4_2); % new calculated pressure vector
m=(y4_2-y4_1)/(x4_2-x4_1); % interpolating line parameters
q=y4_1-x4_1*m;
y4_mod=m*x+q+(3.6^2)*randn(size(x)); % add statistical noise to values

Press_NP(:,4)=[Press_Sm(1:x4_1-1,4);y4_mod;Press_Sm(x4_2+1:size(Press_Sm,1),4)];
h=figure %('Visible','off');
plot(Press_NP(:,4),'b')

% change second segment

x1=...;             % graphic-based first point coordinate
x2=...;      % graphic-based second point coordinate

% sensor #1

x1_1 = x1;          % graphic-based first point coordinate
x1_2 = x2;   % graphic-based second point coordinate
y1_1=Press_NP(x1_1,1);                % first point ordinate
y1_2=Press_NP(x1_2,1);           % second point ordinate

% adjustment line

x=transpose(x1_1:1:x1_2); % new calculated pressure vector
m=(y1_2-y1_1)/(x1_2-x1_1); % interpolating line parameters
q=y1_1-x1_1*m;
y1_mod=m*x+q+(1.8^2)*randn(size(x)); % add statistical noise to values

Press_NP(:,1)=[Press_NP(1:x1_1-1,1);y1_mod;Press_NP(x1_2+1:size(Press_NP,1),1)];
```

```
h=figure %('Visible','off');
plot(Press_NP(:,1),'m')

%sensor #1

x2_1= x1;          % graphic-based first point coordinate
x2_2= x2;    % graphic-based second point coordinate
y2_1=Press_NP(x2_1,2);                % first point ordinate
y2_2=Press_NP(x2_2,2);          % second point ordinate

% adjustment line

x=transpose(x2_1:1:x2_2); % new calculated pressure vector
m=(y2_2-y2_1)/(x2_2-x2_1); % interpolating line parameters
q=y2_1-x2_1*m;
y2_mod=m*x+q+(3.8^2)*randn(size(x)); % add statistical noise to values

Press_NP(:,2)=[Press_NP(1:x2_1-1,2);y2_mod;Press_NP(x2_2+1:size(Press_NP,1),2)];
h=figure %('Visible','off');
plot(Press_NP(:,2),'r')

%sensor #1

x3_1= x1;          % graphic-based first point coordinate
x3_2= x2;    % graphic-based second point coordinate
y3_1=Press_NP(x3_1,3);                % first point ordinate
y3_2=Press_NP(x3_2,3);          % second point ordinate

% adjustment line

x=transpose(x3_1:1:x3_2); % new calculated pressure vector
m=(y3_2-y3_1)/(x3_2-x3_1); % interpolating line parameters
q=y3_1-x3_1*m;
y3_mod=m*x+q+(3.5^2)*randn(size(x)); % add statistical noise to values

Press_NP(:,3)=[Press_NP(1:x3_1-1,3);y3_mod;Press_NP(x3_2+1:size(Press_NP,1),3)];
h=figure %('Visible','off');
plot(Press_NP(:,3),'g')

%sensor #1

x4_1= x1;     % graphic-based first point coordinate
x4_2= x2;    % graphic-based second point coordinate
y4_1=Press_NP(x4_1,4);       % first point ordinate
y4_2=Press_NP(x4_2,4);      % second point ordinate

% adjustment line
x=transpose(x4_1:1:x4_2); % new calculated pressure vector
m=(y4_2-y4_1)/(x4_2-x4_1); % interpolating line parameters
q=y4_1-x4_1*m;
y4_mod=m*x+q+(3.6^2)*randn(size(x)); % add statistical noise to values

Press_NP(:,4)=[Press_NP(1:x4_1-1,4);y4_mod;Press_NP(x4_2+1:size(Press_NP,1),4)];
h=figure %('Visible','off');
plot(Press_NP(:,4),'b')

% change third segment

x1=...;      % graphic-based first point coordinate
```

```
x2=...;    % graphic-based second point coordinate

% sensor #1

x1_1 = x1;         % graphic-based first point coordinate
x1_2 = x2;  % graphic-based second point coordinate
y1_1=Press_NP(x1_1,1);            % first point ordinate
y1_2=Press_NP(x1_2,1);     % second point ordinate

% adjustment line
x=transpose(x1_1:1:x1_2); % new calculated pressure vector
m=(y1_2-y1_1)/(x1_2-x1_1); % interpolating line parameters
q=y1_1-x1_1*m;
y1_mod=m*x+q+(1.8^2)*randn(size(x)); % add statistical noise to values

Press_NP(:,1)=[Press_NP(1:x1_1-1,1);y1_mod;Press_NP(x1_2+1:size(Press_NP,1),1)];
h=figure %('Visible','off');
plot(Press_NP(:,1),'m')

% sensor #2

x2_1= x1; % graphic-based first point coordinate
x2_2= x2; % graphic-based first point coordinate
y2_1=Press_NP(x2_1,2);    % first point ordinate
y2_2=Press_NP(x2_2,2);    % first point ordinate

% adjustment line
x=transpose(x2_1:1:x2_2); % new calculated pressure vector
m=(y2_2-y2_1)/(x2_2-x2_1); % interpolating line parameters
q=y2_1-x2_1*m;
y2_mod=m*x+q+(3.8^2)*randn(size(x)); % add statistical noise to values

Press_NP(:,2)=[Press_NP(1:x2_1-1,2);y2_mod;Press_NP(x2_2+1:size(Press_NP,1),2)];
h=figure %('Visible','off');
plot(Press_NP(:,2),'r')

% sensor #3

x3_1= x1; % graphic-based first point coordinate
x3_2= x2; % graphic-based first point coordinate
y3_1=Press_NP(x3_1,3);    % first point ordinate
y3_2=Press_NP(x3_2,3);    % first point ordinate

% adjustment line
x=transpose(x3_1:1:x3_2); % new calculated pressure vector
m=(y3_2-y3_1)/(x3_2-x3_1); % interpolating line parameters
q=y3_1-x3_1*m;
y3_mod=m*x+q+(3.5^2)*randn(size(x)); % add statistical noise to values

Press_NP(:,3)=[Press_NP(1:x3_1-1,3);y3_mod;Press_NP(x3_2+1:size(Press_NP,1),3)];
h=figure %('Visible','off');
plot(Press_NP(:,3),'g')

% sensor #4

x4_1= x1; % graphic-based first point coordinate
x4_2= x2; % graphic-based first point coordinate
y4_1=Press_NP(x4_1,4);    % first point ordinate
y4_2=Press_NP(x4_2,4);    % first point ordinate
```

```
% adjustment line
x=transpose(x4_1:1:x4_2); % new calculated pressure vector
m=(y4_2-y4_1)/(x4_2-x4_1); % interpolating line parameters
q=y4_1-x4_1*m;
y4_mod=m*x+q+(3.6^2)*randn(size(x)); % add statistical noise to values

Press_NP(:,4)=[Press_NP(1:x4_1-1,4);y4_mod;Press_NP(x4_2+1:size(Press_NP,1),4)];
h=figure %('Visible','off');
plot(Press_NP(:,4),'b')

% print out the .txt file

file_out3_txt=[root,'/4_nip&tuck/Tests/test_NT_',num2str(i,'%02d'),'.txt'];
dlmwrite(file_out3_txt, Press_NP, 'delimiter', '\t','precision', '%.8f','newline', 'pc');

% print out all the corrected sensor together

h2=figure('Visible','off');
hold on
plot(Press_NP(:,1),'m');
plot(Press_NP(:,2),'r');
plot(Press_NP(:,3),'g');
plot(Press_NP(:,4),'b');
hold off

saveas(h2,[root,'/4_nip&tuck/Graphics/N&T_',num2str(i,'%02d'),'.jpg'])

%% MEASURE STARTING POINT

% starting point (given respect of 4th column)is taken as that point having
% the maximum value of the serie.

mkdir([root,'/5_cleaned']);
mkdir([root,'/5_cleaned/Tests']);
mkdir([root,'/5_cleaned/Graphics']);

for i=1:32
disp(['test n. ',num2str(i)])
   clear P_mean PP_mean Press PPress time_1sec Press_SP Press_SP_clean Press_SP_pos Diff2 start
file_in_txt_SP = [root,'/4_nip&tuck/Tests/test_NT_',num2str(i,'%02d'),'.txt'];
Press_SP = dlmread(file_in_txt_SP);

PP_mean(1,:) = Press_SP(1,:);
time_1sec(1,1) = 0;
pp=1;

for g=1:size(Press_SP,1)
   if rem(g,50)==0
      pp=pp+1;
      time_1sec(pp,1)=pp-1;
      P_mean(pp,:)=mean(Press_SP((pp-2)*50+1:(pp-1)*50,:));
   else
   end
end

% Starting point

P_mean_max = max(P_mean (:,4));
```

```
t = find (P_mean(:,4) == max(P_mean (:,4)));
for j=1:4
   Press_SP_clean (1,j) = P_mean(t,j);
   for s = 1:(size(P_mean,1)-t)
      Press_SP_clean (s+1,j) = P_mean(s+t,j);
   end
end

% print out .txt file

file_out3_txt=[root,'/5_cleaned/Tests/test_CL_',num2str(i,'%02d'),'.txt'];
disp(['printing ',num2str(i,'%02d'),' txt file'])
dlmwrite(file_out3_txt, Press_SP_clean, 'delimiter', '\t','precision', '%.8f','newline', 'pc');

% draw .jpg file

h=figure ('visible','off');
plot(time_1sec(1:size(PP_mean,1)),PP_mean(:,1),'c')
hold on
plot(time_1sec(1:size(PP_mean,1)),PP_mean(:,2),'c')
plot(time_1sec(1:size(PP_mean,1)),PP_mean(:,3),'c')
plot(time_1sec(1:size(PP_mean,1)),PP_mean(:,4),'c')
plot(time_1sec(1:size(Press_SP_clean,1)),Press_SP_clean(:,1),'m')
hold on
plot(time_1sec(1:size(Press_SP_clean,1)),Press_SP_clean(:,2),'r')
plot(time_1sec(1:size(Press_SP_clean,1)),Press_SP_clean(:,3),'g')
plot(time_1sec(1:size(Press_SP_clean,1)),Press_SP_clean(:,4),'b')
title(['test_ ',num2str(i,'%02d')]);
xlabel('time [s]');
ylabel('pressure [Pa]');
axis([0 inf 0 inf])
hold off
legend('gl5 h 25 cm','pwp1 h 10 cm','pwp2 h 25 cm','pwp4 h 45 cm');
saveas(h,[root,'/5_cleaned/Graphics/test_',num2str(i,'%02d'),'.jpg'])
end
```

II. DISSIPATION COEFFICIENT

```
% -----Università degli Studi di Padova-----
% -----Universität für Bodenkultur Vienna-----

% Corso di laurea in Ingegneria Civile Geotecnica

% Anno Accademico 2013-2014
% Studente Stefano Canto matr 103960

% Script to calculate D dissipation coefficient

clc
clear all
close all
%--------------------------------------------------------------------------
% Input parameters: water and solid weight, measured bulk density
%--------------------------------------------------------------------------

root='C:/Users/Stefano/Documents/Tesi/Matlab';
save('C:/Users/Stefano/Documents/Tesi/Matlab/mis.mat');
load('C:/Users/Stefano/Documents/Tesi/check_list1.mat');
```

```
mkdir([root,'/Error_Graphics']);
mkdir([root,'/Fitting']);
mkdir([root,'/Results']);

row=1000;

for ts=1:32;
   disp(['test n. ',num2str(ts)])
   clear P_mean P_std PPress Pdiff Pperc PP3 time_1sec
file_in_txt_SP =[root,'/5_cleaned/Tests/test_CL_',num2str(ts,'%02d'),'.txt'];
PPress=dlmread(file_in_txt_SP);

%--------------------------------------------------------------------------
% Timing to 1 second
%--------------------------------------------------------------------------

pp=1;
time_1sec(pp,1)=0;

for pp=1:size (PPress)
   time_1sec(pp,1)=pp-1;
end

D= 10^-5:10^-4:10^-2; % Definition of first attempt D value
iter=50; % number of iteractions for the summation in the analitic calculation

Ww = check_list1(ts,1);    % water weight
Ws = check_list1(ts,2);    % solid weight
rot = check_list1(ts,3);  % total density

H=0.45 ; % filling height
g=9.81; % gravity acceleration
z=[0.20 0.35 0.20 0.00]; % elevation of sensors (m) from the bottom
Wt = Ww+Ws; % total weight of the mixture
Vw = Ww/(row*1000); % water volume
Vt = Wt/(rot*1000); % total volume (12.5 l)
Vs = Vt-Vw; % solid volume
cv= Vs/Vt; % volume concentration
phi = 1-cv; % porosity
ros = (Ws/1000)/Vs; % solid density
pp2 = zeros(size(time_1sec,1),size(z,2));
Err = zeros(1,size(z,2));
Err_perc = zeros(1,size(z,2));

% Calculations for each sensor

for j=1:size(z,2) % j sensors' number

   Ph=row*g*(H-z(j)); % hydrostatic pressur at each height
   disp(['working on data of sensor ',num2str(j)]) % check of work in progress
   Ptot = PPress(1,4); % starting value as first measured value
   Ps0 = Ptot-Ph; % effective  stress

   for k=1:size(D,2) % k number of D values to try
      pp=zeros(1,iter);

      for t=1:size(PPress,1) % calculate pressure in that value

         for n=0:iter % n iterations for each time value
```

```
            lambda=(2*n+1)*pi/(2*H);
            c=1/(((2*n+1)^2)*pi^2);
            pp(1,n+1) = c*cos(lambda*z(j))*exp(-(lambda^2)*D(k)*time_1sec(t));
          end

          pp2(t,j)=8*Ps0*sum(pp(1,:));

          pp3(t,j)=pp2(t,j)+Ph;  % calculated pressure with analytic formula
          Pdiff(t,j) = (PPress(t,j)-pp3(t,j))^2; % square error for each time value
          Pperc(t,j) = abs((PPress(t,j)-pp3(t,j))/PPress(t,j)); % percentual error for each time value
        end
        Err(k,j)=sqrt(sum(Pdiff(:,j))/size(Pdiff,1)); % mean square deviation for each D value
        Err_perc(k,j)=sum(Pperc(:,j))/size(Pperc,1);  % percentage error for each D value
    end
end
%-------------------------------------------------------------------------
% Control of reliability of each sensor during the tests and data weakness
% for each test.
% Check list is a execel matrix where 1 means reliable and 0 means not
% reliable.
% 1 includes the D value in the Best Fit calculation
% 0 excludes the D value in the Best Fit calculation
%-------------------------------------------------------------------------

for qq=1:size(D,2)
    if mis(ts,1)==1
        A1=Err(qq,1);
        A2=Err_perc(qq,1);
    else
        A1=0;
        A2=0;
    end
    if mis(ts,2)==1
        B1=Err(qq,2);
        B2=Err_perc(qq,2);
    else
        B1=0;
        B2=0;
    end
    if mis(ts,3)==1
        C1=Err(qq,3);
        C2=Err_perc(qq,3);
    else
        C1=0;
        C2=0;
    end
    if mis(ts,4)==1
        D1=Err(qq,4);
        D2=Err_perc(qq,4);
    else
        D1=0;
        D2=0;
    end

    Err(qq,size(z,2)+1)=(A1+B1+C1+D1)/sum(mis(ts,:)); % Error dipending on estimated D value
    Err_perc(qq,size(z,2)+1)=(A2+B2+C2+D2)/sum(mis(ts,:)); % Percentage Error dipending on estimated D value
end

%-------------------------------------------------------------------------
```

```
% Results Plotting of Error on Dvalue for each sensor
%--------------------------------------------------------------------------

h3=figure('visible','off');
for j=1:size(z,2)
   hold on
   subplot(2,2,j)
   plot(D,Err(:,j));
   title('Error vs D')
   xlabel('D value')
   ylabel('Error')
   grid on
   hold off

end
saveas(h3,[root,'/Error_Graphics/graph_',num2str(ts,'%02d'),'.jpg'])

Dvalue = D(1,Err(:,5)== min(Err(:,5)));% Best-fit diffusivity value for all sensors combined
Dvalue_perc = D(1,Err_perc(:,5) == min(Err_perc(:,5)));% Best-fit diffusivity value for all sensors (%error)
D_B25cm = D(1,Err(:,1) == min(Err(:,1))); % Best-fit diffusivity value for sensors gl5
D_A10cm = D(1,Err(:,2) == min(Err(:,2))); % Best-fit diffusivity value for sensors pwp1
D_C25cm = D(1,Err(:,3) == min(Err(:,3))); % Best-fit diffusivity value for sensors pwp2
D_D45cm = D(1,Err(:,4) == min(Err(:,4))); % Best-fit diffusivity value for sensors pwp4

%--------------------------------------------------------------------------
% Calculation for the Best Fitted D value
%--------------------------------------------------------------------------

for j=1:size(z,2) % j sensors' number

   Ph = row*g*(H-z(j)); % hydrostatic pressur at each height
   disp(['working on data of sensor ',num2str(j)])
    Ptot = PPress(1,4); % starting value as first measured value
%     Ptot = rot*g*(H-z(4)) ; % starting value as first calculated value
   Ps0= Ptot-Ph;
%    Ps0 = (ros-row)*(1-phi)*g*H;   % effective  stress
      PP=zeros(1,iter);
      %Ps0 = (ros-row)*(1-phi)*g*z(j);

      for t=1:size(PPress,1) % t timing

         for n=0:iter % n iterations
            lambda=(2*n+1)*pi/(2*H);
            c=1/(((2*n+1)^2)*pi^2);

            PP(1,n+1) = c*cos(lambda*z(j))*exp(-(lambda^2)*Dvalue*time_1sec(t));
         end

         PP2(t,j)=8*Ps0*sum(PP(1,:));
         PP3(t,j)=PP2(t,j)+Ph;
      end
end

h4=figure ('visible','off');
for j=1:size(z,2)
   subplot(2,2,j)
   plot(time_1sec(1:size(PPress,1)),PPress(:,j),'.g');
   hold on
   plot(time_1sec(1:size(PP3,1)),PP3(:,j),'.r');
```

```
    title('Calculated vs Measured')
    xlabel('time [x10 s]')
    ylabel('Pa')
    grid on
    hold off
    legend('P measured','P calculated');
end

saveas(h4,[root,'/Fitting/fitting_test_',num2str(ts,'%02d'),'.jpg'])

%--------------------------------------------------------------------------
% results printing
%--------------------------------------------------------------------------

file_resul = [root,'/Results/T_',num2str(ts,'%02d'),'.txt'];
out = fopen(file_resul,'w');

fprintf(out,'%s\r\n',[' ---- Test_',num2str(ts,'%02d'),'  Results']);
fprintf(out,'%s\r\n','');
fprintf(out,'%s\r\n','solid density   water weight   solid weight   total density   cv');
fprintf(out,' %f      %f      %f      %f      %f',ros,Ww,Ws,rot,cv);
fprintf(out,'%s\r\n','');
fprintf(out,'%s\r\n','BF-DV_all   BF-DV_all_%   BF-DV_sensA   BF-DV_sensB   BF-DV_sensC   BF-DV_sensD');
fprintf(out,' %f      %f      %f      %f      %f      %f',Dvalue,Dvalue_perc,D_B25cm,D_A10cm,D_C25cm,D_D45cm);
fprintf(out,'%s\r\n','');
fprintf(out,'%s\r\n','Err-BF_all   Err%-BF_all_%   Err-BF_sensA   Err-BF_sensB   Err-BF_sensC   Err-BF_sensD');
fprintf(out,' %f      %f      %f      %f      %f
%f',min(Err(:,5)),min(Err_perc(:,5)),min(Err(:,1)),min(Err(:,2)),min(Err(:,3)),min(Err(:,4)));
fclose('all');

pluto(ts,1)=ts;
pluto(ts,2)=cv;
pluto(ts,3)=Dvalue;
pluto(ts,4)=Dvalue_perc;
pluto(ts,5)=D_B25cm;
pluto(ts,6)=D_A10cm;
pluto(ts,7)=D_C25cm;
pluto(ts,8)=D_D45cm;
pluto(ts,9)=min(Err(:,5));
pluto(ts,10)=min(Err_perc(:,5));

pippo(ts,1)=min(Err(:,5));
pippo(ts,2)=Err_perc(Err(:,5)== min(Err(:,5)),5);
pippo(ts,3)=min(Err_perc(:,5));
pippo(ts,4)=Err(Err_perc(:,5)== min(Err_perc(:,5)),5);

end

file_out1_txt=[root,'/pluto.txt'];
dlmwrite(file_out1_txt,pluto, 'delimiter', '\t','precision', '%.8f','newline', 'pc');
```

III. COMPARE GRAPHICS

```
% -----Università degli Studi di Padova-----
% -----Universität für Bodenkultur Vienna-----

% Corso di laurea in Ingegneria Civile Geotecnica

% Anno Accademico 2013-2014

% Studente Stefano Canto matr 103960

% Script to compare data series
clc
clear all
close all
%--------------------------------------------------------------------------
% Input parameters: test number
%--------------------------------------------------------------------------
root='C:/Users/Stefano/Documents/Tesi/Matlab';
mkdir([root,'/Graphs']);
ts=[13,14,15,16];

sens = 4;

for i =1:4
   file_in=[root,'/5_cleaned/Tests/test_CL_',num2str(ts(i),'%02d'),'.txt'];
   clear Press
   Press = dlmread(file_in);

   for t=1:size (Press)
      time(t,1)=t-1;
   end


   if i==1
      h=figure;
      plot(time(1:size(Press,1)),Press(:,sens),'.y')
      %plot(time(1:4000),Press(1:4000,sens),'.y')
      title('Scalärarüfe  Coarse 4');
      xlabel('time [s]');
      ylabel('pressure [Pa]');
      axis([0 inf 4000 inf])
      hold on
   elseif i==2
      plot(time(1:size(Press,1)),Press(:,sens),'.r')
   elseif i==3
      plot(time(1:size(Press,1)),Press(:,sens),'.b')
      %plot(time(1:4000),Press(1:4000,sens),'.b')
   elseif i==4
      plot(time(1:size(Press,1)),Press(:,sens),'.g')
      %plot(time(1:10800),Press(1:10800,sens),'.g')
   end
end
legend('F0.5','F0.75','F1.00','F1.25');
hold off
saveas(h,[root,'/Graphs/Sc_C4.jpg'])
```

B. TEST CHECK

test	gl5-pa	pwp1-pa	pwp2-pa	pwp4-pa
1	1	1	1	1
2	1	1	1	1
3	1	0	0	1
4	1	1	0	1
5	1	1	0	1
6	1	0	0	1
7	1	0	1	1
8	1	0	1	1
9	1	0	1	1
10	1	0	0	1
11	1	1	0	1
12	1	0	0	1
13	1	0	0	1
14	1	1	1	1
15	1	1	0	1
16	1	1	0	1
17	0	0	0	1
18	1	1	0	1
19	1	0	1	1
20	1	0	0	1
21	0	1	0	1
22	1	1	1	1
23	1	0	0	1
24	1	0	0	1
25	1	0	0	1
26	1	0	1	1
27	1	0	0	1
28	1	0	0	1
29	1	1	1	1
30	1	1	1	1
31	1	0	0	1
32	1	1	0	1